A Proof-of-Concept Investigation of CPP-Modified ATTEMPTS for Enhanced Toxin-Based Colorectal Cancer Therapy

by

Meong Cheol Shin

A dissertation submitted in partial fulfillment
of the requirements for the degree of
Doctor of Philosophy
(Pharmaceutical Sciences)
in the University of Michigan
2013

Doctoral Committee:

Professor Victor C. Yang, Chair
Professor George A. Garcia
Professor Kyung-Dall Lee
Professor David E. Smith

To my family and friends

With my love and respect

Acknowledgements

I would like to express my sincere gratitude to Dr. Victor C. Yang for his support and insightful guidance throughout my Ph.D. training years. He taught me the attitude to keep up my confidence and bravely work out my experiments. I deeply respect his perseverance and enthusiasm in his research as a scientist. I also would like to thank my committee members, Dr. Kyung-Dall Lee, Dr. David E. Smith, and Dr. George A. Garcia for their suggestions and guidance in my project.

I am also grateful to the Department of Pharmaceutical Sciences and the Rackham Graduate School for supporting me during my Ph.D. I thank all my wonderful friends. They were always there for me to make this long journey for a Ph.D. possible; my classmates, Bei Yang, Kefeng Sun, Deanna Mudie, Maria M. Posada, and Lilly Roy for their friendship and good memories through all the years; my previous lab members, Dr. Yongzhuo Huang, Dr. Allan E. David, Dr. Cheol Moon, Dr. Hee Sun Chung, Dr. Adam J. Cole, Dr. Tien-Yi Lee, Lindsay White, Dr. Yoon Shin Park, Dr. Joon-Beom Park, Dr. Faquan Yu, Dr. Huining He, Dr. Beata Chertok, Dr. Lei Zhang and Dr. Jie Zhou for their valuable advice and support; and my present lab members, Dr. Jian Zhang, Dr. Kyuri Lee, Dr. Mei Wang and Jingwen Zhao for their help and friendship. I would like to dedicate my work to my parents who supported me with love and belief throughout my life. Lastly, I greatly thank my wife, Kyoung Ah and my two sons, Min Seok and Michael, for their love and support.

Table of Contents

List of Tables

List of Figures

Abstract

One of the major hurdles to cure cancer lies in the low potency of currently available drugs, which could eventually be solved by using more potent therapeutic macromolecules. However, although these macromolecules possess greater potency inside the cancer cells, the barely permeable cell membrane remains a formidable barrier in reducing their efficacy. For instance, gelonin, a typical ribosome inactivating protein (RIP) possesses exceptionally high N-glycosidase activity, but the anti-cancer effects of gelonin are rather negligible, due to its inability to enter tumor cells. To overcome the cell membrane barrier, we modified gelonin with two model cell penetrating peptides (CPPs), TAT peptide and low molecular weight protamine (LMWP), *via* both chemical conjugation and genetic recombination methods. Through *in vitro* and *in vivo* studies, these CPP-modified gelonins (i.e. gelonin-LMWP chemical conjugate (cG-L), recombinant gelonin-LMWP chimera (rG-L) and TAT-gelonin chimera (TAT-Gel)) displayed markedly improved cell uptake efficiency and, thereby, significantly enhanced tumoricidal activity, compared with unmodified recombinant gelonin (rGel). On the other hand, this CPP-modification aggravated the potential toxicity concerns of gelonin as the non-specific fashion of CPP-mediated cell uptake led to internalization of the CPP-modified gelonins into any type of cells. Thus, to curb the cell penetration activity of CPP and expose it only to the tumor cells, a modified version of ATTEMPTS (Antibody Targeted Triggered Electrically Modified Prodrug Type Strategy), a heparin/protamine-

based drug delivery system (DDS), featured by ‘antibody-mediated tumor targeting’ and ‘prodrug strategy’ was explored. For targeting, a heparin functionalized monoclonal antibody (mAb) was developed with T84.66 (i.e. T84.66-Hep), an anti-CEA mAb, *via* chemical conjugation. When T84.66-Hep and TAT-Gel was mixed together, they automatically formed a tight complex *via* electrostatic interaction between anionic heparin and cationic TAT. Systemic administration of this T84.66-Hep/TAT-Gel complex enabled much higher accumulation of TAT-Gel (58-fold higher tumor exposure) in LS174T xenograft tumor, compared with injection of TAT-Gel alone. Furthermore, heparin/protamine-based prodrug feature of the DDS provided significantly enhanced tumoricidal efficacy with yet reduced toxicity, compared with administration of TAT-Gel alone. Overall, this study provides a general rationale to enhance the therapeutic efficacy of potent but cell-impermeable macromolecules and, further, safely deliver to their target site.

Chapter 1

Introduction

1.1 Colorectal Cancer and Limitations of Current Chemotherapeutics

In the United States, colorectal cancer is the third most commonly diagnosed cancer (estimate of 140,000 new cases in 2013) and the second leading cause of cancer related deaths (estimate of 50,000 deaths in 2013).[1] Despite certain successes in improving the survival rate of the patients by early cancer detection and appropriate surgical intervention (average 67%), a cure is yet elusive specifically for metastasized cancers which are unable to be removed by surgery (survival rate: 6 %).[1-3] The difficulty to treat those metastasized cancers with current approved small anticancer drugs lies in their low therapeutic efficacy and toxicity issues caused by non-selective mode of the drug action.[4, 5] For example, 5-FU (or fluorouracil) is a pyrimidine analogue drug prescribed for colorectal cancer therapy over 40 years.[6] Although 5-FU still remains the primary choice for treatment, its therapeutic effect is strictly limited (10 – 15% response rate and at most 6 – 8 months extension of life-span).[4] Thus, 5-FU has often been used in combination with 1 or 2 other drugs. Although this combination therapy has been, indeed, more effective than treatment by 5-FU alone, its therapeutic outcome (20 month of

extension of life span) is yet far from achieving cure and, what is worse, frequently induces severe toxicity.[7]

1.2 Gelonin Toxin

To overcome the limitations of current small molecule-based anti-cancer drug therapy, dramatically rising interest has been directed to macromolecules with exceptional therapeutic potency. Specifically, the ribosome-inactivating proteins (RIPs), a family of N-glycosidases, represent promising drug candidates for treatment of cancer.[8] For example, gelonin, originally derived from the seeds of *Gelonium multiflorum*, is a typical RIP that has been clinically studied for its anti-cancer application.[9, 10] This gelonin exerts extreme potency in inhibiting protein synthesis *via* the cleavage of a single adenine residue (A_{4324}) in the 28S ribosomal RNA.[9] Even a single gelonin molecule, assuming its effectiveness of access to the target ribosomes, can kill one tumor cell due to its exceptional catalytic activity, while there requires 10^4–10^5 molecules of its chemotherapeutics counterparts for the same job.[11] However, in spite of the potency, gelonin is not able to cross the cell membrane.[11] Therefore, it is imperative to overcome the membrane barrier to utilize gelonin for tumor treatment.

1.3 Cell Penetrating Peptides (CPPs)

The discovery of the potent cell-penetrating activity of CPPs such as TAT (an arginine-rich, 11-amino acid peptide derived from the human immunodeficiency virus (HIV) protein) or low molecular weight protamine (LMWP; an arginine rich 14-amino acid peptide derived from protamine protein) has shed light of finally solving the

membrane barrier problem.[12-15] Both cell culture and animal studies showed that by covalently linking those CPPs to almost any type of drugs including hydrophilic compounds and large proteins, the CPPs were able to translocate the attached species into cells of all organ types including the brain.[16] Although the mechanism of CPP-mediated cell transduction remains unclear, this event appeared to require a surface adsorption step (likely via the binding of the cationic CPP to the anionic heparan sulfate on the cell surface); because the CPP-mediated cell translocation was completely inhibited by the presence of heparin.[17] Unprecedentedly, this CPP-mediated cell entry was so effective and overwhelming that it could not be matched by any existing cell entry method including receptor-mediated endocytosis. Indeed, in their investigation of cell targeting by a CPP-linked antibody, Niesner *et al* reported that the cell-entering activity of CPP was so potent that it actually overrode the targeting function of the antibody.[18] As a consequence, a whole body distribution of the CPP-antibody conjugates, similar to the profile of CPP alone, was observed before the antibody could ever exert its targeting activity. To this regard, although the unparalleled potency of CPP to transduce all types of compounds (small, large, hydrophobic or hydrophilic) across all types of cell membranes renders it an ideal means to overcome the membrane barrier, the lack of selectivity of CPP on mediated cell internalization unfortunately makes this method an unacceptable practice due to concerns of causing drug-associated toxic effects.

1.4 CPP-Modified ATTEMPTS (Antibody Targeted Triggered Electrically Modified Prodrug-Type Strategy)

The CPP-modified ATTEMPTS system is assembled with a unique architecture that comprises all of the desirable features of a drug delivery system (DDS) including: (1) targeting, (2) prodrug, and (3) the potent CPP-mediated cellular drug uptake.[19] A schematic illustration of this delivery approach is shown in Figure 1. In brief, this system consists of a complex body made of two (i.e. targeting and drug) components. The targeting component consists of a specific targeting moiety (which could be an antibody (Ab) or a peptide ligand) coupled with a heparin (Hep) molecule. The drug component consists of the delivered drug covalently linked with a CPP. These two components can attach to each other automatically by a charge-charge interaction between the anionic heparin (on the targeting component) and the cationic CPP (on the drug component). Binding of heparin to CPP would produce three critical functions: (1) it would inhibit the trans-membrane activity of CPP thereby prohibiting the CPP-Drug/Ab-Hep complex from entering normal cells; (2) it would protect CPP from degradation by plasma trypsin-like proteases; and (3) it would preserve the targeting function of the antibody since the trans-membrane function of CPP is completely masked by heparin. Following *i.v.* administration, the antibody-guided, prodrug-behaved complexes will spare interaction with normal cells during their targeting to the tumor. After reaching the target, protamine sulfate, a clinical heparin antidote that binds heparin stronger than CPP, will be administered as a competing agent to dissociate the CPP-Drug part from its Ab-Hep counterpart. Once relieved from heparin binding, CPP will resume its potent trans-

membrane activity, ferrying the CPP-Drug conjugates into the targeted tumor cells. The drug will then induce apoptosis of the tumor cells.

1.5 Specific Aims

The research objective of this dissertation is to develop a potent CPP-modified gelonin toxin, and investigate the feasibility to apply a modified ATTEMPTS for enhanced CPP-modified toxin-based colorectal cancer therapy. On this basis, the following specific aims will be addressed:

1) To develop CPP-modified gelonin and characterize the anti-cancer activity and applicability for CPP-modified ATTEMPTS.
2) To develop a mAb-Hep and evaluate its ability to selectively deliver a CPP-modified gelonin to the tumor *via* complex formation.
3) To evaluate the feasibility of applying CPP-modified ATTEMPTS for enhanced toxin-based colorectal cancer therapy.

1.6 Figures

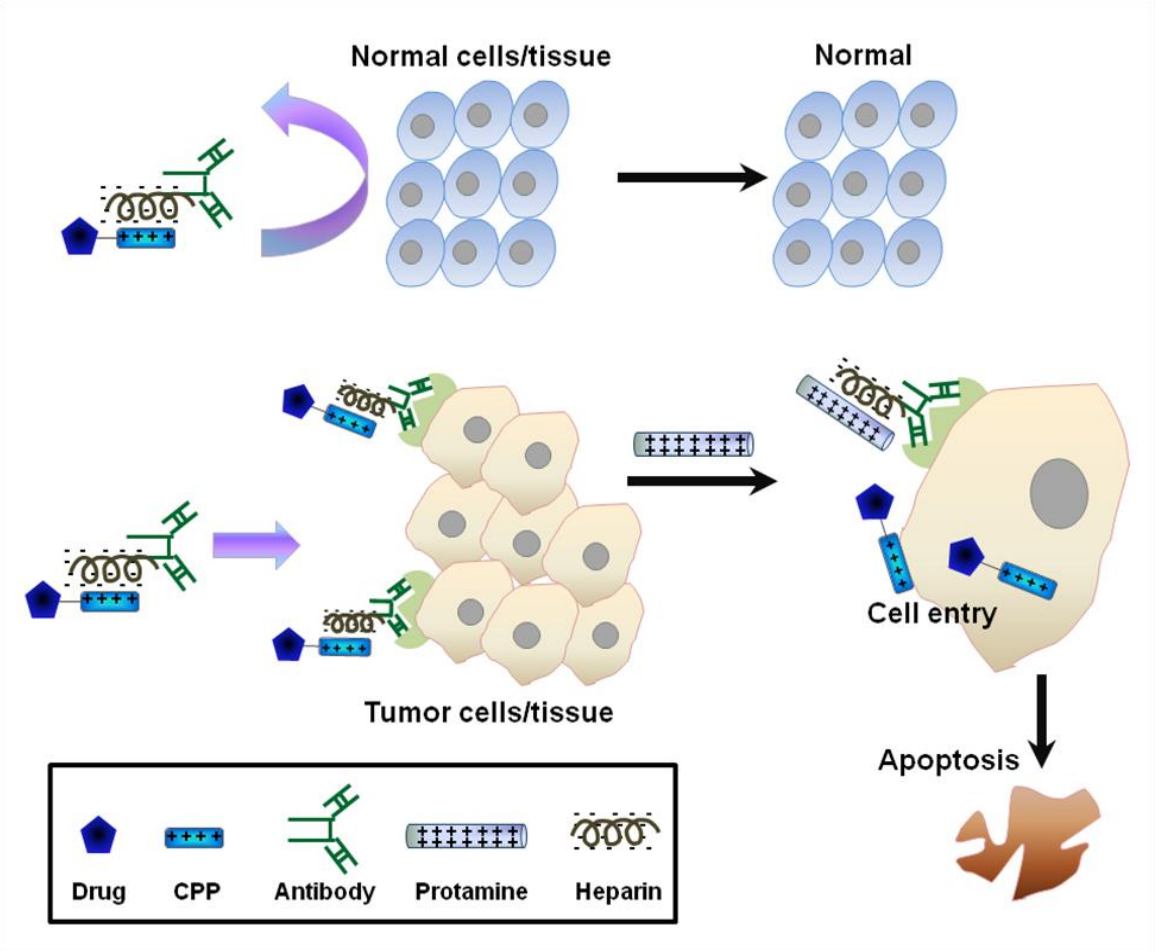

Figure 1-1. Illustration of CPP-modified ATTEMPTS.

1.7 References

1. Siegel R, Naishadham D, Jemal A. Cancer statistics, 2013. CA Cancer J Clin 2013;63:11-30.
2. Rex DK, Johnson DA, Anderson JC, Schoenfeld PS, Burke CA, Inadomi JM, American College of G. American College of Gastroenterology guidelines for colorectal cancer screening 2009 [corrected]. Am J Gastroenterol 2009;104:739-50.
3. Edwards BK, Ward E, Kohler BA, Eheman C, Zauber AG, Anderson RN, Jemal A, Schymura MJ, Lansdorp-Vogelaar I, Seeff LC, van Ballegooijen M, Goede

SL, Ries LA. Annual report to the nation on the status of cancer, 1975-2006, featuring colorectal cancer trends and impact of interventions (risk factors, screening, and treatment) to reduce future rates. Cancer 2010;116:544-73.
4. Zhang DQ, Guo Q, Zhu JH, Chen WC. Increase of cyclooxygenase-2 inhibition with celecoxib combined with 5-FU enhances tumor cell apoptosis and antitumor efficacy in a subcutaneous implantation tumor model of human colon cancer. World J Surg Oncol 2013;11:16.
5. Tzeng CW, Aloia TA. Colorectal liver metastases. J Gastrointest Surg 2013;17:195-201; quiz p -2.
6. Heidelberger C, Chaudhuri NK, Danneberg P, Mooren D, Griesbach L, Duschinsky R, Schnitzer RJ, Pleven E, Scheiner J. Fluorinated pyrimidines, a new class of tumour-inhibitory compounds. Nature 1957;179:663-6.
7. Kelly H, Goldberg RM. Systemic therapy for metastatic colorectal cancer: current options, current evidence. J Clin Oncol 2005;23:4553-60.
8. Barbieri L, Battelli MG, Stirpe F. Ribosome-inactivating proteins from plants. Biochim Biophys Acta 1993;1154:237-82.
9. Stirpe F, Olsnes S, Pihl A. Gelonin, a new inhibitor of protein synthesis, nontoxic to intact cells. Isolation, characterization, and preparation of cytotoxic complexes with concanavalin A. J Biol Chem 1980;255:6947-53.
10. Hertler AA, Frankel AE. Immunotoxins: a clinical review of their use in the treatment of malignancies. J Clin Oncol 1989;7:1932-42.
11. Atkinson SF, Bettinger T, Seymour LW, Behr JP, Ward CM. Conjugation of folate via gelonin carbohydrate residues retains ribosomal-inactivating properties of the toxin and permits targeting to folate receptor positive cells. J Biol Chem 2001;276:27930-5.
12. Torchilin VP. Tat peptide-mediated intracellular delivery of pharmaceutical nanocarriers. Adv Drug Deliv Rev 2008;60:548-58.
13. Frankel AD, Pabo CO. Cellular uptake of the tat protein from human immunodeficiency virus. Cell 1988;55:1189-93.
14. Heitz F, Morris MC, Divita G. Twenty years of cell-penetrating peptides: from molecular mechanisms to therapeutics. Br J Pharmacol 2009;157:195-206.
15. Park YJ, Chang LC, Liang JF, Moon C, Chung CP, Yang VC. Nontoxic membrane translocation peptide from protamine, low molecular weight protamine (LMWP), for enhanced intracellular protein delivery: in vitro and in vivo study. FASEB J 2005;19:1555-7.
16. Schwarze SR, Ho A, Vocero-Akbani A, Dowdy SF. In vivo protein transduction: delivery of a biologically active protein into the mouse. Science 1999;285:1569-72.
17. Derossi D, Calvet S, Trembleau A, Brunissen A, Chassaing G, Prochiantz A. Cell internalization of the third helix of the Antennapedia homeodomain is receptor-independent. J Biol Chem 1996;271:18188-93.
18. Niesner U, Halin C, Lozzi L, Gunthert M, Neri P, Wunderli-Allenspach H, Zardi L, Neri D. Quantitation of the tumor-targeting properties of antibody fragments conjugated to cell-permeating HIV-1 TAT peptides. Bioconjug Chem 2002;13:729-36.

19. Kwon YM, Li YT, Liang JF, Park YJ, Chang LC, Yang VC. PTD-modified ATTEMPTS system for enhanced asparaginase therapy: a proof-of-concept investigation. J Control Release 2008;130:252-8.

Chapter 2

Chemically and Biologically Synthesized CPP-Modified Gelonin for Enhanced Anti-Tumor Activity

2.1 Abstract

The ineffectiveness of small molecule drugs against cancer has generated significant interest in more potent macromolecular agents. Gelonin, a plant-derived toxin with unparalleled N-glycosidase activity to inhibit protein translation, has attracted much attention in this regard. Due to its inability to internalize into cells, however, gelonin only exerts limited tumoricidal effect. To overcome this cell membrane barrier, we modified gelonin with the low molecular weight protamine (LMWP) peptide, a cell penetrating peptide (CPP) which was shown to efficiently ferry various cargos into cells, *via* both chemical conjugation and genetic recombination methods. Results confirmed that while chemically-modified and genetically-modified gelonin-LMWP conjugates (abbreviated as cG-L and rG-L, respectively) possessed equivalent N-glycosidase activity to that of unmodified recombinant gelonin (rGel), they both were able to internalize into tumor cells, unlike rGel. Cytotoxicity studies further demonstrated that both cG-L and rG-L exhibited significantly improved tumoricidal effects, with IC_{50} values reaching 120-fold lower than that of rGel. Moreover, when tested against a CT26 s.c. xenograft tumor

mouse model, significant inhibition of tumor growth was observed, with rG-L doses being as low as 2 μg/tumor, when comparing with rGel which yielded no detectable therapeutic effects even at doses 10-fold higher. Overall, this study shed light on the potential of utilizing CPP-modified gelonin as a highly potent anticancer drug to overcome limitations of currently existing chemotherapeutic agents.

2.2 Introduction

Anti-cancer drug therapies at the present time are primarily focused on small molecule agents. While some have shown to be efficacious, most of these small molecule drugs have suffered from a poor therapeutic index – a ratio of the concentration required for efficacy versus that for toxicity.[1] This issue becomes most apparent in the treatment of cancers, where side-effects often limit the amount of drug dosing which, subsequently result in an accumulation of sub-optimal drug concentrations at the tumor target. With unmatched potency and selectivity, macromolecules have drawn significant interest over the past few decades for their potential to overcome the limitations of small molecule drugs.[2-4] Clinical translation of macromolecular drugs, however, has largely been prohibited, due to the low bioavailability, instability in physiological environment and, in many cases, poor intracellular transport of these agents.[2, 3, 5, 6] A typical example is the plant-derived ribosome-inactivating protein (RIP) toxins. Since the initial discovery of ricin from castor oil plants,[7] more than 50 different RIPs have now been identified.[8, 9] RIPs are extremely potent inhibitors of protein synthesis, and thus have drawn considerable interest for potential use as anticancer drugs[10] Gelonin, for instance, belongs to this RIP family. It is a 30-kDa single chain glycoprotein extracted from seeds of

Gelonium multiflorum, and inactivates ribosomes by the cleavage of a single adenine residue (A_{4324}) in the 28S ribosomal RNA[11] Because of the high substrate specificity, non-stoichiometric mode of action, and repetitive reaction mechanism, the therapeutic efficacy of gelonin cannot be matched by any of the existing anti-tumor agents.[11] It has even been postulated that a single molecule of the gelonin toxin is sufficient enough to completely kill one cancer cell,[12, 13] if the drug can reach the ribosome. Yet, this unparallel therapeutic potency has not been realized clinically, primarily due to the inability of gelonin to cross the cell membrane barrier for effective uptake.[8, 11] A means to deliver gelonin into the intracellular compartment therefore becomes an essential element to utilize this extremely potent N-glycosidase activity for cancer treatment.

The 1988 discovery by Frankel and Pabo that TAT (transactivator of transcription) protein derived from HIV-1 virus could internalize cells[14] led to the identification of a class of peptides with unique and unprecedented cell-penetrating activity[15-17]. Later studies demonstrated that these peptides, so-called "cell penetrating peptides (CPPs)", were also able to efficiently translocate the attached cargos such as protein molecules or nano-scale drug carriers into cells.[15-17] Although the mechanism of cell entry remains unclear and not unified, it now appears that the interaction of the cationic CPP with negatively charged glycosaminoglycans on cell surface is an essential prerequisite, because addition of extracellular heparin, heparan or dextran sulfate would completely abolish the cell-internalizing functions of these CPPs.[18, 19]

Low molecular weight protamine (LMWP) is a 14-mer peptide (VSRRRRRRGGRRRR), previously developed by Yang and coworkers that exhibits CPP-like cell-penetrating behavior.[20] Both *in vitro* and *in vivo* studies demonstrated that

LMWP could transduce proteins, genes and even nano-scale drug carriers like liposomes into living cells.[20-24] Aside from this cell penetrating ability, LMWP also possessed a number of other significant advantages over currently existing CPPs including: 1) the capability for mass production; 2) a thoroughly investigated toxicological and immunological profile; and 3) the *in vivo* safe application as an antidote for heparin reversal.[20, 25-27] Based on these findings, we hypothesized that modification of gelonin with LMWP could effectively and safely deliver gelonin into tumor cells, thereby dramatically enhancing gelonin's cytotoxic effects against tumors.

In this chapter, we present *in vitro* findings of both chemically and biologically modified gelonin. For chemical modification, LMWP was covalently attached to gelonin using a heterobifunctional polyethylene glycol (PEG) cross-linker. For recombinant modification, gene encoding LMWP was inserted at the C-terminus of the gelonin gene, and the resulting fusion protein was expressed in *Escherichia coli* (*E.coli*). The inhibitory activity on protein translation by both chemically synthesized and recombinant gelonin-LMWP conjugates, abbreviated as cG-L and rG-L respectively, was assessed using a cell-free translational system. In addition, the cell-penetrating ability and potency against tumor cells were examined in a variety of cancer cell lines. Furthermore, preliminary *in vivo* investigation of the inhibition on tumor growth was conducted in a CT26 xenograft tumor mice model.

2.3 Materials and Methods

2.3.1 Materials

The pET28a-gelonin vector (pET-Gel) was used for overexpression of recombinant gelonin (rGel). Competent *E.coli* cells (TOP10, BL21star (DE3) and BL21-CodonPlus), pEXP-5-NT/TOPO TA expression kit, AcTEV^{TM} protease, LB broth, fetal bovine serum albumin (FBS), PBS (pH 7.4), Dulbecco's Modified Eagle Medium (DMEM), RPMI1640 and Hoechst 33342 trihydrochloride, trihydrate were purchased from Invitrogen (Carlsbad, CA). Carbenicillin, kanamycin, and isopropyl-β-thiogalactopyranoside (IPTG) were purchased from Fisher Scientific (Pittsburg, PA). Heparin sulfate, rhodamine B isothiocyanate, Traut's reagent (2-iminothiolane; 2-IT) and DTNB (5, 5'-dithiobis-(2-nitrobenzoic acid)) were purchased from Sigma-Aldrich (St. Louis, MO). DNA primers were purchased from Integrated DNA Technologies Inc. (Coralville, IA). DNA restriction endonucleases (NdeI, NheI-HF, EcoRI-HF and XhoI) and T4 DNA ligase were purchased from New England Biolabs (Ipswich, MA). BCA protein assay kit was purchased from Bio-Rad Laboratories (Hercules, CA). Rabbit reticulocyte lysate system, luciferase assay system and recombinant RNasin® ribonuclease inhibitor were purchased from Promega Corporation (Madison, WI). Cell proliferation kit II (XTT) was purchased from Roche Applied Science (Indianapolis, IN). Native gelonin (nGel) was purchased by Enzo Life Sciences Inc. (Farmingdale, NY). LMWP was obtained from ISTN (Lancaster, PA) and heterobifunctional PEG (NHS-PEG-PDP; 2 kDa) was purchased from JenKem Technology USA Inc. (Allen, TX).

2.3.2 Expression and Purification of Recombinant Gelonin (rGel)

The pET-Gel vector was transformed into *E.coli* strain (BL21 (DE3)), and rGel was produced following the method described by Hossann *et al*.[28] Briefly, a single colony of pET-Gel transformed BL21 (DE3), grown on LB agar plate with 80 µg/mL kanamycin, was picked and inoculated into 200 mL of LB medium. This starter culture was incubated overnight at 37°C with shaking at 250 rpm and then used to inoculate 5 L of fresh LB medium, which was incubated at 37°C with shaking at 250 rpm. When the optical density at 600 nm reached 1, IPTG inducer was added to a final concentration of 0.5 mM. The culture was further incubated under the same conditions for 6 hr. Cells were then harvested by centrifugation at 4000 rpm for 20 min at 4°C. The pellet was suspended in 30 mL of 20 mM phosphate buffer saline (PBS, 300 mM NaCl, pH 7) and the cells were lysed by sonication (4 × 30 sec, with 50% output in ice bath). The cell lysate was centrifuged at 20,000 rpm for 30 minutes and the supernatant was loaded onto HisPure® Ni-NTA resin (Bio-Rad Laboratories, Hercules, CA) pre-equilibrated with 20 mM PBS (300 mM NaCl, pH 7). The impurities were washed with 200 mL of PBS and then rGel was eluted with 20 mM PBS containing imidazole (300 mM NaCl, 400 mM imidazole, pH 7). For further purification, the eluent from the Ni-NTA resin was loaded onto a cation exchange column (HiTrap Sepharose CM-FF, GE Healthcare Bio-Sciences, Pittsburgh, PA) connected to a HPLC (Alltech 526 HPLC pump, Deerfield, IL) and rGel was purified by elution with a salt gradient (0 to 2 M NaCl at a rate of 0.02M/min, flow rate: 1 mL/min).

2.3.3 Preparation and Purification of Chemically-Conjugated Gelonin-LMWP (cG-L)

Chemical conjugation of rGel with LMWP was accomplished using Traut's reagent and a heterobifunctional PEG (NHS-PEG-PDP, 2 kDa) as the cross-linker. The NHS group on one side of the PEG chain was amine reactive while the PDP group at the other end was thiol reactive. The conjugation scheme is shown in Figure 1. Briefly, thiol groups were first introduced to rGel (5 mg/mL in 2 mL of 10 mM PBS, 50 mM triethanolamine, 2 mM EDTA, pH 8) by incubation with 10 molar excess of Traut's reagent for 1 hr at room temperature. Unreacted Traut's reagent was removed by ultrafiltration using a centrifugal filtration device (molecular weight cut-off: 10 kDa, Amicon® Centricon® Centrifugal Filter Devices, Millipore Corporation, Billerica, MA) and the generated thiol groups on rGel were quantified by Ellman's assay.

Next, the amine group on the LMWP peptide (10 mg/mL in 20 mM PBS with 0.15 M NaCl, pH 7.4) was reacted with 3-fold molar excess of NHS-PEG-PDP for 4 hr at room temperature with shaking to introduce LMWP with the thiol-reactive PDP group. Unreacted PEG was removed by loading the reaction mixture onto a heparin column (HiTrap Heparin HP, GE Healthcare Bio-Sciences, Pittsburgh, PA) and washing with 50 mM phosphate buffer (pH 7.4). Purified LMWP-PEG-PDP was then eluted with 2 M NaCl (50 mM PBS, 2 M NaCl, pH 7.4) at a flow rate of 1 mL/min. LMWP-bound PDP groups were quantified by the pyridine-2-thione (P2T) assay. Following the preparation of both thiolated-rGel (rGel-SH) and LMWP-PEG-PDP, they were mixed together at a molar ratio of 1:5 (rGel-SH:LMWP-PEG-PDP) and incubated overnight at 4°C. The final cG-L product was purified from unreacted rGel by using a heparin column and elution

with a salt gradient (0 to 2 M NaCl at a rate of 0.02M/min, flow rate: 1 mL/min). Any unreacted LMWP and LMWP-PEG-PDP which might be present in the cG-L peak fraction was further removed by centrifugal filtration (Eppendorf Centrifuge 5702R), using membranes with a 10 kDa molecular weight cut-off pore size. The purified cG-L was stored at 4°C until further use.

2.3.4 Preparation and Purification of the Recombinant Gelonin and LMWP Chimera (rG-L)

Construction of Gelonin-LMWP Genes

The gelonin-LMWP gene was constructed by inserting a PCR fragment encoding the LMWP gene into the pET-Gel vector (pET28a-Gel). Briefly, double stranded DNA fragments containing partial C-terminal gelonin and LMWP encoding codons (646 bp) were prepared by PCR using pET-Gel vector as a template. The primers used for the PCR reaction were as follows: 1) the forward primer was 5'-AAA GCT CGA ATT CTT ATT ACC TTC TCC TTC TAC CTC CCC TTC TCC TTC TCC TTC TTG ATA CAC CTT TCG GAT CTT TGT CG-3' and 2) the backward primer was 5'-AAC GAT AAC GGC CAG CTA GCG GAA ATT GC-3'. The PCR product was purified by 1% agarose gel electrophoresis and inserted into a pEXP-5-NT/TOPO vector using the vendor's protocol (Invitrogen, Carlsbad, CA). Both the pET-Gel vector and the pEXP-5-NT/TOPO vector encompassing the partial gelonin and LMWP genes were then double digested with NheI & EcoRI-HF. The open digested pET-Gel vector and the DNA insert were purified by 1% agarose gel electrophoresis, ligated by T4 ligase reaction and then transformed into TOP10 competent cells. The prepared pET28a-Gel-LMWP vectors were submitted for DNA sequencing analysis.

For expression of rG-L with N-terminal thioredoxin-6x His tag (TRX-Gel-LMWP), the pET-Gel-LMWP vector (pET22b-TRX-Gel-LMWP) was prepared utilizing the pET28a-Gel-LMWP vector. The full length gelonin-LMWP gene was digested from pET28a-Gel-LMWP vector by NdeI & XhoI restriction enzymes and, after purification by 1% agarose gel electrophoresis, it was inserted into the pET22b-TRX vector which contains the gene encoding for thioredoxin-6xHis tag and TEV protease cleavable peptide. The prepared pET-Gel-LMWP vector was submitted for DNA sequencing analysis. The schematic design of the pET-Gel-LMWP vector is depicted in Figure 2A and schematic images of rGel, TRX-Gel-LMWP and rG-L are shown in Figure 2B.

Expression and Purification of rG-L

Prior to large scale (5L) production, the expression of rG-L was tested in a small culture (6 mL) under various conditions, including different media (LB, 2xYT and TB), temperatures (37°C, 25°C and 16°C) and final IPTG concentrations (0.1, 0.5 and 1 mM), using both pET28a-Gel-LMWP and pET-Gel-LMWP vectors. To express the rG-L protein chimera, vectors were separately transformed into BL21star (DE3) *E.coli* strains. For the pET28a-Gel-LMWP vector, a different *E.coli* strain (BL21-CodonPlus) was also used to test the expression. Similar procedures used for expression of rGel were employed for expression of rG-L. After expression and cell lysis, both the supernatant and the pellet of the cell lysate were investigated for rG-L expression *via* SDS-PAGE analysis. The insoluble pellet fraction of rG-L expression was solubilized in 1% SDS solution with boiling and sonication, before separation with SDS-PAGE. Separate batches with no IPTG induction served as controls. The success of the expression was

determined by the presence of the expected rG-L or TRX-Gel-LMWP band in the SDS-PAGE results.

Based on the expression study results, the pET-Gel-LMWP vector was adopted for large scale production of rG-L. The expression and Ni-NTA resin purification procedures applied for production of rGel were identical to those used for TRX-Gel-LMWP and thus would not be reiterated here. After expression and purification, TRX-Gel-LMWP was incubated with TEV protease to remove the thioredoxin-6xHis tag following the vendor's protocol (AcTEV™ protease, Invitrogen, Carlsbad CA). The cleaved product was loaded onto a heparin column, and the final rG-L protein chimera was acquired by salt gradient elution (0 to 1.4 M NaCl at a rate of 0.02 M/min, flow rate: 1 mL/min).

2.3.5 Protein Assays

The products of rGel, cG-L and rG-L were monitored by SDS-PAGE on 10% Tris-HCl gel. Purity of the proteins was assessed by performing densitometry analysis (ImageJ software, National Institutes of Health, Bethesda, MD) on the gels. Protein concentration was determined by the BCA protein assay using native gelonin (nGel; (Enzo Life Sciences Inc) as the standard.

2.3.6 Assessment of the Inhibition of Protein Translation by cG-L and rG-L

The ability of nGel, rGel, cG-L and rG-L to inhibit protein translation was evaluated in a cell-free translational system using rabbit reticulocyte lysate and luciferase mRNA. Briefly, in separate eppendorf tubes, 5 µL of either nGel, rGel, cG-L or rG-L of different concentrations (10^{-12} - 10^{-7} M) were mixed with 35 µL of rabbit reticulocyte lysate, 1 µL of amino acid without methionine, 1 µL of amino acid without leucine, 1.4

μL of potassium chloride, 1 μL of luciferase control mRNA, 1 μL of RNasin® ribonuclease inhibitor and 4.6 μL of ultrapure water (total reaction volume: 50 μL). The reaction mixture was incubated at 30°C for 90 min, and the amount of translated luciferase was then measured by the luciferase assay system (Promega Corp., Madison, WI). Briefly, 2.5 μL of the reaction mixture was added to 50 μL of luciferase substrate and the luminescence intensity was measured by a plate reader (BioTEK® Synergy™ BioTEK, Co., Winooski, VT) following the vendor's protocol. Luminescence intensities were plotted against gelonin concentrations, and the concentration required to inhibit 50% luciferase translation (IC_{50}) was calculated by nonlinear regression using Prism software (Prism version 5.0, GraphPad, San Diego, CA).

2.3.7 Cell Culture

CT26 murine adenocarcinoma cells, LS174T human adenocarcinoma cells, 9L human glioma cells and PC-3 human prostate cancer cells were obtained from American Type Culture Collection (ATCC) (Manassas, VA). The cells were cultured in 75 cm^2 flasks at 37°C in a 95% air/5% CO_2 containing humidified incubator. CT26 cells were maintained in RPMI1640 medium with 1% (v/v) penicillin-streptomycin, and 10% FBS. Both LS174T and 9L cells were cultured in Dulbecco's Modified Eagle Medium (DMEM) with 2 mM L-glutamine, high glucose, 1% (v/v) penicillin-streptomycin, and 10% FBS. PC-3 cells were cultured in 50% RPMI1640 and 50% DMEM with 1% (v/v) penicillin-streptomycin, and 10% FBS. Culture media in the flask was changed every other day. After reaching confluency, cells were transferred into new culture flasks by detaching with 0.25% Trypsin-EDTA and reseeding at a 1:3 split ratio for the continuous cultures.

2.3.8 Evaluation of LMWP-mediated Cellular Uptake of cG-L and rG-L

The rGel, cG-L and rG-L proteins were each labeled with rhodamine dye by mixing the sample (2 mg/mL in 0.1 M sodium bicarbonate buffer, pH 9.3) with rhodamine B isothiocyanate at a molar ratio of 1:5, and then incubated at room temperature for 4 hr. After incubation, unreacted excess rhodamine dye was removed by applying the reaction solution to dye removal resin following the vendor's protocol (Bio-Rad Laboratories, Hercules CA). The protein to dye ratio was determined by measuring the optical density at 280 nm and 520 nm for protein and the dye, respectively.

Prior to the cell uptake study, CT26 cells were seeded onto a 24 well plate with $5x10^4$ cells/well and incubated for 24 hr in complete RPMI1640 medium with 10% FBS. When cell confluency reached approximately 50%, rhodamine-labeled rGel, cG-L and rG-L were added to the cells (~ 5 μM final concentrations with identical fluorescent intensities among the samples) and incubated for 3 hr at 37°C in a humidified CO_2 incubator. The cells were washed three times with heparin/PBS (10 mg/mL heparin in 50 mM phosphate buffer, 0.15 M NaCl, pH 7.4), followed by the addition of the Hoechst 33342 solution (1:1000 dilution of 16.2 mM stock solution) to counter-stain the nucleus of these cells. After 30 min incubation with Hoechst 33342, cells were washed three times with PBS. Images of the live cells were then taken using a Nikon TE2000S epifluorescence microscope equipped with a standard mercury bulb, a charge-coupled device camera (Roper Scientific, Tucson, AZ), a 20 objective ((Nikon Plan Fluor ELWD 20) and a triple-pass DAPI/FITC/TRITC filter set (Chroma Technology Corp., Brattleboro,VT). Cell images were acquired and analyzed by Metamorph software (Molecular Devices Corporation, Sunnyvale, CA).

2.3.9 Anti-cancer Activity of cG-L and rG-L

The anti-cancer activities of rGel, cG-L and rG-L were determined in various cancer cell lines (e.g. CT26, LS174T, 9L and PC-3 cells) by XTT assay. Briefly, cells were detached using trypsin, re-suspended in complete medium and then dispensed into 96-well plates at a density of 10^4 cells per well. After incubation for 24 hr, gelonin samples were added to the wells at varying final concentrations (10^{-10} - 10^{-5} M) and incubated for 48 hr. Relative cell proliferation was measured by XTT assay following the vendor's protocol (Roche Applied Science, Indianapolis IN).

2.3.10 *In Vivo* Evaluation of Inhibition on Tumor Growth by rG-L

Six-week-old male athymic nude mice with an average weight ranging from 22 - 25 g were purchased from Charles River Laboratories (Raleigh, NC). These mice were housed in animal facilities and fed with standard chow diet. Three days after arrival, mice were randomly divided into 5 groups and treated, separately, with: 1) PBS; 2) rGel (injected dose: 20 μg); 3) rG-L (2 μg); 4) rG-L (4 μg); and 5) rG-L (20 μg). Animal experiments were conducted according to protocols approved by the University of Michigan Committee on Use and Care of Animals (UCUCA; protocol No. 08945). Briefly, at day 0 (3 days after arrival of animals), CT26 cells were harvested and implanted to the left hind region of the mice leg (5×10^6 cells in 50 μL). Test samples were administered by intra-tumor injection on day 7, when the tumor size reached about 100 mm^3, and also on day 10. Tumor size was measured daily with a vernier caliper and the tumor volume (mm^3) was calculated as $\boldsymbol{V} = (a^2 \times b)/2$, where a is the width and b is the length of the tumor [29].

2.3.11 Statistical Analysis

All data were presented as mean ± standard deviation. Statistically significant differences among groups were determined using the one-way ANOVA and Tukey's multiple comparison test as post-hoc test (Prism version 5.0, GraphPad, San Diego, CA). Results that yielded p-values less than 0.05 were considered to be statistically significant.

2.4 Results

2.4.1 Expression and Purification of Recombinant Gelonin (rGel)

The rGel protein with N-terminal 6x His tag was successfully over-expressed as a soluble protein from *E.coli* and purified using a Ni-NTA metal affinity column. rGel, which selectively bound to the resin *via* the 6x His tag, was eluted with 400 mM imidazole. When the eluent was further loaded onto a cation exchange column (CM-FF HP column), rGel was found being retained in the column, presumably due to its basic nature (pI = 9.1), and was later eluted as a single peak using 0.4 M NaCl. According to the results (data not shown) from densitometry analysis of the SDS-PAGE gels, the average purity of rGel was $\geq$ 95%. The total amount of expressed rGel in a 5-L culture, as determined by the BCA protein assay, was estimated to be approximately 5 mg (i.e. ~1 mg/L culture).

2.4.2 Synthesis and Purification of Chemically-Conjugated Gelonin-LMWP (cG-L)

The cG-L was successfully synthesized by coupling rGel with LMWP *via* a disulfide bond. Results from the Ellman's assay indicated that an average of 6 active thiol

groups was introduced to each rGel molecule activated by the Traut's reagent. On the other hand, one thiol-active PDP group was introduced to each LMWP molecule through conjugation with NHS-PEG-PDP. Since PEG itself did not have a strong affinity for heparin, unreacted PEG could be readily removed by passing the reaction mixture through a heparin column. Results from the P2T assay showed that approximately 40% of the LMWP eluent from the heparin column contained PEG. Although non-reacted LMWP could also be present in this LMWP fraction, no further purification was deemed necessary, simply because these LMWP molecules lacked the reactive PDP groups and thus would not interact with the above activated rGel. After activation of both rGel and LMWP, disulfide bonds were allowed to form between the thiol groups on rGel and the PDP group on LMWP, yielding the ultimate cG-L chemical conjugates.

After synthesis, the cG-L conjugate was purified using a heparin column. An initial major peak correlating to the elution of rGel was found to come out at 0.4 M NaCl, with a retention time of 5 min (data not shown). A second major peak representing the cG-L conjugate was eluted at above 1 M NaCl and a significantly extended retention time (~ 70 min), presumably due to presence of the heparin-binding LMWP moiety in the conjugate.

Successful synthesis and purification of cG-L was further confirmed by SDS-PAGE. As seen in Figure 3, whereas the unreacted rGel was visible as a single band at the position corresponding to the molecular weight of gelonin (~ 31 kDa; Lane 1), the cG-L conjugate produced multiple bands with molecular weights slightly higher than that of gelonin under non-reducing condition (Lane 2). Assessment from the molecular weight distribution of these bands suggested the presence of a heterogeneous mixture in the final

cG-L product containing 2 to 5 LMWP peptides per gelonin molecule. The disulfide linkage between LMWP and rGel in the cG-L conjugate was also confirmed by comparison of the gel results under reducing (Lane 2R) and non-reducing conditions (Lane 2NR). In the presence of reducing agent, DTT, the disulfide bond between rGel and LMWP was detached and, as a consequence, a single band corresponding to the size of gelonin (31 kDa) was again observed. The yield of the final cG-L product prepared by chemical synthesis was about 35% (3.5 mg cG-L from initially 10 mg rGel).

2.4.3 Expression and Purification of the Recombinant Gelonin-LMWP Chimera (rG-L)

Successful preparation of pET28a-Gel-LMWP and pET-Gel-LMWP (pET22b-TRX-Gel-LMWP) vectors containing the gelonin-LMWP gene was confirmed by DNA sequencing analysis. Test expression of rG-L using the pET28a-Gel-LMWP vector in a small culture displayed very low levels of rG-L, with no soluble protein being observed. In contrast, the pET-Gel-LMWP vector produced obvious expression of rG-L, with a significant portion being identified as soluble proteins (data not shown). The pET-Gel-LMWP vector was therefore selected for the subsequent large scale expression of rG-L.

The gelonin-LMWP fusion protein containing N-terminal thioredoxin-6x His tag (TRX-Gel-LMWP) was produced as soluble protein from *E.coli* in a 5 L culture, and was purified using a Ni-NTA column and eluted with imidazole (400 mM). As shown in the SDS-PAGE (Figure 4), the TRX-Gel-LMWP recombinant protein was clearly identified by the presence of an intense band at 44 kDa (Lane E). Following incubation with the TEV protease, the thioredoxin-6xHis tag was clearly removed, as displayed by the appearance of the 31-kDa band in Lane T of Figure 4.

The rG-L protein chimera was further purified using a heparin column, and the elution profile was presented in Figure 5A. As seen, three major peaks were observed. Anionic (Fraction 1) and slightly cationic (Fraction 2) endogenous bacterial proteins that bound nonspecifically to the Ni-NTA resins and came out with TRX-Gel-LMWP were eluted at 0 and 0.1 M NaCl, respectively. The rG-L product was eluted as a single peak (Fraction 3) at 0.9 M NaCl and with the longest retention time (47 min), presumably due to the presence of the heparin-binding LMWP moiety in the conjugate. Results from SDS-PAGE on these elution fractions were consistent with the above findings (Figure 5B). As shown, Fraction 1 and 2 in Figure 5A displayed multiple bands representing various sizes of bacterial endogenous proteins, while the Fraction 3 in Figure 5A yielded a single band with a MW of 31 kDa. According to densitometry analysis of the gel bands, the purity of rG-L was above 95%. The total yield of rG-L from a 5 L cell culture was about 1.5 mg.

2.4.4 Inhibition of Protein Translation by cG-L and rG-L

The potency of nGel (Enzo Life Sciences Inc), rGel, cG-L and rG-L on the inhibition of protein translation were examined in a cell-free translational system. In the absence of actual cells, all of the four gelonin samples displayed almost identical inhibition profiles of protein translation (Figure 6). The IC_{50} values calculated from these inhibition profiles were summarized in Table 1. Again, no statistically significant differences among the four gelonin samples were observed. It should be noted the IC_{50} value of rGel determined from our experiments was in good accordance to that reported by Hossann *et al*.[28] These results demonstrated that neither chemical conjugation nor

biological insertion of LMWP to gelonin would alter the N-glycosidase activity of gelonin on its inhibition of protein translation in a cell-free system.

2.4.5 Cellular Uptake of cG-L and rG-L

Cell-internalizing function of r-Gel, cG-L and rG-L was examined by uptake studies in CT26 cells utilizing rhodamine-labeled gelonin samples. Figure 7 depicted the fluorescence microscopy images taken after incubation of CT26 cells with the gelonin samples and Hoechst 33342 counter-stain solution. While only minimal fluorescence intensity was observed in rGel-treated cells (Figure 7A), strong fluorescence signals were clearly visible inside the cells that were treated either with cG-L or rG-L (Figure 7B and 7C, respectively). Moreover, the merged images in Figure 7B and 7C suggested an even distribution of cG-L and rG-L throughout the entire cell, rather than being confined in certain specific sub-cellular compartments such as endosomes.

2.4.6 Cell Culture Analyses of the Anti-Tumor Activity of cG-L and rG-L

To evaluate whether LMWP-mediated cell internalization would enhance the cytotoxic effects of gelonin, the rGel, cG-L and rG-L samples were tested against four different cancer cell lines (CT26, LS174T, 9L and PC-3). As seen in Figure 8, against the four cancer cell lines tested, rGel displayed cytotoxic effects only at concentrations above the micro-molar level. This toxicity may be attributed to the uptake of gelonin *via* fluid phase pinocytosis.[11, 30] In a sharp contrast, both cG-L and rG-L yielded significantly magnified cytotoxicity against all of the tested cancer cell lines. The IC_{50} values, estimated from the curves in Figure 8 and summarized in Table 2, were in full agreement with the above findings. As seen, the IC_{50} values of both cG-L and rG-L were about 20- to 120-fold lower than that of r-Gel against the four tested cancer cell lines. It is

interesting to note that there was basically no significant difference in cytotoxicity between cG-L and rG-L across all of the tested cancer cell lines.

2.4.7 *In Vivo* Evaluation of the Inhibition on Tumor Growth by rG-L

Preliminary animal studies using the CT26 s.c. xenograft tumor model were conducted to assess the *in vivo* cytotoxic effects of the rG-L protein chimera. To limit other pharmacokinetic factors, intra-tumor injection was selected for drug administration. As illustrated in Figure 9, mice treated with 20 μg rGel displayed a slight (14%) reduction in the measured tumor size at day 17, when comparing with the control of PBS-treated animals. As described earlier, this minor cytotoxic effect by the cell-impermeable rGel was probably attributed to gelonin's uptake *via* the fluid phase pinocytosis mechanism.[11, 30] In sharp contrast, animals treated with 2, 4 or 20 μg of rG-L, exhibited significant, dose-dependent inhibition on tumor growth, with the measured tumor size being reduced considerably by 58, 80 and 86%, respectively. These finding provided a "proof-of-concept" to our hypothesis that incorporation of the cell-penetrating LMWP would significantly augment the anti-tumor effects of gelonin.

2.5 Discussion

While macromolecular drugs have drawn significant recognition as the next generation of anticancer agents due to their unmatched reaction efficiency and the repetitive mode of action, their inability to cross the membrane barrier of tumor cells remains as a bottleneck challenge to potential clinical applications, as most of the machineries for tumor cytotoxicity are present in the cell cytosol. In this study, we made a rational hypothesis that modification of the macromolecular drug, such as the protein

toxin gelonin, with the non-toxic cell-penetrating peptide LMWP would enable the transduction of gelonin into tumor cells, thereby drastically augmenting its anti-tumor efficacy *in vivo*. To prove this concept, gelonin-LMWP conjugates were synthesized *via* both chemical conjugation and recombinant methods (the products were termed as cG-L and rG-L, respectively). Although both conjugation methods proved feasible, they both possessed several advantages and pitfalls. For chemical conjugation, one of the benefits was that LMWP and gelonin were linked with a disulfide bond that would be automatically cleaved once entering the cells, due to the presence of a reducing condition in the cytosol by the elevated concentrations of glutathione and reductase.[31] Detachment of LMWP from gelonin would allow the delivered gelonin to be entrapped in the cytosol, eliminating the possibility of trafficking into the nucleus, which was reported to be the destiny of many CPPs.[32-34] The other benefit was that, although remained unproven, many investigators were speculating that the CPP-mediated protein translocation was a reversible process, implicating the probability that the ferried protein cargos could be fluxed back from the cells. The use of a cytosol-cleavable disulfide bond would alleviate this concern.

The primary drawback from chemical conjugation was that the final cG-L product was a mixture of gelonin conjugates containing various numbers of LMWPs per gelonin molecule; as demonstrated by our SDS-PAGE results in Figure 3. Although many studies reported that a single CPP was sufficient to transduce a large protein into cells,[35, 36] it was nevertheless postulated that extra CPP chains on the protein cargo might increase the extent of cell transduction. Hence, the heterogeneous nature of the chemically synthesized cG-L conjugates would not only affect the batch-to-batch reproducibility of

the product, but also the uptake results of these conjugates. In addition, chemical synthesis practically was not really suitable for mass production of the conjugates, therefore hindering its potential for clinical applications.

On the contrary, the benefits and shortcomings of the recombinant approach were exactly the opposite to those of the chemical conjugation method. Recombinant engineering would allow synthesis of a homogeneous 1:1 gelonin-LMWP protein chimera, and also expression of rG-L from *E.coli* was one of the most efficient and economic means for recombinant production of heterologous proteins, thereby being suitable for mass-scale production; both were the pitfalls of the chemical method. However, recombinant engineering lacked the ability to create a protein chimera through the disulfide linkage, thereby being unable to enjoy the afore-mentioned benefits of the chemical method resulting from formation of the cytosol-cleavable –S-S- bond between gelonin and LMWP.

For chemical synthesis of the gelonin-LMWP conjugate, two criteria must be met concerning the selection of a cross-linking method: 1) preservation of gelonin activity after conjugation, and 2) external-exposure of LMWP on the conjugate thereby fully retaining it cell-penetrating activity. Herein we selected the Traut's reagent to achieve thiol-activation of the gelonin molecule because, when comparing with other conventional activating agents to produce a reactive –SH group, such as *N*-succinimidyl 3-(2-pyridyldithio)-propionate) (SPDP), N-succinimidyl iodoacetate, or 4-(iodoacetamido)-l-cyclohexenyl-1,2-dicarboxylic acid anhydride), etc., the Traut's reagent was reported to not impair gelonin's biological activity.[37, 38] In addition, the good aqueous solubility and slow hydrolysis rate (half-life: 1 hour in 50mM triethanolamine

buffer at pH 8) of the Traut's reagent rendered it a more favorable choice.[39] As shown from our results in Section 3.2., thiol groups were successfully introduced to gelonin using the Traut's reagent, as confirmed by the Ellman's assay.[40] Alternatively, to ensure an external exposure of LMWP, a short PEG chain containing heterobifunctional activated groups on both ends was employed as the cross-linker to produce the cG-L conjugate. Our results on the binding of cG-L to the heparin column (Section 3.2) indeed confirmed the exposure of LMWP on cG-L after chemical conjugation. Most importantly, SDS-PAGE findings in Figure 3 clearly demonstrated the formation of a disulfide linkage between gelonin and LMWP.

Regarding recombinant synthesis, LMWP gene was initially inserted to the C-terminus of the gelonin-encoding gene (pET-Gel vector) to produce the pET28a-Gel-LMWP vector. Despite that rGel was successfully expressed using this vector, there was almost no expression of the rG-L conjugate under tested conditions. This poor expression of rG-L was likely due to inefficient translation of the LMWP gene caused by codon usage bias, a finding previously reported by Lee and other investigators.[33, 41] Indeed, LMWP was known to consist of abundant arginine residues that was translated by the rarest codons in *E.coli*,[33] hence severely limiting its expression level. To this regard, the poor translation of LMWP appeared to significantly impair the overall expression of the ultimate rG-L chimera. On the other hand, the use of the BL21-CodonPlus *E.coli* strain, which contained extra copies of genes encoding the tRNAs for rare amino acids, also did not provide any enhancement on rG-L expression.

Aside from the low expression, the low solubility of rG-L also presented a concern. When eukaryotic proteins were expressed by prokaryotic *E.coli* cells, improper

folding of proteins often occurred, resulting in insoluble aggregates called inclusion bodies.[42, 43] This seemed to be the major hurdle that must be overcome in order to succeed in the production of rG-L, since the total expression level of rG-L was already very low. A strategy often used to improve the expression of so-called "difficult-to-produce" proteins was by inclusion and co-expression of a highly expressible fusion partner. Thioredoxin (TRX), for instance, was a small 12-kDa redox protein known for its extraordinary high level of expression (up to 40% of total cellular proteins) and high solubility could thus be conferred to fused proteins.[42] Based on this principle, we inserted the full length gelonin-LMWP gene into the pET-TRX vector to create the pET-Gel-LMWP vector (PET22b-TRX-Gel-LMWP) that also contained the TRX gene (Figure 2). Results from Figure 3 clearly demonstrated the plausibility of this strategy, as the thioredoxin-6xHis tag-gelonin-LMWP fusion protein (TRX-Gel-LMWP) was successfully over-expressed and produced in large quantities as a soluble protein in *E.coli.*

Maintenance of the functions of both cG-L and rG-L to inhibit protein translation was a major initial concern, since it was demonstrated in the literature that even a slight conformational change of the 3-D structure could result in a significant alteration on the biological activities of proteins.[44, 45] Notably, data obtained using a cell-free translational system confirmed that all of the rGel, cG-L and rG-L products possessed activities equivalent to that of the commercial native gelonin (nGel), displaying no significant difference in the measured IC_{50} values. Although the rGel results were somewhat expected, it was a little surprising to notice that there was virtually no loss in activity for both the cG-L and rG-L chimeras. Nevertheless, gelonin was known to be extremely

stable due to its specific structure,[46-48] which consequently could contribute to the retention of its activity even after modification with LMWP.

While the results showing retention of the biological activity of both cG-L and rG-L was truly encouraging, intracellular transport of gelonin was also required to enable it access to the ribosomes of cancer cells. With the incorporation of the cell-penetrating LMWP peptide, fluorescence microscopy data in Figure 7 clearly demonstrated that both cG-L and rG-L were able to internalize cells, while little, if any, of the impermeable rGel was found inside the cytosol of the test tumor cells. More importantly, the transduced cG-L and rG-L appeared to be evenly distributed within the cytosol, enabling them to maximize their cytotoxic effects. Comparison of the IC_{50} values of both cG-L (32 - 113.4 nM) and rG-L (55.4 - 95.4 nM) with that of rGel (1630 - 5870 nM) summarized in Table 1 yielded a solid support to our initial crucial hypothesis that modification of gelonin with LMWP would lead to a much improved anti-tumor activity. Also of significance was that this greatly enhanced cytotoxic activity of gelonin appeared to be indiscriminative to cancer types, as all of the four tested cancer cell lines yielded similar responses. This phenomenon may be accounted for in terms of the universal cell transduction mechanism of most CPPs, which, in principal and practice, suggests that all cell types including brain cells and erythrocytes are tranducible.[19, 23, 49] Also noteworthy was that both cG-L and rG-L yielded almost identical cytotoxic activities toward cancer cells. This was somewhat unexpected, considering the fact that the two major factors affecting tumor-killing capability of the LMWP-gelonin conjugates lied in the enzymatic activity and cell-penetrating ability. Although the intrinsic activities to inhibit protein translation were shown to be identical for cG-L and rG-L (Table 1), the cG-L conjugate actually

possessed a higher ratio of the CPP moieties (2-5 LMWP chains per gelonin molecule) comparing to that (1 LMWP chain per gelonin molecule) of rG-L. This result seemed to suggest that one well-exposed LMWP would be sufficient to effectively facilitate the cell entry of gelonin; consistent with findings reported by other investigators.[20, 23, 33]

Albeit that cG-L and rG-L exhibited equivalent IC_{50} values and equally promising *in vitro* cell culture cytotoxicity, rG-L was nevertheless selected for subsequent preliminary animal studies, simply because of its homogeneity, batch-to-batch manufacturing consistency, and, most critically, the possibility for mass production to satisfy the need of large quantities for animal investigation. In a CT26 xenograft tumor mice model, the rG-L product displayed a significantly enhanced tumoricidal activity of over controls administered with either PBS solution or non-modified gelonin (i.e. rGel). A dose-dependent reduction on tumor growth was observed for rG-L, with a total gelonin dose being as low as only 2 μg. On the contrary, non-modified rGel displayed virtually no effect on tumor growth, even at a total gelonin dose of 20 μg. Previously, Park *et al*. reported, by using the same animal tumor model, that intra-tumoral administration of gelonin at a dose as high as 100 μg did not yield visible reduction on tumor size.[20] Overall, both *in vitro* and *in vivo* findings provided strong evidence to support our hypothesis, i.e. modification of gelonin with the cell-penetrating LMWP would drastically enhance gelonin's clinical potential for cancer treatment.

2.6 Conclusions

Despite decades of efforts, a cure to the vast majority of cancers remains elusive. Highly potent and specific macromolecular drugs have shown promise to overcome the

limitations of traditional small molecule drugs. Effective intracellular delivery of these large drugs, however, continues to be the main hurdle to clinical realization of these drugs. Recent discovery of the cell-penetrating peptides offers hope to finally solve this intracellular delivery problem. In this study, we reported the "first" synthesis, *via* both chemical conjugation and genetic engineering methods, of gelonin modified with a potent yet non-toxic cell-penetrating peptide, LMWP. A novel coupling method based on the use of the Traut's reagent and a heterobifunctional PEG cross-linker was developed to synthesize the chemical gelonin-LMWP conjugate (cG-L), whereas an innovative strategy based on the incorporation co-expression of a highly expressible fusion partner, thioredoxin (TRX), was adopted to produce the recombinant gelonin-LMWP (rG-L) protein chimera containing the "difficult-to-produce" LMWP sequence with abundant arginine residues, the rarest codons in *E. coli*. *In vitro* cell culture studies revealed that cG-L and rG-L not only retained the protein translation-inhibiting activity and cell-penetrating capability, but also yielded 20- to 120-fold lower IC_{50} values than that of the unmodified recombinant gelonin (r-Gel). Preliminary *in vivo* studies using a xenograft tumor mouse model showed that while intra-tumor injection of the cell-impermeable r-Gel resulted in virtually no inhibition on tumor growth, both of the LMWP- modified gelonin conjugates exhibited significantly enhanced anti-tumor cytotoxic effects. Overall, our investigation shed light on the possibility to realize clinical application of the potent protein toxin drugs for cancer treatment.

2.7 Tables

Table 2-1. Summary of the IC_{50} values of nGel, rGel, cG-L and rG-L for inhibition of protein translation in cell-free translational system

Samples	IC_{50} [a]
nGel	15.0 ± 3.4 (-1.6)
rGel	14.4 ± 3.6 (-1.8)
cG-L	13.5 ± 4.9 (-1.7)
rG-L	12.9 ± 3.1 (-1.5)

[a]Concentration for half inhibition of luciferase translation (IC_{50}), calculated by applying nonlinear regression model using Prism software (GraphPad), are displayed as pM. The Hill slope is shown in the parenthesis behind the IC_{50}. For all experiments, N=3. (nGel: native gelonin, rGel: recombinant gelonin, cG-L: chemically modified gelonin-LMWP, rG-L: genetically modified gelonin-LMWP)

Table 2-2. Cytotoxicity levels (IC_{50}) of rGel, cG-L and rG-L in various cancer cell lines (CT 26, LS174T, 9L and PC-3)

Samples	CT 26 [a]	LS174T [a]	9L [a]	PC-3 [a]
RGel	1630 ± 500	5870 ± 1000	3100 ± 400	3400 ± 1000
cG-L	$37.3 \pm 15.7^{***}$	$123 \pm 27^{***}$	$106 \pm 23^{***}$	$57.8 \pm 23.4^{**}$
rG-L	$79.1 \pm 21.4^{***}$	$67.8 \pm 13.7^{***}$	$61.3 \pm 12.2^{***}$	$83.6 \pm 28.3^{**}$

[a]IC_{50} values are displayed as nM. $^{**}P < 0.001$, $^{***}P < 0.0001$. For all experiments, N=3. (rGel: recombinant gelonin, cG-L:chemically modified gelonin-LMWP, rG-L: genetically modified gelonin-LMWP)

2.8 Figures

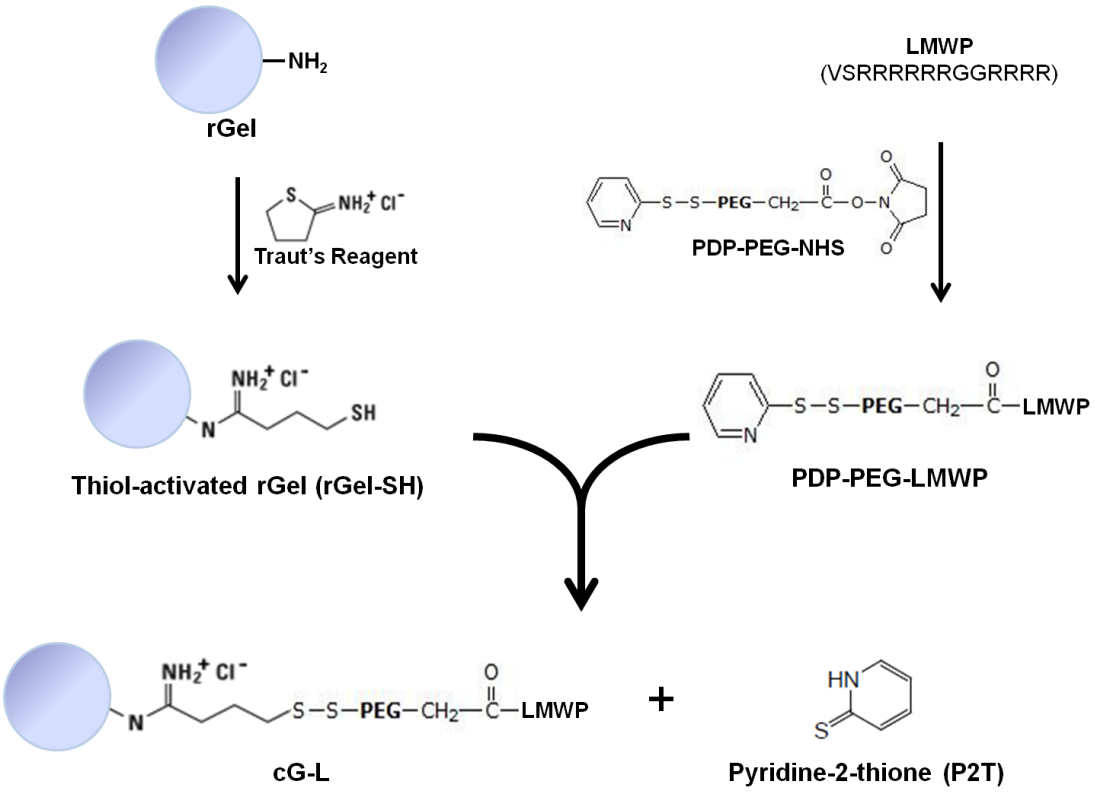

Figure 2-1. Scheme of gelonin-LMWP chemical conjugation *via* a disulfide bond using heterobifunctional PEG as the cross-linker. (rGel: recombinant gelonin, cG-L: chemically modified gelonin-LMWP).

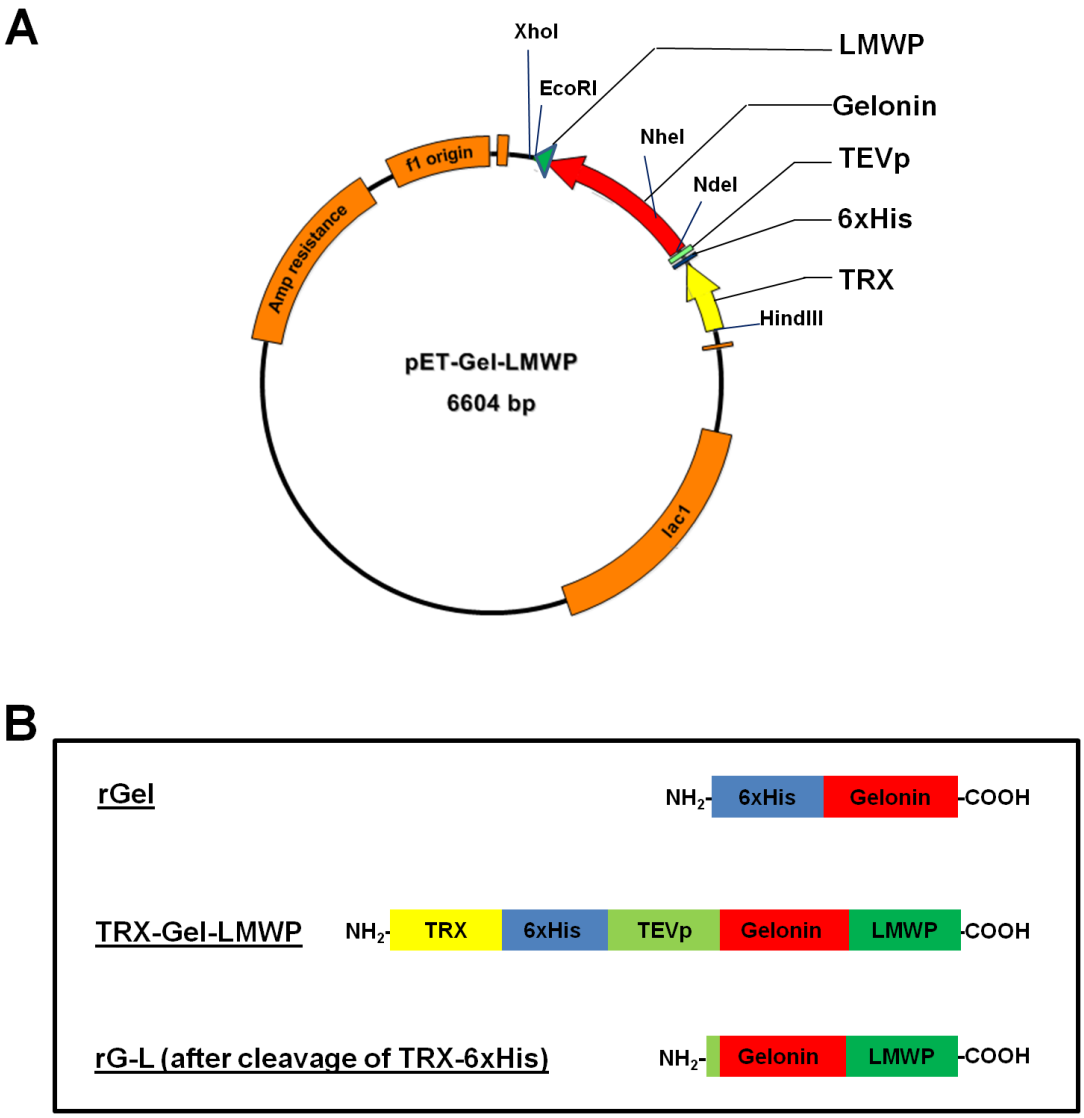

Figure 2-2. Schematic design of (A) pET-Gel-LMWP vector, and (B) image of rGel, TRX-Gel-LMWP and rG-L.

The pET-Gel-LMWP vector was constructed by inserting the full sequence of gelonin-LMWP gene into the pET-22b vector containing thioredoxin-6xHis tag and TEVp gene. (rGel: recombinant gelonin, TRX-Gel-LMWP: thioredoxin-6xHis tagged gelonin-LMWP, rG-L: genetically modified gelonin-LMWP, TEVp: TEV protease cleavable peptide).

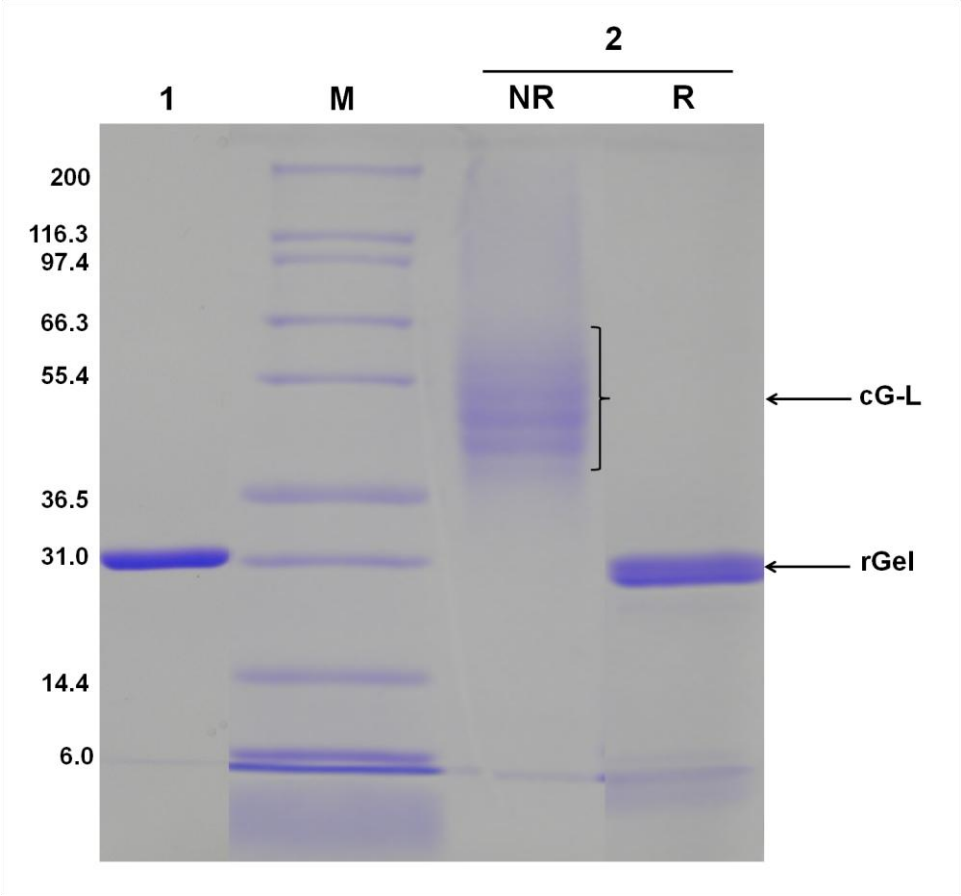

Figure 2-3. SDS-PAGE results of cG-L purified by a heparin column.

Lane 1: 1st elution peak fraction, Lane M: markers of the protein molecular weight standard (Invitrogen), Lane 2: 2nd elution peak fraction (NR: non-reducing condition, R: reducing condition). Recombinant gelonin migrated at its expected molecular weight of 31 kDa whereas cG-L migrated at higher molecular weight under non-reducing (NR) conditions; suggesting approximately 2 - 5 LMWP molecules were conjugated to each recombinant gelonin. Disulfide bond formation between recombinant gelonin and LMWP-PEG-PDP was confirmed by the size reduction of cG-L to gelonin size under reducing (R) conditions. (rGel: recombinant gelonin, cG-L: chemically modified gelonin-LMWP).

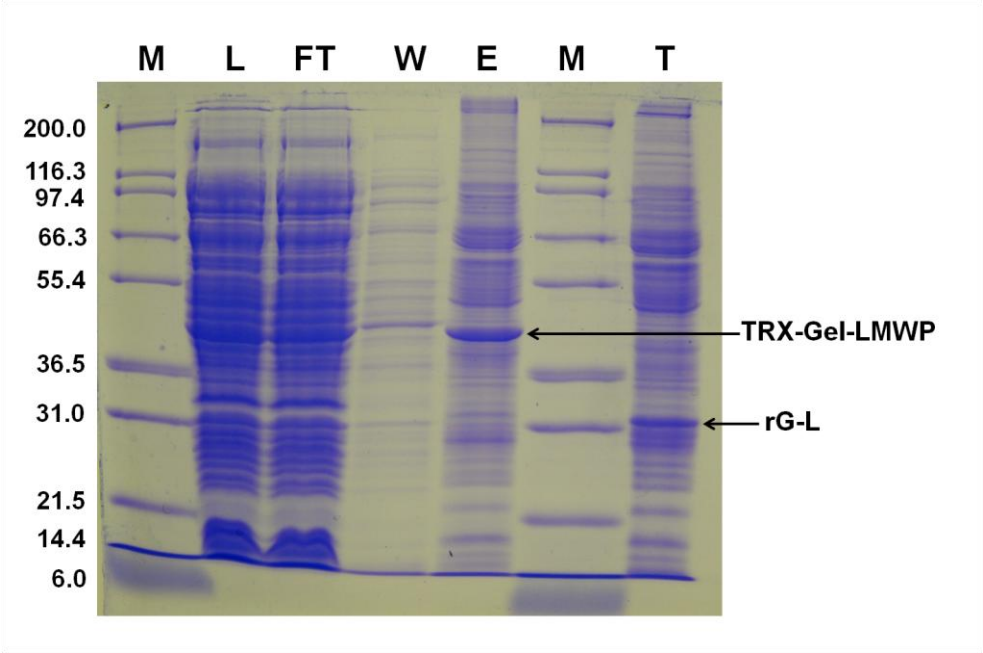

Figure 2-4. SDS-PAGE results of the Ni-NTA column purification of rG-L.

Lane M: markers of the protein molecular weight standard (Invitrogen), Lane L: supernatant fraction of the cell lysate. Lane FT: flow through fraction. Lane W: wash fraction. Lane E: elution fraction representing TRX-Gel-LMWP. Lane T: elution fraction after incubation with TEV protease. TRX-Gel-LMWP overexpression was confirmed from the intense band (MW: 44 kDa) in Lane E, and TEV protease cleavage of TRX was observed by appearance of the band (MW 31 kDa) in Lane T. (rG-L: genetically modified gelonin-LMWP, TRX-Gel-LMWP: thioredoxin-6xHis tagged gelonin-LMWP).

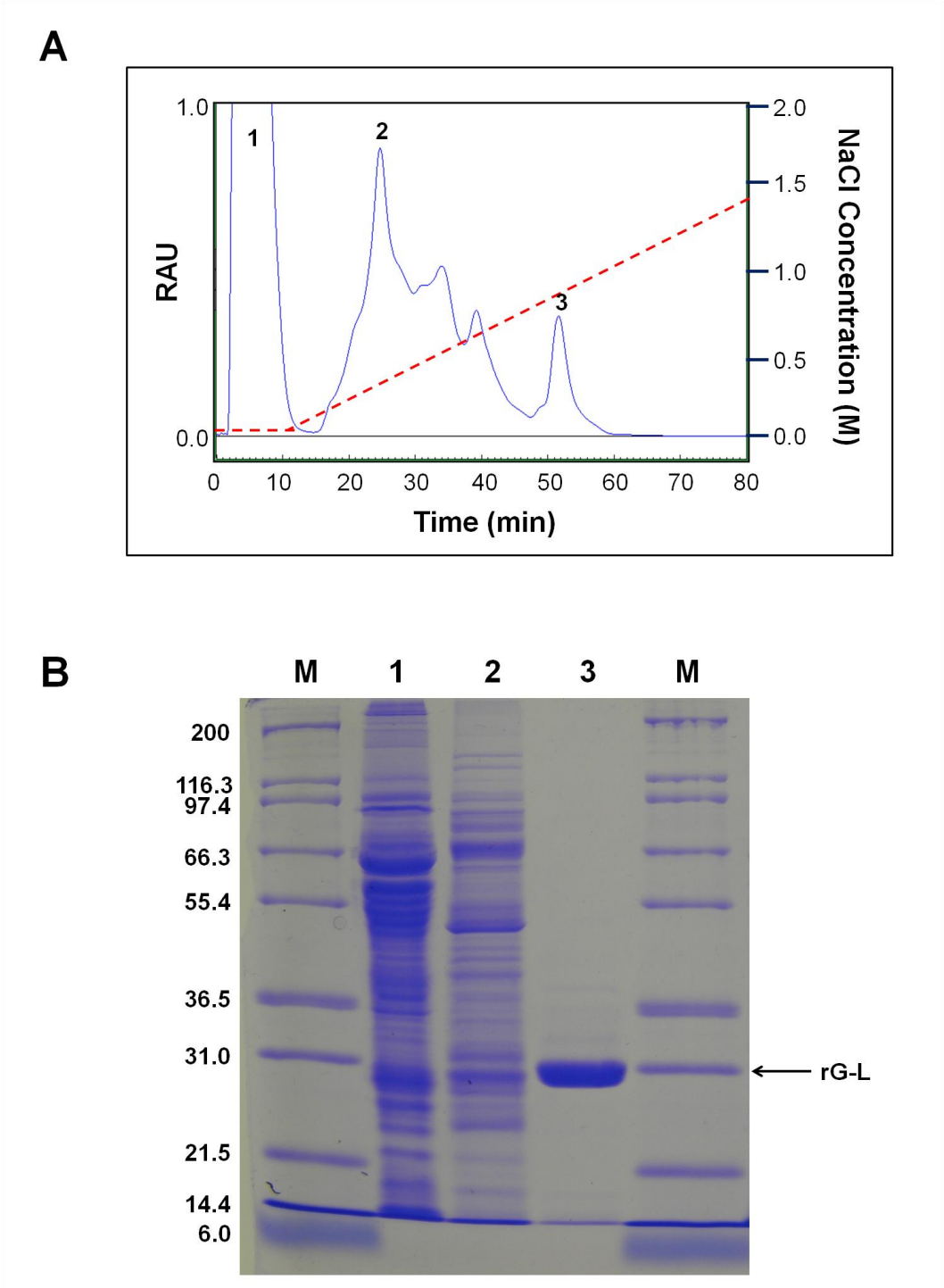

Figure 2-5. Purification of the recombinant gelonin-LMWP (rG-L) conjugate by a heparin column.

The cell monolayer without Eluent from the Ni-NTA column containing TRX-Gel-LMWP was incubated with TEV protease to cleave the thioredoxin-6xHis tag and then loaded onto a heparin column. (A). Elution profile from the heparin column using a NaCl

salt gradient from 0 to 1.4 M (red line). Three major fractions labeled as Peak 1 - 3 eluted at 0, 0.1 and 0.9 M NaCl (with retention time of 2, 15 and 47 min, respectively) were observed; (B) SDS-PAGE analysis of the fractions from the heparin column. Lane M: markers of the protein molecular weight standard (Invitrogen). Lane 1, 2, and 3 represented results from the three peak fractions (1, 2, and 3, respectively) in (A). Results showed that rG-L was eluted from the 3rd peak at 0.9 M NaCl.

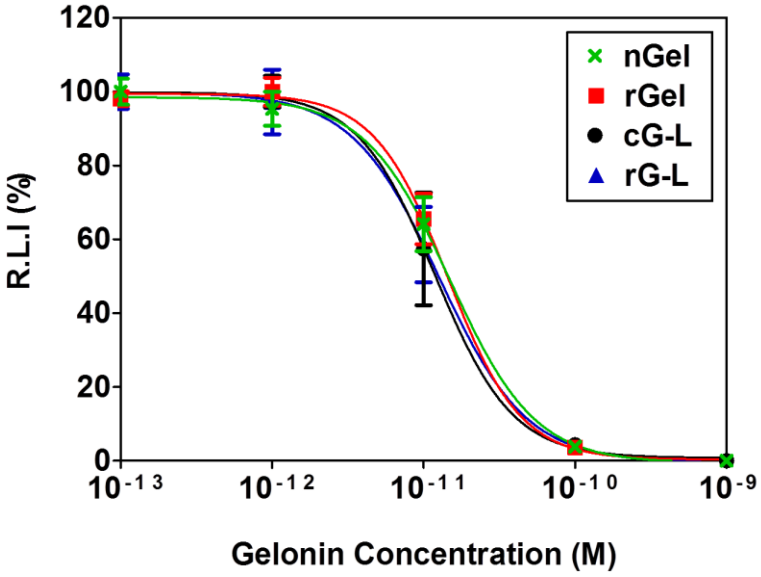

Figure 2-6. Inhibition of protein translation by native (commercial) Gel (nGel; circle), recombinant gelonin (rGel; square), chemical gelonin-LMWP (cG-L; cross) conjugate, or recombinant gelonin-LMWP (rG-L; triangle) conjugate using a cell-free translational system and luciferase as the marker.

The quantity of the translated luciferase was measured by the chemiluminescent assay (Promega) (N=3). The curves were fitted by applying the nonlinear regression model to the plots using Prism software (GraphPad).

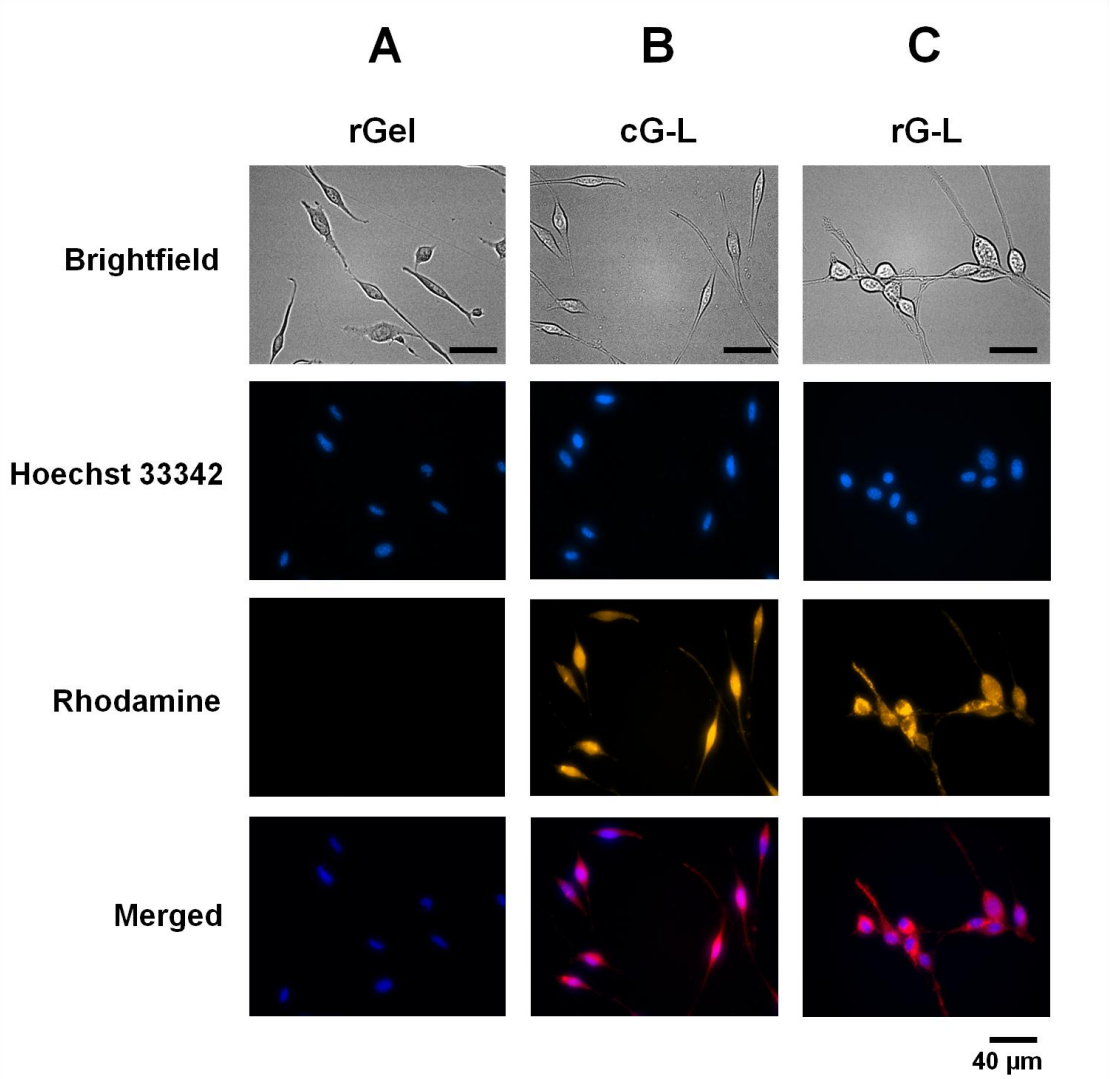

Figure 2-7. LMWP-mediated cellular uptake by tumor cells of: (A) recombinant gelonin (rGel), (B) chemical gelonin-LMWP (cG-L) conjugate, and (C) recombinant gelonin-LMWP (rG-L) conjugate.

CT26 cells were treated with rhodamine-labeled gelonin samples for 3 hrs at 37°C in 5% CO_2 humidified incubator. After stringent wash with 10 mg/mL heparin/PBS solution, nuclei were counter-stained with Hoechst 33342. Images of the cells were captured by different channels (brightfield (gray), Hoechst 33342 (blue) and rhodamine (gold)) by Nikon epifluorescence microscope. Merged images were obtained by overlapping images taken with Hoechst 33342 and rhodamine channels.

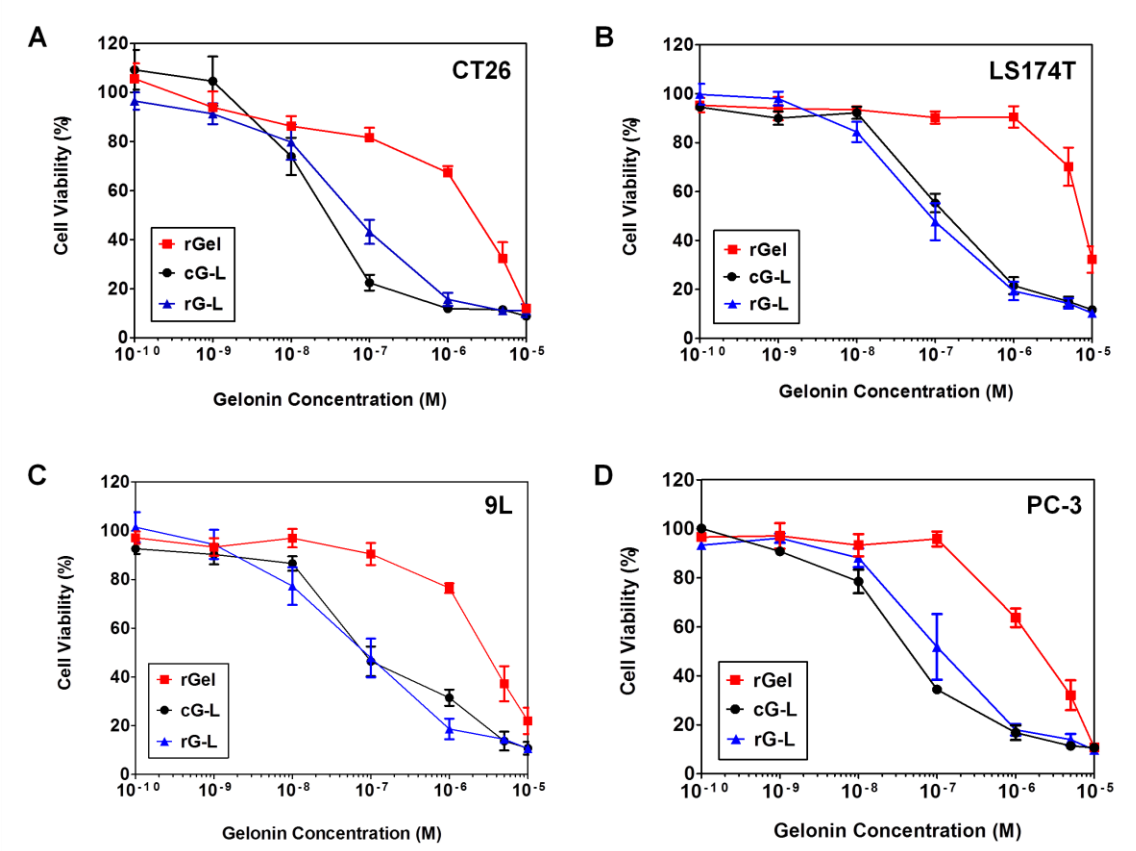

Figure 2-8. Cytotoxic effect of recombinant gelonin (rGel), chemical gelonin-LMWP (cG-L) conjugate, and recombinant gelonin-LMWP (rG-L) conjugate against (A) CT26, (B) LS174T, (C) 9L and (D) PC-3 cell lines.

Cells were plated onto 96 well plates (10^4 cells/well) and cytotoxicity was measured using the XTT assay (N=3). Both cG-L and rG-L displayed significantly higher cytotoxicity against all of the tested cancer cell lines than that of rGel, confirming the event of LMWP-mediated uptake in tumor cells.

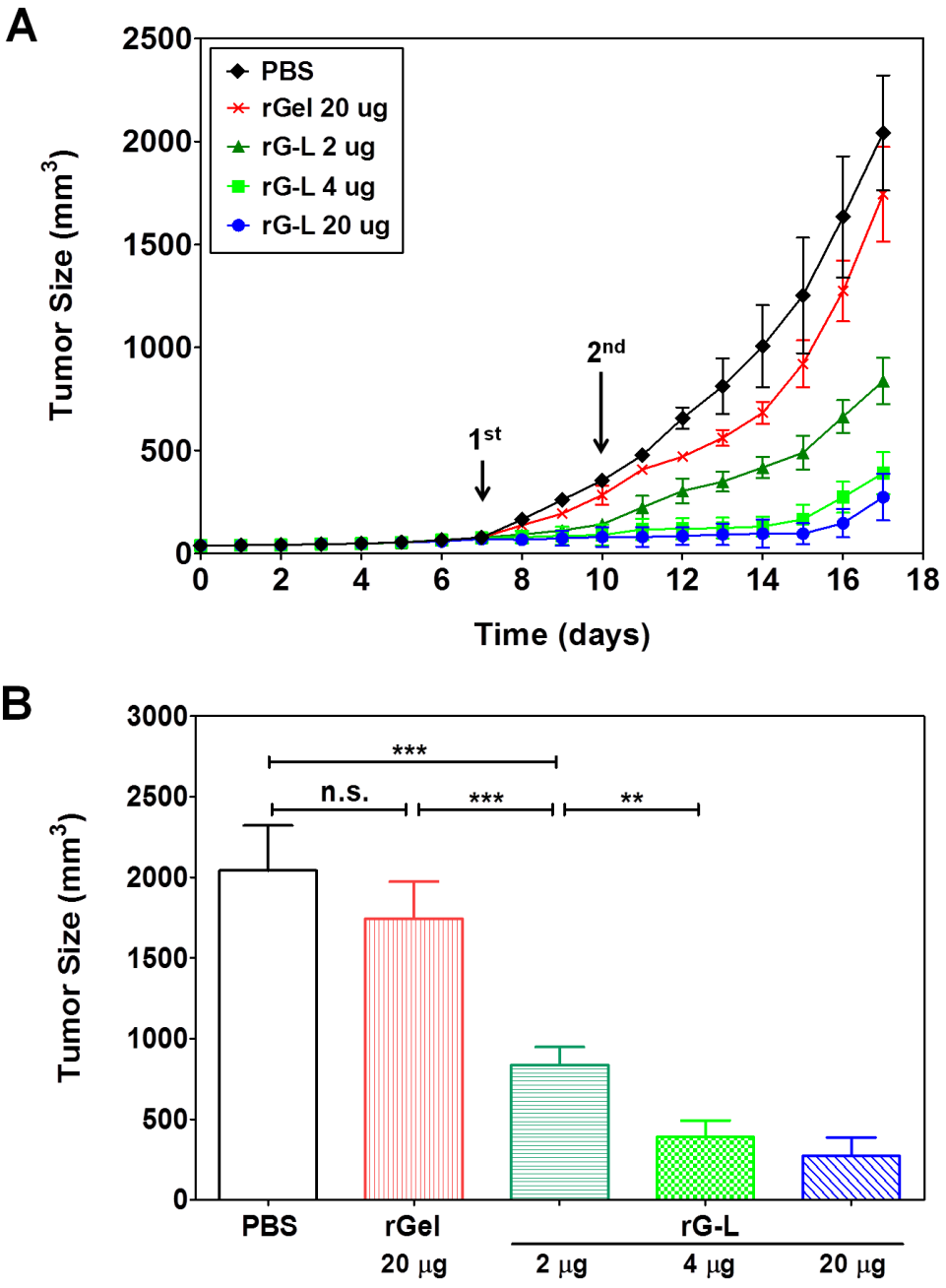

Figure 2-9. Inhibition of tumor growth by intra-tumor injection of PBS solution (control; diamond), recombinant gelonin (rGel; cross) and 2 μg (triangle), 4 μg (square), or 20 μg (circle) of recombinant gelonin-LMWP (rG-L) conjugate in a CT26 s.c. xenograft tumor mouse model (N=5).

Treatment was carried out at Day 7 and 10 after tumor implantation. Tumor size was measured daily using a vernier caliper right after tumor inoculation (Day 0). Tumor volume (mm^3) was calculated by using the following equation: $V = (a^2xb)/2$, where *a* represented the width and *b* represented the length of the tumor.

2.9 References

1. Blagosklonny MV. The power of chemotherapeutic engineering: arresting cell cycle and suppressing senescence to protect from mitotic inhibitors. Cell Cycle 2011;10:2295-8.
2. Kreitman RJ. Immunotoxins. Expert Opin Pharmacother 2000;1:1117-29.
3. Devi GR. siRNA-based approaches in cancer therapy. Cancer Gene Ther 2006;13:819-29.
4. Adams GP, Weiner LM. Monoclonal antibody therapy of cancer. Nat Biotechnol 2005;23:1147-57.
5. Foged C, Nielsen HM. Cell-penetrating peptides for drug delivery across membrane barriers. Expert Opin Drug Deliv 2008;5:105-17.
6. Snyder EL, Dowdy SF. Cell penetrating peptides in drug delivery. Pharm Res 2004;21:389-93.
7. Stirpe F. On the action of ribosome-inactivating proteins: are plant ribosomes species-specific? Biochem J 1982;202:279-80.
8. Puri M, Kaur I, Perugini MA, Gupta RC. Ribosome-inactivating proteins: current status and biomedical applications. Drug Discov Today 2012;17:774-83.
9. Stirpe F. Ribosome-inactivating proteins. Toxicon 2004;44:371-83.
10. Tumer NE, Li XP. Interaction of ricin and Shiga toxins with ribosomes. Curr Top Microbiol Immunol 2012;357:1-18.
11. Stirpe F, Olsnes S, Pihl A. Gelonin, a new inhibitor of protein synthesis, nontoxic to intact cells. Isolation, characterization, and preparation of cytotoxic complexes with concanavalin A. J Biol Chem 1980;255:6947-53.
12. Atkinson SF, Bettinger T, Seymour LW, Behr JP, Ward CM. Conjugation of folate via gelonin carbohydrate residues retains ribosomal-inactivating properties of the toxin and permits targeting to folate receptor positive cells. J Biol Chem 2001;276:27930-5.
13. Yamaizumi M, Mekada E, Uchida T, Okada Y. One molecule of diphtheria toxin fragment A introduced into a cell can kill the cell. Cell 1978;15:245-50.
14. Frankel AD, Pabo CO. Cellular uptake of the tat protein from human immunodeficiency virus. Cell 1988;55:1189-93.
15. Heitz F, Morris MC, Divita G. Twenty years of cell-penetrating peptides: from molecular mechanisms to therapeutics. Br J Pharmacol 2009;157:195-206.
16. Koren E, Torchilin VP. Cell-penetrating peptides: breaking through to the other side. Trends Mol Med 2012;18:385-93.
17. Magzoub M, Graslund A. Cell-penetrating peptides: [corrected] from inception to application. Q Rev Biophys 2004;37:147-95.
18. Derossi D, Calvet S, Trembleau A, Brunissen A, Chassaing G, Prochiantz A. Cell internalization of the third helix of the Antennapedia homeodomain is receptor-independent. J Biol Chem 1996;271:18188-93.
19. Kwon YM, Li YT, Liang JF, Park YJ, Chang LC, Yang VC. PTD-modified ATTEMPTS system for enhanced asparaginase therapy: a proof-of-concept investigation. J Control Release 2008;130:252-8.

20. Park YJ, Chang LC, Liang JF, Moon C, Chung CP, Yang VC. Nontoxic membrane translocation peptide from protamine, low molecular weight protamine (LMWP), for enhanced intracellular protein delivery: in vitro and in vivo study. FASEB J 2005;19:1555-7.
21. Choi JK, Jang JH, Jang WH, Kim J, Bae IH, Bae J, Park YH, Kim BJ, Lim KM, Park JW. The effect of epidermal growth factor (EGF) conjugated with low-molecular-weight protamine (LMWP) on wound healing of the skin. Biomaterials 2012;33:8579-90.
22. Xia H, Gao X, Gu G, Liu Z, Zeng N, Hu Q, Song Q, Yao L, Pang Z, Jiang X, Chen J, Chen H. Low molecular weight protamine-functionalized nanoparticles for drug delivery to the brain after intranasal administration. Biomaterials 2011;32:9888-98.
23. Kwon YM, Chung HS, Moon C, Yockman J, Park YJ, Gitlin SD, David AE, Yang VC. L-Asparaginase encapsulated intact erythrocytes for treatment of acute lymphoblastic leukemia (ALL). J Control Release 2009;139:182-9.
24. Park YS, Huang Y, Park YJ, David AE, White L, He H, Chung HS, Yang VC. Specific down regulation of 3T3-L1 adipocyte differentiation by cell-permeable antisense HIF1alpha-oligonucleotide. J Control Release 2010;144:82-90.
25. Chang LC, Lee HF, Yang Z, Yang VC. Low molecular weight protamine (LMWP) as nontoxic heparin/low molecular weight heparin antidote (I): preparation and characterization. AAPS PharmSci 2001;3:E17.
26. Chang LC, Liang JF, Lee HF, Lee LM, Yang VC. Low molecular weight protamine (LMWP) as nontoxic heparin/low molecular weight heparin antidote (II): in vitro evaluation of efficacy and toxicity. AAPS PharmSci 2001;3:E18.
27. Lee LM, Chang LC, Wrobleski S, Wakefield TW, Yang VC. Low molecular weight protamine as nontoxic heparin/low molecular weight heparin antidote (III): preliminary in vivo evaluation of efficacy and toxicity using a canine model. AAPS PharmSci 2001;3:E19.
28. Hossann M, Li Z, Shi Y, Kreilinger U, Buttner J, Vogel PD, Yuan J, Wise JG, Trommer WE. Novel immunotoxin: a fusion protein consisting of gelonin and an acetylcholine receptor fragment as a potential immunotherapeutic agent for the treatment of Myasthenia gravis. Protein Expr Purif 2006;46:73-84.
29. Urva SR, Yang VC, Balthasar JP. Physiologically based pharmacokinetic model for T84.66: a monoclonal anti-CEA antibody. J Pharm Sci 2010;99:1582-600.
30. Madan S, Ghosh PC. Interaction of gelonin with macrophages: effect of lysosomotropic amines. Exp Cell Res 1992;198:52-8.
31. Saito G, Swanson JA, Lee KD. Drug delivery strategy utilizing conjugation via reversible disulfide linkages: role and site of cellular reducing activities. Adv Drug Deliv Rev 2003;55:199-215.
32. Joliot A, Prochiantz A. Transduction peptides: from technology to physiology. Nat Cell Biol 2004;6:189-96.
33. Lee TY, Park YS, Garcia GA, Sunahara RK, Woods JH, Yang VC. Cell permeable cocaine esterases constructed by chemical conjugation and genetic recombination. Mol Pharm 2012;9:1361-73.

34. Vives E, Brodin P, Lebleu B. A truncated HIV-1 Tat protein basic domain rapidly translocates through the plasma membrane and accumulates in the cell nucleus. J Biol Chem 1997;272:16010-7.
35. van den Berg A, Dowdy SF. Protein transduction domain delivery of therapeutic macromolecules. Curr Opin Biotechnol 2011;22:888-93.
36. Mae M, Langel U. Cell-penetrating peptides as vectors for peptide, protein and oligonucleotide delivery. Curr Opin Pharmacol 2006;6:509-14.
37. Lambert JM, Senter PD, Yau-Young A, Blattler WA, Goldmacher VS. Purified immunotoxins that are reactive with human lymphoid cells. Monoclonal antibodies conjugated to the ribosome-inactivating proteins gelonin and the pokeweed antiviral proteins. J Biol Chem 1985;260:12035-41.
38. McIntyre GD, Scott CF, Jr., Ritz J, Blattler WA, Lambert JM. Preparation and characterization of interleukin-2-gelonin conjugates made using different cross-linking reagents. Bioconjug Chem 1994;5:88-97.
39. Traut RR, Bollen A, Sun TT, Hershey JW, Sundberg J, Pierce LR. Methyl 4-mercaptobutyrimidate as a cleavable cross-linking reagent and its application to the Escherichia coli 30S ribosome. Biochemistry 1973;12:3266-73.
40. Ellman GL. Tissue sulfhydryl groups. Arch Biochem Biophys 1959;82:70-7.
41. Kane JF. Effects of rare codon clusters on high-level expression of heterologous proteins in Escherichia coli. Curr Opin Biotechnol 1995;6:494-500.
42. LaVallie ER, DiBlasio-Smith EA, Collins-Racie LA, Lu Z, McCoy JM. Thioredoxin and related proteins as multifunctional fusion tags for soluble expression in E. coli. Methods Mol Biol 2003;205:119-40.
43. Singh SM, Panda AK. Solubilization and refolding of bacterial inclusion body proteins. J Biosci Bioeng 2005;99:303-10.
44. Ebert RF, Spryn LA. Immunotoxin construction with a ribosome-inactivating protein from barley. Bioconjug Chem 1990;1:331-6.
45. Battelli MG, Barbieri L, Stirpe F. Toxicity of, and histological lesions caused by, ribosome-inactivating proteins, their IgG-conjugates, and their homopolymers. APMIS 1990;98:585-93.
46. Hosur MV, Nair B, Satyamurthy P, Misquith S, Surolia A, Kannan KK. X-ray structure of gelonin at 1.8 A resolution. J Mol Biol 1995;250:368-80.
47. Mujoo K, Cheung L, Murray JL, Rosenblum MG. Pharmacokinetics, tissue distribution, and in vivo antitumor effects of the antimelanoma immunotoxin ZME-gelonin. Cancer Immunol Immunother 1995;40:339-45.
48. Li Z, Qu Y, Li H, Yuan J. Truncations of gelonin lead to a reduction in its cytotoxicity. Toxicology 2007;231:129-36.
49. Goncalves E, Kitas E, Seelig J. Binding of oligoarginine to membrane lipids and heparan sulfate: structural and thermodynamic characterization of a cell-penetrating peptide. Biochemistry 2005;44:2692-702.

Chapter 3

Heparin/Protamine-Mediated Regulation on Cell Transduction of CPP-Modified Gelonin

3.1 Abstract

Therapeutically relevant macromolecules, such as gelonin toxin, are highly desirable anti-cancer drugs due to their unparalleled reaction efficiency and substrate specificity. Nevertheless, there are two key hurdles to be overcome for their successful use in cancer therapy. The first is the membrane barrier that only allows the permeation of small molecules into cells. The other is the lack of tumor-selective drug actions, which leads to toxic side effects. The recent discovery of cell-penetrating peptides (CPP) that possess potent transmembrane activity provides an effective strategy to solve the first problem, but it aggravates the second problem of unwanted toxicity due to the increased yet nonspecific cell penetration ability. Herein we developed a CPP-modified ATTEMPTS system to solve both problems. First, TAT-gelonin fusion protein (TAT-Gel) was engineered *via* genetic recombination method and its anti-cancer activity was characterized *in vitro*. This TAT-Gel exhibited significantly greater cytotoxic effects with average half maximal inhibitory concentration (IC_{50}) of 22.6 nM, showing 2 to 3 orders of magnitude lower than rGel (avg. IC_{50}: 4633 nM). Next, the TAT-Gel was incorporated

into the modified ATTEMPTS, a heparin/protamine based-DDS, for tumor-selective delivery. TAT-mediated translocation was curbed due to the heparin-TAT interaction, and restored by addition of protamine. Our *in vitro* findings validate the applicability of heparin/protamine-based regulation of cell internalization of TAT-Gel. Moreover, the feasibility of this strategy is demonstrated using an LS174T xenograft tumor mouse model.

3.2 Introduction

CPP-mediated intracellular delivery has emerged as a prominent strategy for protein drugs in the recent decade. As a case in point, TAT, through cellular and animal studies, has been well demonstrated of its ability to translocate various cargos (e.g., peptides, proteins, genes or nanoparticles) into different types of cells in our lab as well as other groups.[1, 2] To this regard, the TAT is considered a highly desirable carrier for gelonin delivery into tumor cells. However, the other side of the coin is the non-selectivity of TAT-mediated cell penetration, causing unwanted drug exposure to normal tissues and cells. The worse is that the TAT-mediated penetration appears to be too violent to be site-specifically directed, as evidenced by the findings that an antibody with conjugation of TAT lost its targeting ability but follow the non-selective penetration pattern of the TAT.[3] Therefore, to achieve tumor cell-specific penetration for protein delivery is still a formidable challenge.[4]

To address the paradox of potent yet nonselective penetration feature of CPP and its related potential toxicity, the CPP-modified ATTEMPTS (Antibody Targeted Triggered Electrically Modified Prodrug-Type Strategy), a heparin/protamine-based drug

delivery system (DDS), has been recently developed by our laboratory.[5, 6] Herein, we engineered TAT-Gel *via* genetic recombination method and evaluated its potentials for use as an anti-cancer drug. The applicability of the CPP-modified ATTEMPTS for TAT-Gel delivery was then investigated both *in vitro* and *in vivo* utilizing heparin and protamine.

3.3 Materials and Methods

3.3.1 Materials

The pET28a-Gel plasmid vector for the expression of rGel was a generous gift from Dr. Wolfgang E. Trommer (University of Kaiserslautern, Germany).[7] Kanamycin, carbenicillin and isopropyl-β-thiogalactopyranoside (IPTG) were purchased from Fisher Scientific (Pittsburg, PA). Heparin sulfate, protamine sulfate, rhodamine B isothiocyanate and fluorescein isothiocyanate (FITC) were purchased from Sigma-Aldrich (St. Louis, MO). Competent *Escherichia coli (E.coli)* strains (TOP10 and BL21star (DE3)), pEXP-5-NT/TOPO TA expression kit, AcTEV™ protease, PBS (pH 7.4), Dulbecco's Modified Eagle Medium (DMEM), fetal bovine serum albumin (FBS) and Hoechst 33342 were purchased from Invitrogen (Carlsbad, CA). BCA protein assay kit was purchased from Bio-Rad Laboratories (Hercules, CA). DNA primers were purchased from Integrated DNA Technologies Inc. (Coralville, IA). DNA restriction enzymes (BamHI and XhoI) and T4 DNA ligase were purchased from New England Biolabs (Ipswich, MA). Rabbit reticulocyte lysate assay system, Luciferase assay system and recombinant RNasin® ribonuclease inhibitor were purchased from Promega Corporation (Madison, WI). Cell proliferation kit II (XTT) was purchased from Roche Applied Science (Indianapolis, IN).

3.3.2 Construction of the TAT-Gel Genes

For the expression of TAT-Gel with an N-terminal thioredoxin-6xHis tag (TRX-TAT-Gel), the pET-TAT-Gel vector (pET21a-TRX-TAT-Gel) was prepared in two steps. In the first step, the double-stranded DNA encompassing the full length of the TAT-Gel encoding gene was constructed by PCR using the pET-Gel vector as a template. The primers used for the PCR (TG-forward and TG-backward) are shown in Table 1. The PCR product was purified by 1% agarose gel electrophoresis and inserted into the pEXP-5-NT/TOPO TA vector following the vendor's protocol (Invitrogen, Carlsbad, CA). The TOPO-TA vector containing the TAT-Gel gene was then transformed into TOP10 *E.coli* cells, and the prepared vector was submitted for DNA sequencing analysis. Next, the pET-TAT-Gel vector was prepared by insertion of the TAT-Gel gene into the pET21a-TRX vector (ProMab Biotechnologies, Inc., Richmond, CA) containing the thioredoxin (TRX) gene. Prior to TAT-Gel gene insertion, genes encoding the TEV protease cleavable peptide (TEVp), 6xHis and the BamHI restriction enzyme site were engineered at the N-terminal of the TAT-Gel gene. Also, the XhoI restriction enzyme site was generated at the C-terminal *via* PCR reactions. The PCR primers (pTG-forward-1 ~ 3 and pTG-backward) are summarized in Table 1. The final PCR product for TAT-Gel was double digested by restriction enzymes (BamHI and XhoI) and then inserted into the pET21a-TRX vector. The prepared pET-TAT-Gel vector was submitted for DNA sequencing analysis. The schematic design of the pET-TAT-Gel plasmid vector and the schematic images of TRX-TAT-Gel, TAT-Gel and rGel are depicted in Figure 1.

3.3.3 Expression and Purification of TAT-Gel

For the expression of TRX-TAT-Gel, pET-TAT-Gel vector was transformed into an *E.coli* strain. A single colony was picked from the pET-TAT-Gel vector transformed BL21 (DE3), grown on an LB agar plate containing 50 µg/mL carbenicillin, and inoculated into 200 mL LB medium (50 µg/mL carbenicillin). The starter culture was incubated overnight at 37°C with shaking at 250 rpm and then diluted into 5 L fresh LB medium. The large culture (5 L) was incubated under the same conditions and, when the optical density at 600 nm reached 1, TRX-TAT-Gel expression was induced by the addition of IPTG to a final concentration of 0.5 mM. The large culture was further incubated for an additional 6 hr.

After expression of the TRX-TAT-Gel, the *E.coli* cells were harvested by centrifugation at 4000 rpm for 20 min, then, re-dispersed in 30 mL of 20 mM PBS (300 mM NaCl, pH 7). The cells were lysed by sonication (4 × 30 seconds with 50% output in ice) and the supernatant fraction containing the soluble TRX-TAT-Gel collected by centrifugation (15,000 rpm for 30 min) was incubated with 2 mL of Ni-NTA resin suspension (HisPure® Ni-NTA resin, Bio-Rad Laboratories, Hercules, CA). After incubation for 2 hrs at 4ºC, the resins were washed with 200 mL of 20 mM PBS (300 mM NaCl, pH 7), and then, TRX-TAT-Gel was eluted with PBS containing imidazole (20 mM PBS, 300 mM NaCl, 400 mM imidazole, pH 7).

To acquire TAT-Gel, the eluent containing TRX-TAT-Gel was incubated with TEV protease to remove the thioredoxin-6xHis tag following the vendor's protocol (AcTEV™ protease, Invitrogen, Carlsbad, CA). Briefly, 150 µL of 20 × TEV protease reaction buffer, 30 µL 0.1 M DTT and 300 units of AcTEV™ protease were added to 3

mL of TRX-TAT-Gel solution and incubated overnight (18 hr) at 4°C. The final TAT-Gel product was obtained after heparin column purification (HiTrap Heparin HP, GE Healthcare Bio-Sciences, Pittsburgh, PA) with a salt gradient elution (0 to 1.4 M NaCl at a rate of 0.02 M/min, flow rate: 1 mL/min). The expression and purification of TAT-Gel was monitored by SDS-PAGE in 10% Tris-HCl gel, and the purity was measured *via* densitometry analysis of the observed bands using ImageJ software (National Institutes of Health, Bethesda, MD). The protein concentration was determined based on BCA protein assay using native gelonin as the standard.

3.3.4 Determination of TAT-Gel's N-glycosidase Activity

The N-glycosidase activity of TAT-Gel was assessed in a cell-free translational system using rabbit reticulocyte lysate assay system (Promega Corp., Madison, WI) with modification of the protocol. Briefly, 5 µL of TAT-Gel or recombinant gelonin (rGel) (at final concentration of 1 pM, 10 pM, 100 pM, 1 nM, 10 nM or 100 nM) was mixed with 35 µL of rabbit reticulocyte lysate, 1.4 µL of potassium chloride, 1 µL of amino acid without methionine, 1 µL of amino acid without leucine, 1 µL of luciferase control mRNA, 1 µL of RNasin® ribonuclease inhibitor and 4.6 µL of Mili-Q water (total reaction volume: 50 µL). After incubation for 90 min at 30°C, luciferase translation from each reaction was quantified by measuring the luciferase activity with the luciferase assay system following the vendor's protocol (Promega Corp., Madison WI). The IC_{50} of TAT-Gel to inhibit luciferase translation was calculated by nonlinear regression using Prism software (Prism version 5.0, Graphpad, CA).

3.3.5 Cell Culture

LS174T and HT116 human adenocarcinoma cells and Madin-Darby Canine Kidney (MDCK) cells were purchased from American Type Culture Collection (ATCC, Manassas, VA). The cells were cultured in 75 cm^2 flasks and maintained in a humidified CO_2 incubator (5% CO_2/95% air) at 37°C. The cells were cultured in Dulbecco's Modified Eagle Medium (DMEM) with 2 mM L-glutamine, high glucose, 1% (v/v) penicillin-streptomycin, and 10% FBS. During the cultures, the culture media in the flasks was replaced with fresh media every two days, and the cells were subcultured when the confluency reached 90% by detaching with 0.25% trypsin-EDTA at a 1:3 split ratio.

3.3.6 Evaluation of TAT-Gel Cell Internalization

TAT-mediated cell internalization was evaluated in a cell entry study using confocal microscopy. For detection, rGel and TAT-Gel (2 mg/mL in 0.1 M bicarbonate buffer, pH 9.0) were both labeled with a fluorescence dye by incubation with 5-fold molar excess of rhodamine B isothiocyanate for 3 hr at room temperature. The unreacted rhodamine was removed by loading the reaction solutions into a dye removal resin following the vendor's protocol (Bio-Rad, Hercules, CA). Successful rhodamine labeling was determined by measuring the optical density at 280 nm and 520 nm for protein and the dye, respectively.

LS174T cells were seeded onto an 8-well chambered coverglass (Nunc® Lab-Tek II Chambered Coverglass, Thermo Scientific, Rockford, IL) at a density of 10^5 cells/well and incubated for 24 hr in complete medium. When the cells were attached to the bottom of the plates, rhodamine-labeled rGel and TAT-Gel were separately added to the cells and

incubated for 3 hr at 37°C in the humidified CO_2 incubator. The cells were then washed with a 10 mg/mL heparin/PBS solution once and with PBS three times. Images of the live cells were taken with a Nikon A1R-A1 confocal laser microscope with a 60 × objective (Nikon Instruments Inc., Melville, NY). The cell images were acquired and analyzed using NIS-Elements Microscope Imaging software (Nikon Instruments Inc., Melville, NY).

3.3.7 Assessment of TAT-Gel Anti-Tumor Activity

The anti-tumor activity of TAT-Gel was determined in various cell lines (e.g., LS174T and HCT116 human adenocarcinoma cells and non-cancerous MDCK cells) using an XTT assay. Briefly, the cells were dispensed into 96-well plates at a density of $5x10^3$ cells per well, and when the cells were attached on the bottom of the plates, rGel and TAT-Gel were separately added to the wells at different final concentrations (100 pM, 1 nM, 10 nM, 100 nM, 1 μM or 10 μM) (N=3). The cells were incubated with rGel or TAT-Gel for 72 hrs, and the relative cell proliferation was measured using an XTT assay following the vendor's protocol (Roche Applied Science, Indianapolis IN). The IC_{50} values were calculated by nonlinear regression using Prism software (Prism version 5.0, Graphpad, CA).

3.3.8 Evaluation of *In Vitro* Plasma Stability of TAT-Gel Binding to Heparin and Protamine-induced Release of the TAT-Gel

TAT-Gel was labeled with a fluorescence dye by mixing the TAT-Gel (2 mg/mL in 0.1 M bicarbonate buffer, pH 9.0) with 5-fold molar excess of fluorescein isothiocyanate (FITC) and incubation for 4 hrs at room temperature. The unreacted FITC

was removed by loading the reaction solution into a dye removal resin (Bio-Rad, Hercules CA).

The FITC-labeled TAT-Gel (200 µg/mL in PBS) was loaded in 50 µg aliquots onto heparin bead slurries (Heparin HyperD® M, Pall Corporation, Port Washington, NY; 50% (v/v) in PBS) pre-dispensed into separate eppendorf tubes (100 µL slurry per tube). After incubation for 1 hr at room temperature, the unbound TAT-Gel was removed by centrifugation at 10,000 rpm for 5 min. The FITC-labeled TAT-Gel loaded beads were re-dispersed in 250 µL of rat plasma and incubated up to 24 hr at 37°C. At intended time points (0, 1 hr, 4 hr, 6 hr, 12 hr and 24 hr), the beads (3 tubes per time point) were washed with PBS 3 times, and the FITC-labeled TAT-Gel remaining on the bead surface was eluted with 2 M NaCl solution. To test the protamine-triggered release, 100 µL of protamine solution (10 mg/mL) was added to eppendorf tubes where FITC-labeled TAT-Gel bound heparin beads were prepared in the presence of rat plasma. After incubation for 30 min, the beads were washed with PBS 3 times, and the remaining FITC-labeled-TAT-Gel was eluted with 2 M NaCl solution. For the control, FITC-labeled TAT-Gel was incubated with beads and, after wash with PBS, eluted with 2 M NaCl solution without incubation in rat plasma. The fluorescence intensity of each eluent was measured using a plate reader (excitation/emission wave length: 485 nm/530 nm, BioTEK® Synergy™ BioTEK, co., Winooski, VT). The portion of TAT-Gel binding to the heparin beads (%) was calculated by dividing the fluorescence intensities of the eluent of the test groups (N=3 per each time point and the protamine tested group) by the average fluorescence intensity of the eluent of the control group (N=3).

3.3.9 *In Vitro* Characterization of Heparin/Protamine-Mediated Regulation on TAT-Gel Cell Transduction

The heparin/protamine-mediated regulation on TAT-Gel cell transduction was evaluated by confocal microscopic imaging and cytotoxicity studies. For the imaging study, TAT-Gel (2 mg/mL in 0.1 M bicarbonate buffer, pH 9.0) was labeled with rhodamine dye using the same protocol described at Methods section 3.3.6.

Twenty four hrs prior to the study, LS174T cells were seeded onto an 8-well chambered coverglass (Nunc® Lab-Tek II Chambered Coverglass, Thermo Scientific, Rockford, IL) at a density of 10^5 cells/well and incubated in complete medium. When the cells were attached to the bottom, rhodamine-labeled TAT-Gel was added to the cells and incubated for 3 hr at 37°C in the humidified CO_2 incubator. The TAT-Gel/Hep (complex of TAT-Gel and heparin) was prepared by incubating TAT-Gel with a 3-fold molar excess of heparin for 30 min. To evaluate the protamine-induced reversal of the heparin block, a 3-fold molar excess of protamine sulfate to heparin was immediately added to the cells pre-treated with the TAT-Gel/Hep complex. After incubation with the different TAT-Gel samples, the cells were washed with a 10 mg/mL heparin/PBS solution, and the nuclei were counterstained with Hoechst 33342 (1:1000 dilution of 10 mg/mL stock solution). The cells were then washed with PBS three more times. Images of the live cells were taken with a Nikon A1R-A1 confocal laser microscope with a 20 × objective (Nikon Instruments Inc., Melville, NY). The cell images were acquired and analyzed using NIS-Elements Microscope Imaging software (Nikon Instruments Inc., Melville, NY).

The heparin/protamine-mediated regulation on cell internalization of TAT-Gel was further evaluated by cytotoxicity studies on LS174T, HCT116 and MDCK cells. The

cells were dispensed into 96-well plates at a density of 5 $\times 10^3$ cells per well. When the cells were attached on the bottom of the plates, TAT-Gel was added to the wells at final concentrations of either 100 nM or 1 μM (N=3). Preparation of the TAT-Gel/Hep and protamine treatment was performed as the same for the confocal microscopic imaging studies. The cells were incubated with the samples for 72 hr at 37°C under 5% CO_2 in the humidified incubator and then the relative cell proliferation was measured using an XTT assay.

3.3.10 Evaluation of Heparin/Protamine-Based Prodrug Feature of ATTEMPTS in LS174T S.C. Xenograft Tumor Model

Six-week-old male athymic nude mice (body weight: 23 - 26 g) were purchased from Charles Rivers Laboratories (Raleigh, NC). Three days after arrival (day 0), LS174T cells (5 $\times 10^6$ cells/mice) were implanted into the left hind region of the legs of the nude mice. When the tumor size reached 100 mm^3 (day 16), the mice were randomly divided into 5 groups (N=5 per group) and treated with: 1) PBS, 2) TAT-Gel (injected dose: 2 μg), 3) TAT-Gel/Hep (TAT-Gel 2 μg and heparin 3 μg), 4) TAT-Gel/Hep+Pro (TAT-Gel 2 μg and heparin 3 μg; separate injection of protamine 3 μg) or 5) Protamine (injected dose: 3 μg). The test samples were administered twice at day 16 and 22 *via* intra-tumor injection. For every treatment, the TAT-Gel/Hep was freshly prepared by mixing TAT-Gel with heparin and incubation for 30 min at 4ºC. For the TAT-Gel/Hep+Pro group, the TAT-Gel/Hep was injected into mice as described above, and the protamine was injected separately into the tumor 5 min after the TAT-Gel/Hep administration. The tumor size was monitored daily, and the volume was calculated using the following formula: V (mm^3) = (w^2 x l) / 2. In this equation, w is the width and l is the

length of the tumor. All animal experiments were conducted according to protocols approved by the University of Michigan Committee on the Use and Care of Animals (UCUCA).

3.4 Results

3.4.1 Expression and Purification of TAT-Gel

The thioredoxin-6xHis tagged-TAT-Gel (TRX-TAT-Gel) was successfully expressed as soluble protein from the *E.coli* and purified by Ni-NTA metal affinity chromatography (Figure 2A). After incubation of TRX-TAT-Gel with TEV protease and subsequent heparin column purification, TAT-Gel was acquired as a single peak fraction at 0.75 M NaCl (Figure 2B). The production of TAT-Gel was further confirmed by SDS-PAGE gel analysis (Figure 2B inbox). The yield of TAT-Gel was 3 mg per liter culture, and the purity was higher than 95% according to densitometry analysis.

3.4.2 N-glycosidase Activity of TAT-Gel

The N-glycosidase activity of TAT-Gel was determined by rabbit reticulocyte lysate assay using luciferase as a marker. As shown in Figure 3, the profiles of recombinant gelonin (rGel) and TAT-Gel were almost identical and the IC_{50} values of TAT-Gel (20 ± 12 pM; Hill slope: -1.46) and rGel (15 ± 4 pM; Hill slope: -1.02) had no statistical difference ($p > 0.05$ by student's t-test). Notably, the IC_{50} value of rGel was in good accordance with the value reported by Hossan *et al.*[7]

3.4.3 Intracellular Uptake and Anti-cancer Activity of TAT-Gel

TAT-mediated cell internalization of gelonin was evaluated by confocal microscopic imaging of LS174T cells after incubation with rhodamine-labeled TAT-Gel or rGel. Virtually no fluorescence intensity was detected from the rGel-treated cells (Figure 4B). As a comparison, strong fluorescence was clearly visible in the cells after incubation with TAT-Gel (Figure 4A). The results indicated that TAT-Gel could translocate into tumor cells.

Cytotoxicity studies for TAT-Gel were performed on two cancerous cell lines (LS174T and HCT116) and a non-cancerous cell line (MDCK) using an XTT assay. For all the tested cells, the rGel showed low cytotoxicity at concentrations above micro-molar, while TAT-Gel exerted significantly greater cytotoxic effects. Remarkably, the IC_{50} values of TAT-Gel were 2 to 3 orders lower than those of the rGel (Figure 5 and Table 2).

3.4.4 Plasma Stable Binding of TAT-Gel to Heparin and Protamine-triggered Release of the TAT-Gel

FITC-labeled TAT-Gel was loaded onto heparin beads, and the release was monitored during incubation with rat plasma at 37ºC with or without protamine. The majority (~ 80%) of TAT-Gel load onto the beads were found stably binding on the surface of the heparin beads for 24 hr (Figure 7). In contrast, addition of protamine induced release of most of the TAT-Gel (75% release) in less than 30 min (Figure 6).

3.4.5 In Vitro Characterization of Heparin/Protamine-mediated Regulation on TAT-Gel Cell Internalization

Heparin block of the TAT-mediated cell internalization and the protamine-induced reversal of this heparin inhibition were evaluated by confocal microscopic

imaging and cytotoxicity studies. As shown in Figure 7A, under the confocal miscroscope, rhodamine-labeled TAT-Gel was visible inside the LS174T cells, while no fluorescence signal was detected from the cells incubated with TAT-Gel/Hep. In comparison, when protamine was added to the TAT-Gel/Hep pre-treated cells (TAT-Gel+Pro), the strong fluorescence intensity was observed from the cells (Figure 7A).

In the cytotoxicity studies on various cells (LS174T, HCT116 and MDCK), TAT-Gel showed significant cell death in all the tested cells at concentration of either 100 nM or 1 μM, but almost no cytotoxicity was observed from the cells incubated with TAT-Gel/Hep (Figure 7B, 7C and 7D). However, when protamine was added to the cells pre-treated with the TAT-Gel/Hep (TAT-Gel/Hep+Pro), cytotoxicity level was recovered to that of the TAT-Gel (Figure 7B, 7C and 7D). Protamine, by itself, did not show any cytotoxicity below 10 μM (> 90% cell viability, data not shown).

3.4.6 In Vivo Evaluation of Heparin/Protamine-Based Prodrug Feature of ATTEMPTS

The heparin/protamine-mediated regulation on tumoricidal efficacy of TAT-Gel was tested in s.c. LS174T xenograft tumor mice. As shown in Figure 8, mice administered with TAT-Gel/Hep complex exerted only low therapeutic effects with 12% inhibition of tumor growth (at day 38). In contrast, the mice received TAT-Gel/Hep+Pro treatment, exhibited significant inhibition of tumor growth (67% inhibition), which was close to that observed from TAT-Gel treatment (78% inhibition) (Figure 8) However, protamine alone did not show any therapeutic effects (5% inhibition).

3.5 Discussion

Although the cell penetrating peptides (CPPs) have been considered highly favorable intracellular drug carriers for therapeutically potent macromolecules, non-specific fashion of their cell penetration mechanism prohibits the clinical use because of potential toxicity issues, especially if the macromolecules have low selectivity for the diseased tissue. In this study, a recombinant TAT-gelonin chimera protein (TAT-Gel) was developed as a model CPP-modified macromolecular drug and, after characterization of its potency, the feasibility to apply a heparin/protamine-based drug delivery system (DDS), CPP-modified ATTEMPTS, for regulation on the intracellular delivery of TAT-Gel was explored.

For the synthesis of TAT-Gel, genetic recombination method was adopted because of the following advantages: 1) site-specific attachment of TAT to gelonin (generally to the N- or C- terminal of the protein gene), alleviating the risk of activity loss induced by a random incorporation of the TAT; 2) homogeneous expression of TAT-Gel, which allows the utilization of TAT-Gel activity with greater reproducibility; 3) efficient mass production from the *E.coli* expression system. Using this recombinant engineering technique, the TAT-Gel was, indeed, successfully prepared and purified.

After preparation of the TAT-Gel, its potentials to be used as an anti-cancer drug were characterized *in vitro*. According to the rabbit reticulocyte lysate assay results, the TAT-Gel showed equipotent N-glycosidase activity to rGel (Figure 3), indicating no activity loss by conjugation of TAT. Furthermore, cell entry and cytotoxicity studies (Figure 4 and 5) revealed improved cell internalization and significantly enhanced anti-cancer activity of the TAT-Gel, compared with the unmodified recombinant gelonin

(rGel). Apparent cell internalization of TAT-Gel was observed from the confocal microscopic images (Figure 4), and the cytotoxicity studies further evidenced the access of internalized TAT-Gel to their target cytosolic ribosomes. Notably, by TAT conjugation to gelonin, 2 to 3 orders lower IC_{50} (avg. IC_{50}: 22.6 nM (± 20.2)) was achieved, compared with rGel (avg. IC_{50}: 4633 nM (± 635)) (Figure 5 and Table 2).

From the cytotoxicity study results, however, comparable cytotoxic effects of TAT-Gel on cancer cell lines were also observed with the non-cancerous MDCK cells (Figure 5C and Table 2), which was expected due to the non-specific cell uptake mechanism of the CPPs (Chapter 2). Therefore, in an effort to prevent any toxicity issues caused by TAT-Gel, the applicability of the CPP-modified ATTEMPTS for this TAT-Gel delivery was explored.

In order to successfully apply CPP-modified ATTEMPTS for TAT-Gel delivery, there are two requisites to be fulfilled: 1) a tight complex formation between TAT-Gel and the antibody-heparin conjugate (Ab-Hep) and 2) the efficient release of TAT-Gel from the Ab-Hep counterpart by protamine. In a simply designed *in vitro* binding study using heparin beads (Figure 6), the interaction between TAT-Gel and heparin was proven enough strong to hold each other under simulated physiological conditions (in the presence of rat plasma at 37 ºC). Moreover, addition of protamine to those heparin beads yielded significant release of the TAT-Gel (Figure 6).

Based on the finding that TAT-Gel and heparin can form a stable but reversible complex, the heparin/protamine-based regulation on TAT-Gel cell internalization was evaluated *in vitro*. The confocal microscopic images of the cells showed an obvious difference in the cell entry of TAT-Gel with and without the presence of heparin and

protamine (Figure 7A). By forming a complex with heparin, the TAT-Gel was unable to enter the cells. However, the addition of protamine to the TAT-Gel/Hep treated cells markedly enhanced the cell uptake of TAT-Gel. Accordingly, TAT-Gel/Hep (3-fold molar excess of TAT-Gel) exhibited no cytotoxic effects, while the addition of protamine (3-fold molar excess of heparin) to the cells pre-treated with this complex induced significant cell death (Figure 7B). Remarkably, the complex formation of TAT-Gel with heparin could completely abolish the cell translocation ability of TAT in all of the tested cell lines, including the non-cancerous MDCK cells. This finding provides an insight that, if protamine can be administered to the body when the TAT-Gel/Ab-Hep complex is selectively targeted to the tumor, the potential toxicity induced by TAT-Gel might be effectively avoided.

In that the *in vitro* study results were promising, the heparin/protamine regulation on TAT-Gel cell internalization was further evaluated in an LS174T s.c. xenograft tumor mouse model. Compared with TAT-Gel (78% tumor growth inhibition), TAT-Gel/Hep did not yield a significant therapeutic effect (16% tumor growth inhibition) (Figure 8). However, when protamine was administered to the tumor after injection of TAT-Gel/Hep (TAT/Gel+Pro), the tumor growth was significantly inhibited (67%) (Figure 8). This *in vivo* study results support our hypothesis that TAT-Gel/Hep complex can stably maintain in the tumor and that protamine is able to release the TAT-Gel from heparin inside the tumor.

3.6 Conclusions

In this Chapter, TAT-Gel was developed using a genetic recombination method and successfully produced from the *E.coli* cells. Through *in vitro* studies, TAT-Gel was proven for its great potency to kill tumor cells. However, potential toxicity issues related to non-cell specific internalization of the TAT-Gel were also recognized. To overcome this problem, the feasibility of employing the CPP-modified ATTEMPTS for TAT-Gel-based cancer therapy was investigated, specifically focusing on the heparin/protamine-based regulation of the cell entry of TAT-Gel, a key feature of the DDS. Both our *in vitro* and *in vivo* studies showed that masking TAT with heparin can completely block the cell internalization of TAT-Gel, but this inhibition can be efficiently reversed by protamine.

3.7 Tables

Table 3-1. Summary of PCR primers for preparation of pET-TAT-Gel vector

PCR primers for construction of TAT-Gel encoding gene	
TG-forward	5’- AGCCATATGGGTtatggccgtaaaaaacgtcgtcagcgtcgtcgtGGC GGCCTGGATACCGTG-3’
TG-backward	5’-TTCTTATTATTTCGGATCTTTGTCGACGAATTTCAGCAGCGC-3’
PCR primers for preparation of pET-TAT-Gel vector	
pTG-forward-1	5’-GCGAAAACCTGTATTTTCAGTCCCTTAGCCATATG GGTtatggccgtaaaaaacg-3’
pTG-forward-2	5’-CATCATCATCATCATCATGGTAGCAGCGGCGAAAACCTGTA TTTTCAG-3’
pTG-forward-3	5’-GCCGTCTCGGATCCCATCATCATCATCATCATGGT-3’
pTG-backward	5’-GCCGTCTCCTCGAGTTATTATTTCGGATCTTTGTC-3’

TAT codons are shown in lower case.

Table 3-2. Summary for the cytotoxicity study results (IC_{50}) of gelonin and TAT-Gel

Samples	LS174T [a]	HCT116 [a]	MDCK [a]
Gelonin	5749 ± 829	5506 ± 1563	3900 ± 1200
TAT-Gel	17.3 ± 11.7***	5.6 ± 3.2***	45.2 ± 23.1***

[a] IC_{50} values are displayed as nM. ***$P < 0.0001$ by Student t-test. For all experiments, N=3. (TAT-Gel: TAT-gelonin fusion protein)

3.8 Figures

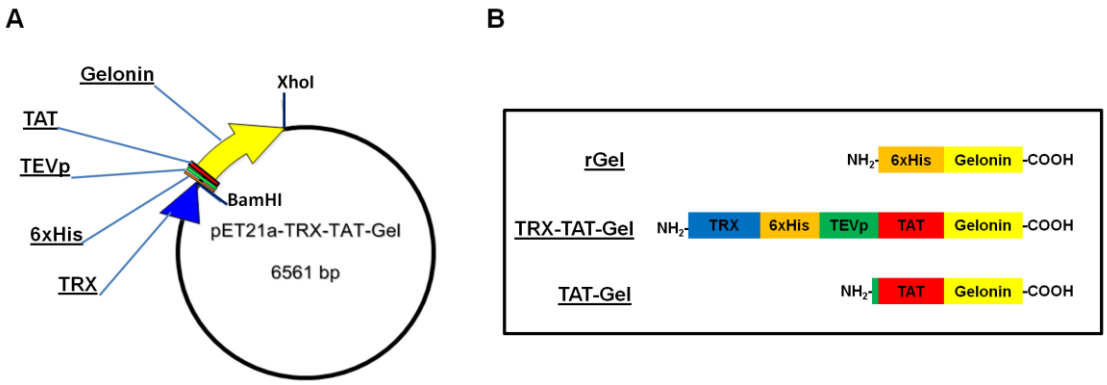

Figure 3-1. Schematic design of (A) pET-TAT-Gel vector, and images of (B) rGel, TRX-TAT-Gel and TAT-Gel.

(rGel: recombinant gelonin, TRX-TAT-Gel: thioredoxin-6xHis tagged TAT-gelonin fusion protein, TAT-Gel: TAT-gelonin fusion protein)

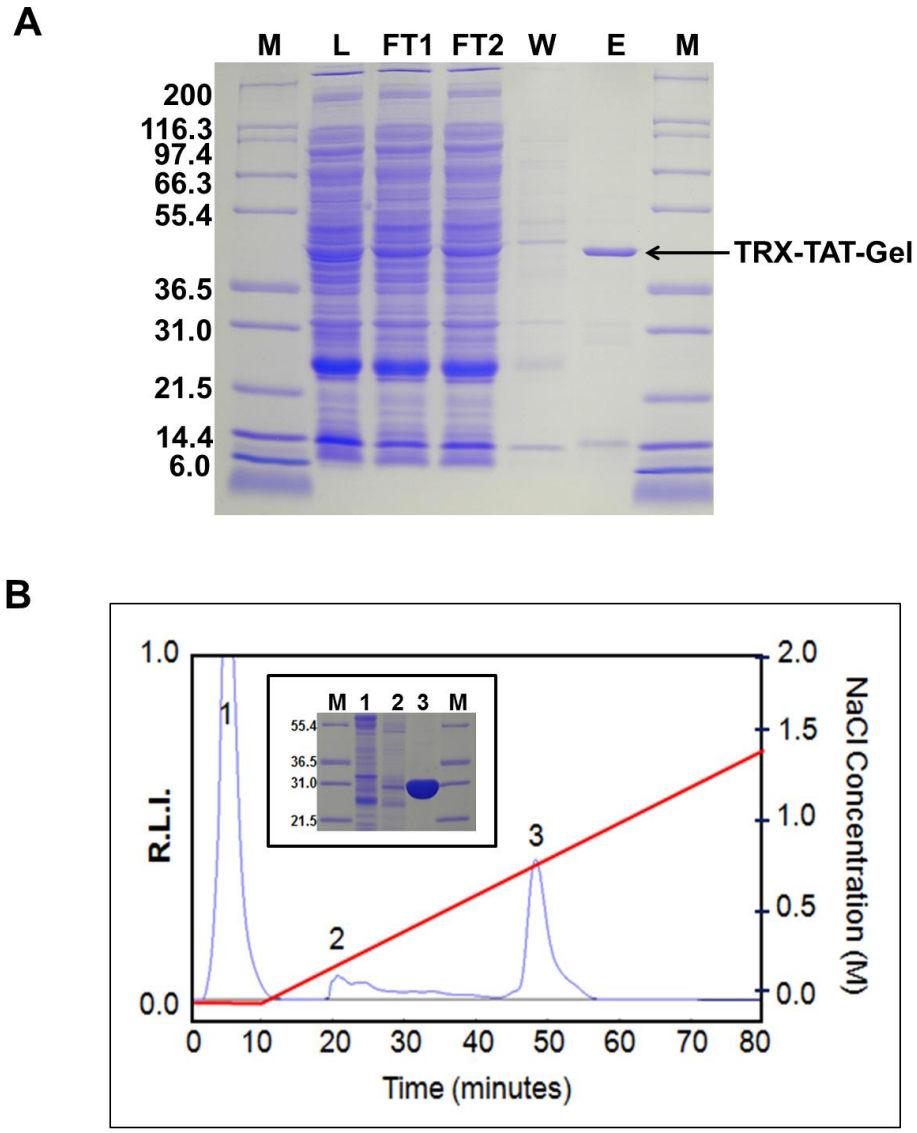

Figure 3-2. Expression and purification of TAT-Gel. (A) SDS-PAGE results of Ni-NTA column purification of TRX-TAT-Gel.

Lane M: Mark12 protein molecular weight standard (Invitrogen, Carlsbad, CA). Lane L: the supernatant fraction of cell lysate. Lane FT1 & FT2: 1st and 2nd flow through fractions. Lane W: wash fraction. Lane E: elution fraction containing TRX-TAT-Gel. Lanes FT1 to E were obtained after loading cell lysate to the Ni-NTA column; (B) Heparin chromatograpy trace for purification of TAT-Gel. TAT-Gel was acquired by incubation of TRX-TAT-Gel with TEV protease and heparin column purification with elution buffer A: 50 mM phosphate; B: 50 mM phosphate, pH 7.4 + 2 M NaCl. The NaCl salt gradient applied for elution is showed as a red line. Three major peaks (1 (eluted out with no salt), 2 (eluted out at 0.2 M NaCl) and 3 (eluted out at 0.75 M NaCl)) are displayed with the RAU (relative absorbance unit) according to the retention time (min); In box: SDS-PAGE

results of the three peak fractions obtained from the heparin chromatography. Lane M: Mark12 protein molecule weight standard. Lane 1 to 3: 3 elution fractions. (TRX-TAT-Gel: thioredoxin-6-His tagged TAT-gelonin fusion protein, TAT-Gel: TAT-gelonin fusion protein)

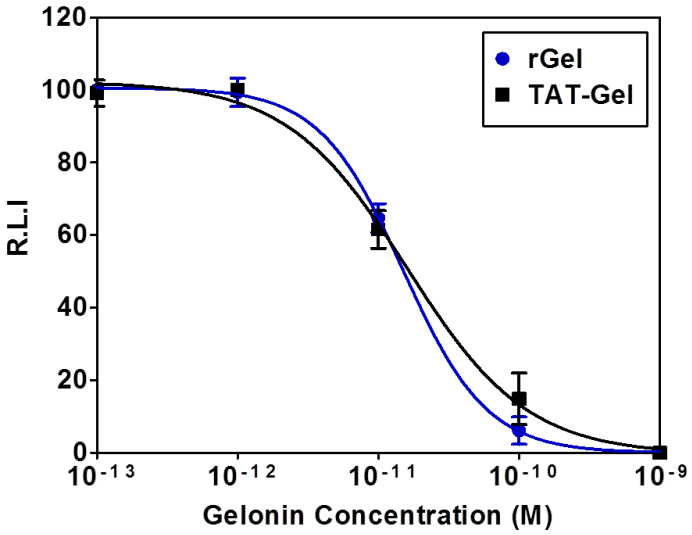

Figure 3-3. N-glycosidase activity of TAT-Gel determined by rabbit reticulocyte lysate assay.

Inhibition of luciferase translation by rGel (closed circle) or TAT-Gel (closed square) was measured by a chemiluminescent assay (Promega Corp., Madison, WI) and IC_{50} values were calculated by nonlinear regression using Prism software (Prism version 5.0, Graphpad, CA). (TAT-Gel: TAT-gelonin fusion protein, rGel: recombinant gelonin)

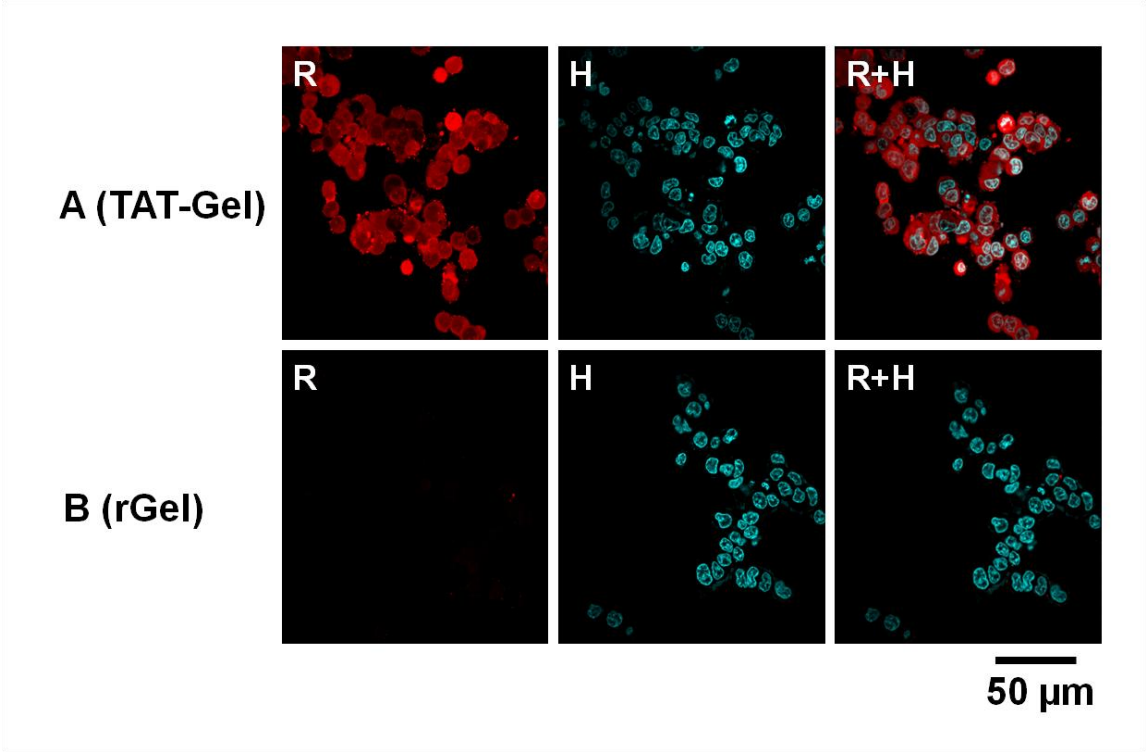

Figure 3-4. Confocal microscopic images of LS174T human adenocarcinoma cells incubated with rhodamine-labeled (A) TAT-Gel or (B) rGel.

Cells were incubated with 5 µM of rhodamine-labeled TAT-Gel or rGel for 3 hrs at 37°C, and, after washed once with 10 mg/mL heparin/PBS and 3 times with PBS, the cell images were taken by a Nikon A1R-A1 confocal laser microscope with a 60x objective (Nikon Instruments Inc., Melville, NY). (TAT-Gel: TAT-gelonin fusion protein, rGel: recombinant gelonin)

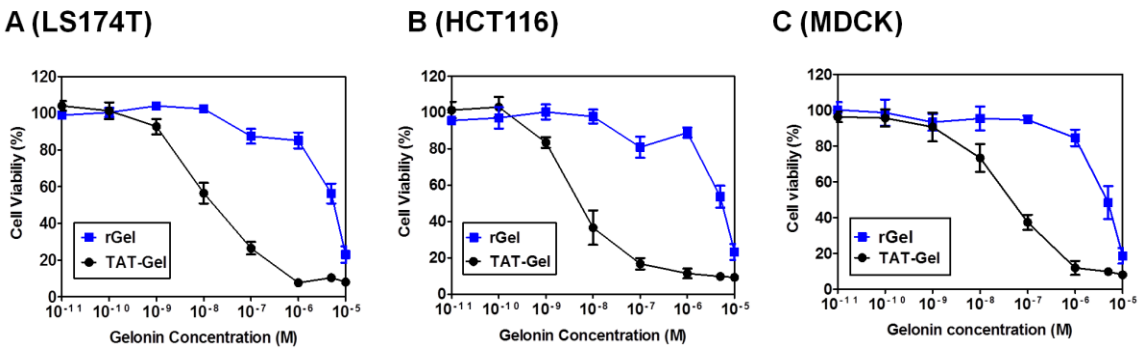

Figure 3-5. Anti-cancer activity of TAT-Gel.

(A) LS174T, (B) HCT116 and (C) MDCK cells, plated onto 96 wells (cell density: $5x10^3$ cells/well), were incubated with rGel or TAT-Gel for 72 hrs and the cytotoxicity level was determined by XTT assay (N=3).

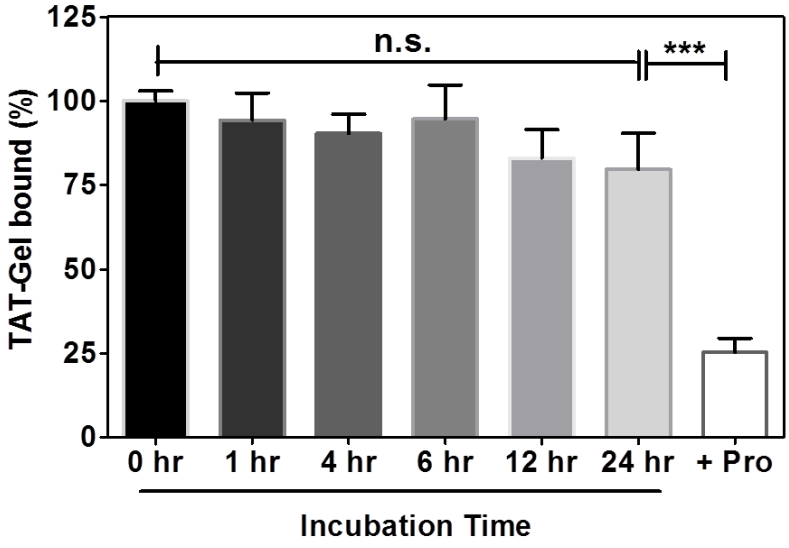

Figure 3-6. *In vitro* plasma stability of TAT-Gel/Hep and protamine-induced release of TAT-Gel.

FITC-labeled TAT-Gel was loaded onto heparin beads and the release was monitored for 24 hrs in the presence of rat plasma at 37ºC. Release of TAT-Gel by addition of excessive protamine was also observed. *** $P < 0.0001$, n.s.: not significant. For all experiments, N=3. (TAT-Gel: TAT-gelonin fusion protein, TAT-Gel/Hep: TAT-Gel and heparin complex; Pro: Protamine)

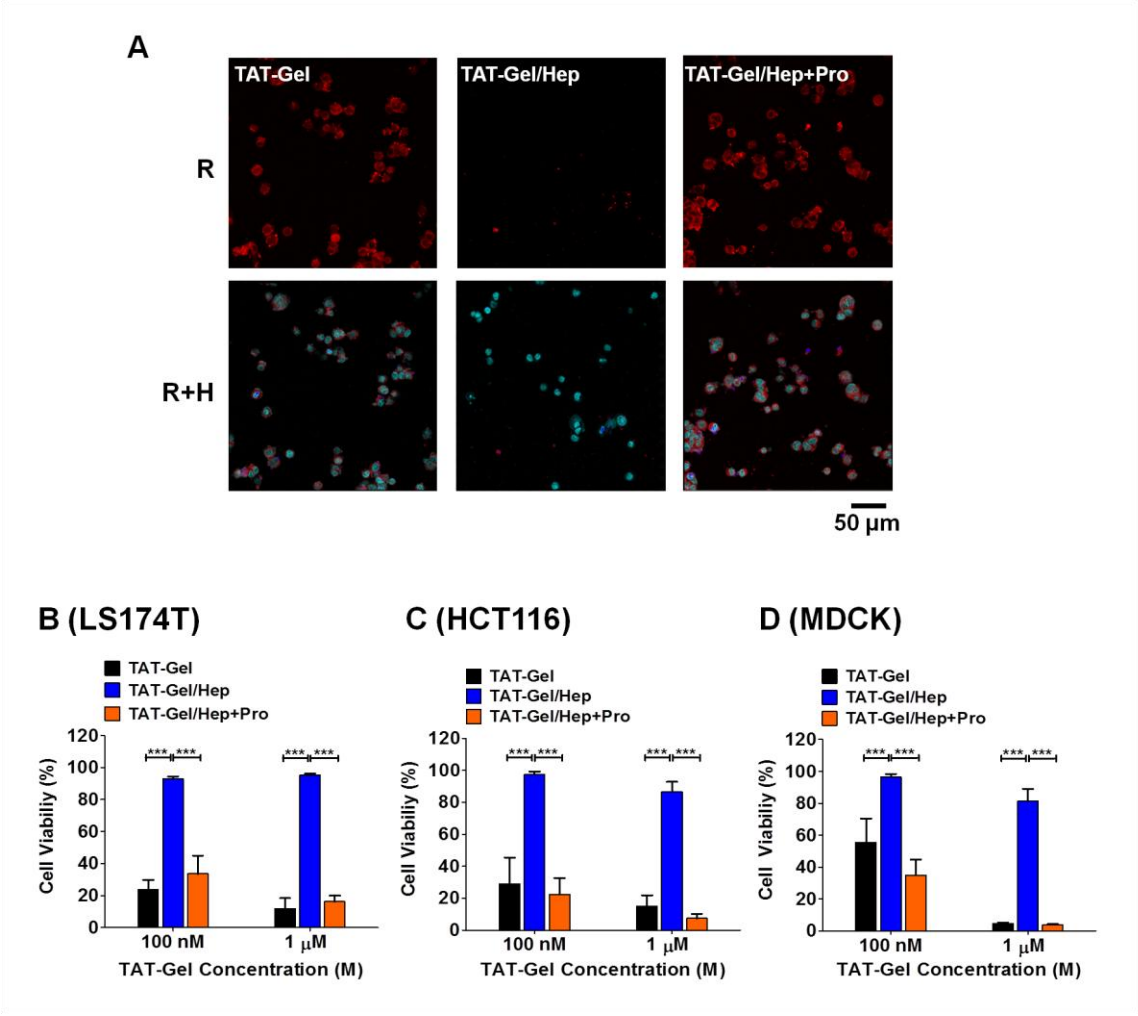

Figure 3-7. Heparin/protamine-mediated regulation on TAT-Gel cell internalization evaluated by cell entry and cytotoxicity studies.

(A) Confocal microscopic images of LS174T cells after incubation with rhodamine-labeled TAT-Gel, by itself (TAT-Gel; 1st column), a complex with heparin (TAT-Gel/Hep; 2nd column) or a complex with heparin and later addition of protamine (TAT-Gel/Hep+Pro; 3rd column). The upper row shows the cell images acquired by a rhodamine filter (R) and the lower row exhibits the merged cell images obtained by a rhodamine filter (R) and a Hoechst filter (H). Cytotoxicity study results on (B) LS174T, (C) HCT116 and (D) MDCK cells, after TAT-Gel, TAT-Gel/Hep or TAT-Gel/Hep+Pro treatment. Data represent mean ± SD, *** $P < 0.0001$. For all experiments, N=3. (TAT-Gel: TAT-gelonin fusion protein, TAT-Gel/Hep: TAT-Gel and heparin complex)

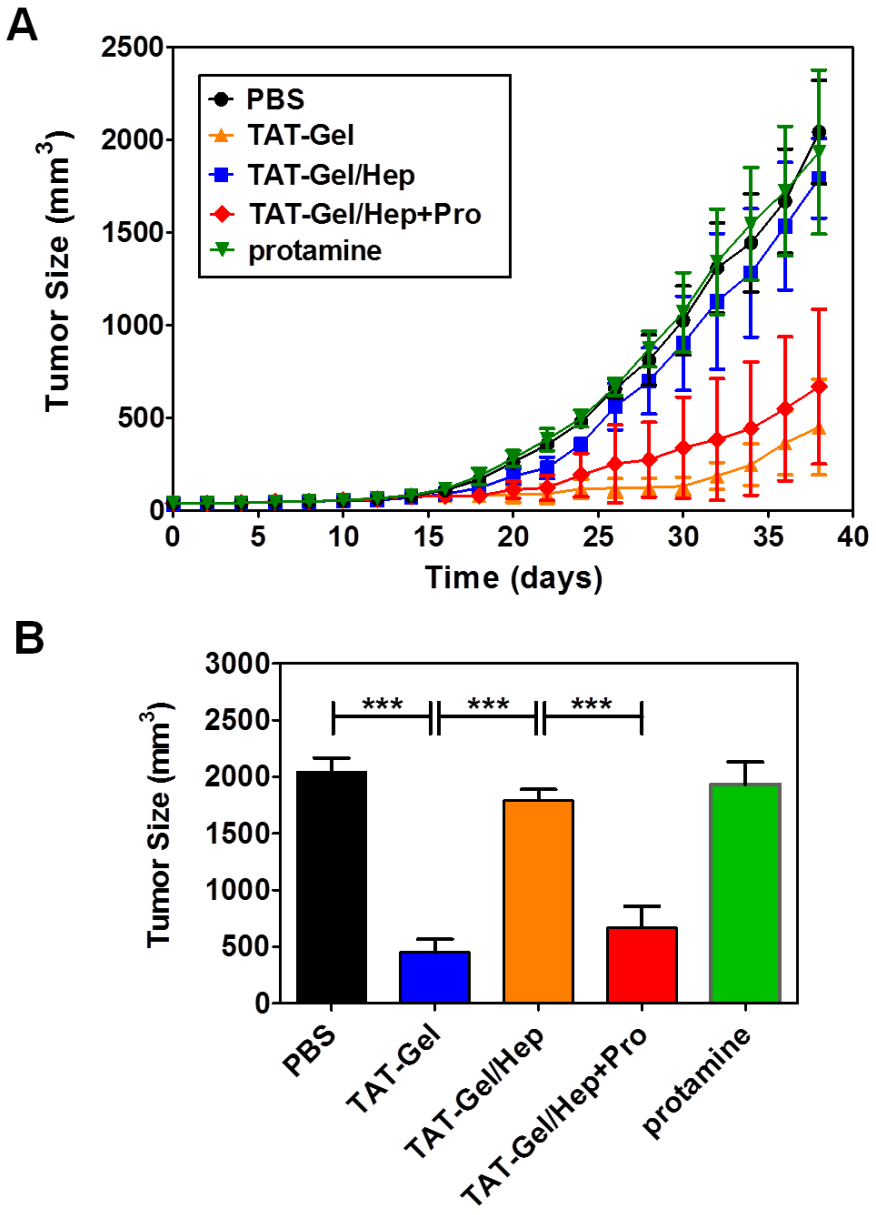

Figure 3-8. *In vivo* evaluation of heparin/protamine-mediated regulation on TAT-Gel tumoricidal efficacy in a LS174T s.c. xenograft tumor mice model.

(A) Tumor volume profiles as a function of time (days). When the tumor size reached 100 mm^3, mice were divided into 5 groups (N=5) and received PBS (circle), TAT-Gel (triangle), TAT-Gel/Hep (square), TAT-Gel/Hep+Pro (diamond) or protamine (reverse triangle) treatment. For TAT-Gel/Hep+Pro treatment, the TAT-Gel/Hep was first administered to the tumor and, 5 min later, protamine injection was followed. The treatments were given by intra-tumor injection at day 16 and 22. Tumor size was measured daily using a vernier caliper after tumor inoculation (day 0) and the volume (mm^3) was calculated by the following equation, $V = (a^2 \times b) / 2$. In this equation, *a*

represents the width and *b* represents the length of the tumor. (B) Average tumor size of each group at day 38 when the tumor size of the PBS treated group reached 2000 mm^3. Data represent mean ± SD. *** $P < 0.0001$. (TAT-Gel: TAT-gelonin fusion protein, TAT-Gel/Hep: TAT-Gel and heparin complex)

3.9 References

1. Brooks H, Lebleu B, Vives E. Tat peptide-mediated cellular delivery: back to basics. Adv Drug Deliv Rev 2005;57:559-77.
2. Wadia JS, Dowdy SF. Transmembrane delivery of protein and peptide drugs by TAT-mediated transduction in the treatment of cancer. Adv Drug Deliv Rev 2005;57:579-96.
3. Niesner U, Halin C, Lozzi L, Gunthert M, Neri P, Wunderli-Allenspach H, Zardi L, Neri D. Quantitation of the tumor-targeting properties of antibody fragments conjugated to cell-permeating HIV-1 TAT peptides. Bioconjug Chem 2002;13:729-36.
4. Huang Y, Jiang Y, Wang H, Wang J, Shin MC, Byun Y, He H, Liang Y, Yang VC. Curb challenges of the "Trojan Horse" approach: Smart strategies in achieving effective yet safe cell-penetrating peptide-based drug delivery. Adv Drug Deliv Rev 2013.
5. Kwon YM, Li YT, Liang JF, Park YJ, Chang LC, Yang VC. PTD-modified ATTEMPTS system for enhanced asparaginase therapy: a proof-of-concept investigation. J Control Release 2008;130:252-8.
6. Kwon YM, Li Y, Naik S, Liang JF, Huang Y, Park YJ, Yang VC. The ATTEMPTS delivery systems for macromolecular drugs. Expert Opin Drug Deliv 2008;5:1255-66.
7. Hossann M, Li Z, Shi Y, Kreilinger U, Buttner J, Vogel PD, Yuan J, Wise JG, Trommer WE. Novel immunotoxin: a fusion protein consisting of gelonin and an acetylcholine receptor fragment as a potential immunotherapeutic agent for the treatment of Myasthenia gravis. Protein Expr Purif 2006;46:73-84.

Chapter 4

Heparin Functionalized Monoclonal Antibody Mediated Tumor Targeted Delivery of CPP-Modified Gelonin

4.1 Abstract

Monoclonal antibodies (mAbs) are attractive drug carriers for cancer therapy, as they can provide effective means of tumor targeting. Specifically, by attaching extrememly potent toxins to those mAbs, certain clinical successes have been accomplished. Herein, we investigated the feasibility to exploit the strong electrostatic interaction between anionic heparin and cationic cell penetrating peptides (CPPs) for coupling the mAb with a toxin, gelonin. A heparin-functionalized mAb was developed *via* chemical conjugation of heparin with T84.66, a murine anti-carcinoembryonic antigen (CEA) mAb. This T84.66 is well-known for its excellent targeting ability toward tumors, such as colorectal cancer. Through *in vitro* assays, it was confirmed that the T84.66-heparin conjugate (T84.66-Hep) still retains specificity for CEA, and, moreover, can strongly bind to cationic peptides (e.g., protamine) in the presence of plasma. Live animal imaging studies further showed that T84.66-Hep can selectively deliver a CPP-modified toxin, TAT-Gel, to tumor *via* forming a complex. Through administration of

T84.66-Hep/TAT-Gel, markedly enhanced (58-fold) tumor exposure of TAT-Gel was accomplished, compared with injection of TAT-Gel alone.

4.2 Introduction

The mAbs are attractive macromolecules for cancer therapy due to their ability to selectively bind to tumor cells *via* interaction with specific tumor associated antigens.[1, 2] Carcinoembryonic antigen (CEA) which was first isolated from human colon cancer extracts is a GPI-linked highly glycosylated cell surface protein (MW ~ 200 kDa).[3, 4] The CEA is known to have strictly limited expression in normal tissues (e.g., columnar epithelial cells and goblet cells in colon), but over-expressed in various human adenocarcinomas (e.g., colon, ovarian, lung, breast and pancreatic cancer).[4] Moreover, although normal colon cells express CEA, its expression is exclusively limited to the apical surface, which allows very limited access from the blood stream. However, colon cancer cells lose their polarity and have distribution of CEA all around the cell surface.[4] Therefore, CEA has been considered a suitable tumor associated antigen for tumor detection and targeted drug delivery.[5-8] Among the anti-CEA mAbs, T84.66 from murine origin possesses exceptionally high binding affinity (2.6×10^{10} M^{-1}) and specificity toward the CEA.[9] Thus, T84.66 has shown exceptional tumor targeting efficiency. According to Urva and Balthasar, over 85% of the injected T84.66 (at 1 mg/kg dose) was found to accumulate in tumor.[10]

Binding to the antigens, the mAbs, by itself, can elicit anti-tumor activity mediated *via* complement dependent cytotoxicity (CDC), antibody dependent cell cytotoxicity (ADCC) or induction of direct signaling.[2] However, the above effects tend to

be various among the mAbs and eventually not curative.[1] An effective way to improve the therapeutic efficacy of the mAbs is to couple them with potent toxin molecules.[11, 12] This approach has received enormous interest in the past decades and, indeed, accomplished certain clinical successes.

In this chapter, we describe the development of a heparin functionalized mAb, T84.66-Hep, by chemical conjugation method using a heterobifunctional PEG (NH_2-PEG-MAL) as a cross-linker. The CEA binding specificity of T84.66-Hep, evaluated by cell binding and ELISA studies, is reported. Also, the *in vitro* plasma stability of T84.66-Hep binding with cationic peptides (e.g. protamine) is discussed. Finally, we examine the feasibility of T84.66-Hep mediated tumor targeted delivery of TAT-Gel *via* complex formation in a LS174T *s.c.* xenograft tumor model.

4.3 Materials and Methods

4.3.1 Materials

Carbenicillin and isopropyl-β-thiogalactopyranoside (IPTG) were purchased from Fisher Scientific (Pittsburg, PA). Heparin sulfate and rhodamine B isothiocyanate, fluorescein isothicyanate (FITC), Traut's reagent (2-iminothiolane), MES (2-(*N*-morpholino) ethanesulfonic acid), EDC (1-Ethyl-3-[3-dimethylaminopropyl] carbodiimide Hydrochloride), goat anti-mouse-IgG (Fc specific)-alkaline phosphatase, rat plasma and murine IgG were purchased from Sigma-Aldrich (St. Louis, MO). Competent *E.coli* strain (BL21star (DE3)), AcTEV™ protease, PBS (pH 7.4), Dulbecco's Modified Eagle Medium (DMEM), Hybridoma serum free medium (SFM), fetal bovine serum albumin (FBS), Hoechst 33342 trihydrochloride, trihydrate were purchased from

Invitrogen (Carlsbad, CA). 1-step PNPP, Dylight 679-C5 and Dylight 775-B4 were purchased from Thermo Scientific (Rockford, IL). PEG (NH_2-PEG-MAL; 3.5 kDa) was purchased from JenKem Technology USA Inc. (Allen, TX). Recombinant CEA (rCEA) was purchased from R&D SYSTEMS (Minneapolis, MN).

4.3.2 Production of T84.66

T84.66 was produced from hybridoma cells purchased from American Type Culture Collection (ATCC # HB-8747, Manassas, VA). Cells were grown in 2L spinner flasks containing serum free media (Hybridoma SFM, Invitrogen), and the culture supernatant was harvested every 3 days. T84.66 was purified by loading the culture supernatant onto protein G column (Protein G Sepharose™ 4 Fast Flow, GE Healthcare Biosciences, Pittsburg, PA) pre-equilibrated with 20 mM phosphate buffer (PB, pH 7). After wash with 200 mL of above PB, the T84.66 was eluted with 0.1 M glycine buffer (pH 2.8) and collected in a tube where 1 M Tris buffer was pre-dispensed for instant neutralization of the elution buffer. The T84.66 was then dialyzed (Dialysis Tubing Cellulose Membrane, molecular weight cutoff: 12,000 Da, Sigma-Aldrich, St. Louis, MO) for overnight against 20 mM phosphate buffer saline (PBS, 0.15 M NaCl, pH 7.4) for buffer exchange. The final T84.66 product was quantified by measuring the optical density at 280 nm and kept at 4ºC until use.

4.3.3 Preparation and Purification of Heparin Functionalized T84.66 (T84.66-Hep)

T84.66 was conjugated with heparin *via* a stable thioether bond utilizing a heterobifunctional PEG (NH_2-PEG-MAL, 3.5 kDa, JenKem Technology USA Inc.) as a cross-linker. The conjugation scheme is depicted in Figure 1. Thiol groups were introduced to T84.66 by incubation of the T84.66 (10 mg/mL in 50 mM HEPES buffer, 5

mM EDTA, pH 8) with 10-fold molar excess of Traut's reagent for 1 hr at room temperature. The unreacted Traut's reagent was removed by ultrafiltration using centrifugal filtration device (molecular weight cut off: 10 kDa, Amicon® Centricon® Centrifugal Filter Devices, Millipore Corporation, Billerica, MA) and the generated thiol groups were quantified by Ellman's assay.[13] To introduce thiol reactive maleimide groups to heparin, heparin (40 mg/mL in 0.1 M MES buffer 1 mL, pH 5) was incubated with 5-fold molar excess of NH_2-PEG-MAL (40 mg/mL in 0.1 M MES buffer 1 mL) and EDC (40 mg/mL in 0.1 M MES buffer 0.5 mL) for 2 hr at room temperature. The conjugate, heparin-PEG-MAL, was loaded onto an anion exchange column (Bio-Scale™ Mini UNOsphere™ Q Cartridge, Bio-Rad Laboratories, Hercules, CA) connected to HPLC (Alltech 526 HPLC pump, Deerfield, IL) and eluted with salt gradient (0 to 2 M NaCl at a rate of 0.02 M/min, flow rate: 1 mL/min). The heparin-to-PEG conjugation ratio was determined by measuring the heparin and NH_2-PEG-MAL content by azure A assay[14] and barium iodide assay,[15] respectively. The prepared heparin-PEG-MAL was slowly added to the thiol activated T84.66 (T84.66-SH), and the conjugation reaction was performed at room temperature for overnight. The T84.66-Hep was purified from T84.66-SH using an anion exchange column and elution with a salt gradient (0 to 2 M NaCl at a rate of 0.02M/min, flow rate: 1 mL/min, detection: 280 nm). Any unreacted heparin and heparin-PEG-MAL was further removed by ultrafiltration (molecular weight cut off: 100 kDa). All the peak fractions including the final T84.66-Hep product was analyzed by SDS-PAGE and the T84.66 and heparin contents were quantified by measuring the optical density at 280 nm (OD_{280}) and azure A assay, respectively.

4.3.4 Cell Culture

LS174T and HT116 human adenocarcinoma cells were purchased from American Type Culture Collection (ATCC) (Manassas, VA). The cells were cultured in 75 cm^2 flasks and maintained in a humidified atmosphere of 5% CO_2 at 37°C. The cells were cultured in DMEM with 2 mM L-glutamine, high glucose, 1% (v/v) penicillin-streptomycin, and 10% FBS. During the cultures, culture media in flasks was replaced by fresh media every other day, and the cells were sub-cultured when confluent, by detaching with 0.25% trypsin-EDTA.

4.3.5 Specific Cell Binding Assay

Specific binding of T84.66-Hep to cell surface expressed CEA was evaluated *in vitro* by cell binding assay using confocal microscopy. Prior to the cellular studies, T84.66-Hep (2 mg/mL in 0.1 M bicarbonate buffer, pH 9.0) was labeled with a fluorescence dye by incubation with 5-fold molar excess of rhodamine B isothiocyanate (TRITC) at room temperature for 2 hr. The unreacted TRITC was removed using dye removal resin following the vendor's protocol (Bio-Rad Laboratories, Hercules, CA).

For the cell binding assay, LS174T (CEA high expression cell line) and HCT116 (CEA low expression cell line) cells were seeded onto an 8-well chambered coverglass (Nunc® Lab-Tek II Chambered Coverglass, Thermo Scientific, Rockford, IL) at a density of 10^5 cells/well and incubated for overnight in complete medium. When the cells were attached on the bottom of the wells, rhodamine-labeled T84.66-Hep (final concentration of 5 μM) was incubated with the cells for 2 hr at 37°C in a humidified atmosphere of 5% CO_2. Additionally, to investigate whether T84.66-Hep binding to the cells is *via* specific interaction with the CEA, LS174T cells were pre-incubated with 10-

fold molar excess of unlabeled T84.66 for 1 hr, and then, incubated with the rhodamine-labeled T84.66-Hep for 2 hr. After washing the cells with PBS, the images of the live cells were taken with a Nikon A1R-A1 confocal laser microscope with a 60x objective (Nikon Instruments Inc., Melville, NY). The cell images were acquired and analyzed using NIS-Elements microscope imaging software (Nikon Instruments Inc., Melville, NY).

4.3.6 ELISA Assay

Specific binding of T84.66-Hep to CEA was determined by ELISA assay using the protocols by Urva *et al*. with modification.[16] Briefly, 96-well plates (Corning® 96 well EIA/RIA clear flat bottom polystyrene high bind microplate, Tewksbury, MA) were coated with recombinant CEA (rCEA, 400 ng/mL in 20mM phosphate buffer, 250 µL/well, R&D SYSTEMS) and incubated at 4ºC for overnight. The unbound rCEA was removed and the wells were washed by PB-Tween (20 mM phosphate buffer with 0.05% Tween 20) three times, followed by wash with MQ water twice. Various concentrations of T84.66 and T84.66-Hep (0, 10, 50 and 100 ng/mL) were then separately added to the wells (200 µL/well). After incubation for 2 hr at room temperature, the wells were washed and goat anti-mouse-IgG (Fc specific)-alkaline phosphatase (1:1000 in PB-Tween, 100 µL/well, Sigma-Aldrich) was added to the wells and incubated for 2 hr at room temperature. After washing as above, 100 µL of p-nitrophenyl phosphate (1-step PNPP, Thermo Scientific) was added to each well and the change in absorbance at 405 nm was monitored by a microplate reader (BioTEK® Synergy™ BioTEK, co., Winooski, VT) using kinetic mode. The absorbance of each well was measured every minute for

total 6 minutes and the initial rate (slope, dA/dt) was calculated by linear regression using Prism software (Prism version 5.0, GraphPad, San Diego, CA).

4.3.7 Evaluation of the *In Vitro* Plasma Stability of T84.66-Hep Binding to Cationic Protamine

In vitro plasma stability of T84.66-Hep binding to cationic CPP was evaluated at physiologically simulated condition using protamine beads (Protamine-Agarose, Sigma-Aldrich, St. Louis, MO) as an alternative for the CPPs. Prior to the study, T84.66-Hep was labeled with a fluorescent dye. Briefly, T84.66-Hep (2 mg/mL in 0.1 M bicarbonate buffer, pH 9.0) was incubated with 5-fold molar excess of FITC for 2 hr at room temperature and the unreacted FITC was removed using dye removal resins (Bio-Rad Laboratories).

The FITC-labeled T84.66-Hep (200 µg/mL in PBS) was loaded 50 µg each onto 100 µL of protamine beads (50% (v/v) slurry) and incubated at room temperature for 1 hr. The unbound FITC-labeled T84.66-Hep was removed by centrifugation at 10,000 rpm for 5 min. The FITC-labeled T84.66-Hep loaded beads were then re-dispersed in 250 µL of rat plasma (Sigma-Aldrich) and incubated up to 24 hr. At intended time points (0, 1hr, 2 hr, 4 hr, 6 hr, 12 hr and 24 hr), the beads were washed with PBS for 3 times and the FITC-labeled T84.66-Hep remaining on the bead surface was eluted with 2 M NaCl solution. For the control, the FITC-labeled T84.66-Hep was eluted from the beads without incubation in the rat plasma. The fluorescence intensities of the eluents were measured by a plate reader (excitation/emission (Ex/Em) wave length: 485nm/530 nm, BioTEK® Synergy™ BioTEK, co., Winooski, VT). The bound fraction (%) of FITC-

labeled T84.66-Hep was calculated by dividing the mean fluorescence intensities of the eluents by that of the control (N=3 for each time point).

4.3.8 LS174T S.C. Xenograft Tumor Mouse Model

Male athymic nude mice (body weight: 21 ~ 25 g, 6 weeks old) were purchased from Charles Rivers Laboratories (Raleigh, NC). Mice were housed in sterile animal facilities, handled under aseptic conditions in a laminar hood, and fed by standard chow diet. At day 0 (three days after arrival), LS174T cells (5×10^6 cells/mice) were injected (s.c.) into the left flank of the mice. After tumor implantation, the mice were fed by special alfalfa-free diet (AIN-76A rodent diet, gamma-irradiated, Research Diets, Inc., New Brunswick, NJ) to reduce the background autofluorescence during the imaging studies.[17, 18] Tumor size was measured using a vernier caliper and the volume was calculated by the formula of volume, V (mm^3) = (w^2 x l) / 2. In the equation, w is the width and l is the length of the tumor. When the tumor size reached average 200 mm^3, the imaging study was performed.

4.3.9 Live Animal Imaging

Prior to the imaging studies, antibody (Ab) samples (T84.66-Hep, nonspecific mouse IgG and IgG-heparin conjugate (IgG-Hep)) and TAT-Gel were labeled with near infrared (NIR) dyes, Dylight 679-C5 (C5, Thermo Scientific) and Dylight 775-B4 (B4, Thermo Scientific), respectively. The C5 and B4 were chosen based on their minimal overlapping of excitation and emission (Ex/Em) wavelengths, in order to simultaneously image both the antibody samples and TAT-Gel in the same mouse. To assess any interference or quenching between the two dyes, the fluorescence intensities of C5, B4 and 1:1 mixture of C5 and B4 were measured at Ex/Em wavelengths of 675 nm/720 nm

(optimal for C5) and 745 nm/800 nm (optimal for B4), using the IVIS® spectrum imaging system (Xenogen, Alameda, CA).

Dye labeling was performed following the vendor's protocol (Thermo Scientific). Briefly, non-specific IgG, IgG-Hep and T84.66-Hep (5 mg/mL in 50 mM sodium bicarbonate buffer, pH 9.3) were separately incubated with 5-fold molar excess of C5 (10 mg/mL stock solution in DMF) at room temperature for 2 hr. Similarly, TAT-Gel (2 mg/mL in 50 mM sodium bicarbonate buffer, pH 9.3) was incubated with 5-fold molar excess of B4 (10 mg/mL in DMF). The unreacted C5 and B4 were removed using the dye removal resins (Bio-Rad Laboratories). The dye-to-protein ratio was calculated based on the vendor's protocol (Thermo Scientific).

For the live animal imaging, the LS174T s.c. xenograft tumor mice were randomly divided into 6 groups (N=3 per group) and administered with: 1) PBS, 2) C5, 3) nonspecific IgG-C5 (360 µg), 4) TAT-Gel-B4 (135 µg), 5) IgG-Hep-C5/TAT-Gel-B4 (345 µg of IgG-Hep-C5 and 135 µg of TAT-Gel-B4) or (6) T84.66-Hep-C5/TAT-Gel-B4 (400 µg of T84.66-Hep-C5 and 135 µg of TAT-Gel-B4). The above prepared C5, IgG-C5 and T84.66-Hep-C5 sample solutions contained similar C5 content. The Ab-Hep/TAT-Gel complex was prepared by incubation of the Ab-Hep-C5 with TAT-Gel-B4 at 4ºC for 1 hr, prior to the imaging studies. The samples were injected *via* tail vein injection and the live animal imaging was performed using IVIS® spectrum imaging system (Xenogen, Alameda, CA). During imaging, mice were maintained anesthetized with isoflurane (Abbott Laboratories, Chicago, IL). The animal images were obtained at 5 min, 30 min, 1hr, 2 hr, 6 hr, 24 hr, 48 hr and 72 hr after the injection of the samples. Animal

experiments were conducted according to the protocol approved by the University of Michigan Committee on Use and Care of Animals (UCUCA; protocol No. 08945).

To acquire the images of the C5-labeled Ab samples in the animal body, Cy5.5 filter (Ex/Em: 675 nm/720 nm) was used and, for the detection of TAT-Gel-B4, ICG filter (Ex/Em: 745 nm/800 nm) was utilized, respectively. Identical illumination settings, such as exposure time (1 s), binning (8), *f*/stop (4 for C5-labeled Ab samples and 2 for TAT-Gel-B4) and fields of view (25 cm x 25 cm) were used for the imaging. The images were analyzed using Living Image 2.5 software (Xenogen, Alameda, CA) and the signal was normalized to photon per second per centimeter squared per steradian ($ps^{-1}cm^{-2}sr^{-1}$).

Intra-tumor accumulation of TAT-Gel-B4 was assessed by measuring the fluorescence intensity of the tumor, designated as the region of interest (ROI), from each animal image. The fluorescence intensity of each ROI was acquired by subtracting the mean fluorescence intensity of the corresponding ROI on the control blank mice. The mean fluorescence intensity was plotted as a function of time and the area under the curve (AUC) for each plot was calculated using Metamorph software (Molecular Devices Corporation, Sunnyvale, CA).

4.3.10 Statistical Analysis

All data are presented as mean ± standard deviation. Statistical comparisons were made using student t-test (unpaired t-test, two-tailed, Prism version 5.0, GraphPad, San Diego, CA). Less than p-values of 0.05 were considered significant.

4.4 Results

4.4.1 Purification of T84.66

The T84.66 was expressed from the hybridoma cells and purified by protein G affinity chromatography. Successful purification of T84.66 was confirmed by SDS-PAGE gel analysis (data not shown). The T84.66 was observed at the position corresponding to the size of about 170 kDa. The average yield of T84.66 was 2 mg per L culture and the purity was higher than 95% based on the densitometry analysis using imageJ software.

4.4.2 Preparation and Purification of Heparin Functionalized T84.66 (T84.66-Hep)

The T84.66 was conjugated to heparin *via* a thioether bond using a heterobifunctional PEG (NH_2-PEG-MAL, 3.5 kDa) as a cross-linker (Figure 1). To prepare the conjugate, thiol activation of T84.66 (T84.66-SH) was achieved using Traut's reagent. Ellman's assay indicated that an average of 5 thiol groups was introduced to each T84.66. Moreover, a thiol active maleimide group was successfully introduced to heparin by conjugation with NH_2-PEG-MAL. As the PEG does not have strong binding affinity to anion exchange resins, the heparin-PEG-MAL was purified from unreacted PEG by anion exchange chromatography. The eluent contained both heparin and PEG at a molar ratio of 1:0.4 (heparin:PEG), determined by Azure A and Barium iodide assay. The conjugation reaction was performed by incubation of the T84.66-SH with 5-fold molar excess of the heparin-PEG-MAL and the T84.66-Hep was successfully purified from T84.66-SH by anion exchange chromatography using NaCl salt gradient (Figure 2A). Whereas T84.66 did not bind to the column (Figure 2A), T84.66-Hep elution profile showed two distinct peak fractions, F#1 (eluted with no salt) and F#2 (retention time: 50

min, elution with 0.8 - 1.8 M NaCl) (Figure 2A). SDS-PAGE analysis indicated that F#2 contained the T84.66-Hep (Figure 2B). After removal of the unreacted heparin and heparin-PEG-MAL that contained in the F#2 by ultrafiltration (MWCO:100 kDa), the final yield of T84.66-Hep was 25% (2.5 mg of T84.66-Hep from initial 10 mg T84.66) and the average T84.66-to-heparin conjugation molar ratio was 1:3 (see Figure 2C).

4.4.3 CEA-mediated Specific Cell Binding of T84.66-Hep

To determine whether T84.66-Hep can specifically bind to CEA overexpressed on tumor cell surface, cell binding studies were performed on CEA high expressing LS174T cell line and CEA low expressing HT116 cell line. After 2 hr incubation with rhodamine-labeled T84.66-Hep, whereas no apparent fluorescence intensity was observed from the HT116 cells, strong fluorescence signal was clearly visible on the surface of LS174T cells (Figure 3). However, when the LS174T cells were incubated with rhodamine-labeled T84.66-Hep after pre-incubation with 10-fold molar excess of T84.66, only minimal signal was observed (Figure 3).

4.4.4 ELISA Assay

The specific binding of T84.66-Hep to CEA was further evaluated using ELISA assay. With all the tested concentrations (10, 25, 50, 75 and 100 ng/mL), T84.66-Hep showed lower CEA binding profile than the T84.66 (Figure 4 and Table 1) with averaging 69% T84.66-Hep/T84.66 rate ratio ($R_{T84.66\text{-}Hep/T84.66}$).

4.4.5 Plasma Stability of T84.66-Hep Binding to Cationic Protamine

The plasma stability of the interaction between T84.66-Hep and cationic CPPs was evaluated *in vitro* utilizing protamine beads as alternatives for the CPPs. By simple

mixing, the FITC-labeled T84.66-Hep was able to bind to the protamine beads (65% loading efficiency). When the T84.66-Hep-loaded protamine beads were incubated with plasma, 25% FITC-labeled T84.66-Hep was released within an hour. However, the majority of the FITC-labeled T84.66-Hep stably remained on the surface of the beads for 24 hrs (68% remaining on the surface of the beads) (Figure 5).

4.4.6 *In Vivo* Evaluation of Tumor Targeted Delivery of TAT-Gel *Via* Complex Formation with T84.66-Hep

A live animal imaging study was performed with near infrared (NIR) dye-labeled samples, C5-labeled antibodies samples (non-specific IgG, IgG-Hep, T84.66-Hep) and TAT-Gel-B4, in an LS174T *s.c.* xenograft tumor mice model. Little, if any, interference between the C5 and B4 was observed, specifically at their low concentrations (< 6.25 μg/mL) that was used in this study (Figure 6).

The absence of any fluorescence signal from the PBS-treated mice (Figure 7B) evidenced no autofluorescence from the tissues. After administration of T84.66-Hep-C5/TAT-Gel-B4, the T84.66-Hep-C5 was observed in the tumor over 72 hr with a localized fashion and its major disposition site appeared to be the liver (Figure 7A). In comparison, the control mice (administered with PBS, C5 or IgG-C5) displayed no fluorescence intensity in the tumor at either 5 min or 48 hr post-injection (Figure 7B).

The TAT-Gel-B4 was observed from the body for a short period (less than 6 hrs) when administered alone (Figure 8A). However, by administration as a complex with IgG-Hep-C5 or T84.66-Hep-C5, the TAT-Gel-B4 was visible over 48 hr (Figure 8B and 8C). Furthermore, by administration as a complex with IgG-Hep-C5 or T84.66-Hep-C5, enhanced accumulation of TAT-Gel-B4 was observed in the tumor (Figure 8B and 8C).

When the mean fluorescence intensity of TAT-Gel-B4 in the tumors was plotted as a function of time (Figure 9A), a 7-fold and a 58-fold increase in tumor exposure (AUC) of the TAT-Gel-B4 was observed by administration as a complex with IgG-Hep-C5 and T84.66-Hep-C5, respectively (Figure 9A). The relative fluorescence intensities of the TAT-Gel-B4 in the dissected tumors are shown in Figure 9B.

4.5 Discussion

Heparin, a clinically approved anticoagulant,[19] is an attractive biomaterial applicable for developing drug delivery systems (DDS), as it is biodegradable, biocompatible and less toxic.[20] Added to the above characteristics, heparin possesses a unique property, exceptionally high negative charge density on the molecule surface, which enables heparin to serve as an effective affinity tag for coupling two molecules.[21] On the other hand, CPPs which are well known for their cell translocating ability also have potentials to serve as an affinity linker due to their highly cationic nature.[22] In this work, by utilizing the exquisite merits of both the heparin and CPPs, we developed a heparin functionalized mAb, T84.66-Hep, by chemical conjugation method and evaluated the *in vivo* applicability for tumor targeted delivery of a CPP-modified toxin was explored.

The T84.66-Hep was prepared *via* a thioether linkage between the thiol group introduced to T84.66 and the maleimide group of the heparin-PEG conjugate. Structurally, heparin consists of a linear polymer with repeating units of disaccharide which are abundant in carboxyl groups.[23] The sugar residues and the carboxyl groups of heparin have been the main target sites for chemical conjugation. In previous studies, the

sugar residues have been successfully utilized for conjugation of heparin to nanoparticle[24] and antibody[25] by generating amine-reactive aldehyde groups using nitrous acid-induced deamination reaction[25, 26]. However, this method has a major drawback. During heparin activation with nitrous acid, fragmentation of heparin inadvertently occurs under the acidic environment (pH 2.5) which is necessary for the reaction.[25, 26] Hence, this method is not suitable to conjugate the full length heparin. Another method for heparin activation is using the EDC chemistry to functionalize the carboxyl groups on the heparin. The EDC enables heparin activation without causing degradation of the heparin.[27] Furthermore, EDC-activated carboxyl groups of heparin which are not incorporated in the conjugation reaction are rapidly reversed to their original carboxyl groups *via* hydrolysis.[27] Therefore, considering the merits of the EDC activation method, in this study, we chose to use the EDC for the heparin activation.

For conjugation of T4.66 with the EDC-activated heparin, a short heterobifunctional PEG (NH_2-PEG-MAL, 3.5 kDa) was used as a cross-linker. Compared with the small molecule cross-linkers, the PEG composed of extended and flexible polymer chain can provide an effective way to alleviate aggregation issues which frequently occurs during conjugation of highly charged bio-molecules. Indeed in this study, by utilizing the EDC for heparin activation and the PEG as a cross-linker, T84.66 and heparin could be successfully conjugated to each other with no aggregation. The preparation and purification of final the T84.66-Hep product was confirmed by the anion exchange chromatogram (Figure 2A), SDS-PAGE result (Figure 2B) and the T84.66 and heparin quantification results (Figure 2C).

Once the T84.66-Hep was successfully prepared, the CEA binding specificity of T84.66-Hep was evaluated *in vitro via* cell binding assay and ELISA. From the cellular studies using confocal microscopy, the binding of T84.66-Hep to the LS174T CEA high expression cells was clearly visible (Figure 3), while, the T84.66-Hep showed only minimal binding to the HCT116 CEA low expression cells and the LS174T cells pre-treated with excess of unlabeled T84.66 (Figure 3). The CEA binding ability of T84.66-Hep was, further, confirmed by the ELISA assay results. It was found that the T84.66-Hep can bind to the CEA with slightly lower binding affinity (69% of T84.66) compared with the T84.66 (Figure 4 and Table 1). However, caution is required for interpreting the ELISA results, as it might be underestimating the actual CEA binding ability of T84.66-Hep, because heparin conjugation to the T84.66 can not only affect the binding of T84.66 to the CEA, but also interfere the binding of goat anti-mouse-IgG-alkaline phosphatase to the T84.66. Thus, the T84.66-Hep binding affinity to CEA might be higher than what is reported here.

While the results showing specific CEA binding was encouraging, it is also required for the T84.66-Hep to form a tight complex with the TAT-Gel to achieve tumor targeted delivery. The plasma stability of the interaction between T84.66-Hep and TAT-Gel was investigated *in vitro* using protamine beads. The study results showed that majority of the T84.66-Hep (68%) could stably bind to the surface of protamine beads up to 24 hrs (Figure 5). Although the interaction between T84.66-Hep and TAT-Gel is likely to be weaker than that between T84.66-Hep and protamine, as protamine consists of more basic residues (21 arginines) than TAT (6 arginines and 2 lysines)[28, 29], the result suggests that T84.66-Hep can strongly bind to cationic peptides and maintain the bond in the

plasma. In a previous study, the plasma stability of TAT-Gel binding to immobilized heparin was also investigated under similar experimental condition. It was found that more than 80% of the TAT-Gel remained bound on the heparin beads after 24 hrs of incubation at 37°C in the presence of plasma (Chapter 3). Considering the above study results, the formation and maintenance of T84.66-Hep/TAT-Gel complex *in vivo* appeared feasible.

Inspired by the promising *in vitro* assay results, the applicability of T84.66-Hep for tumor targeted delivery of the TAT-Gel was investigated *in vivo*. Previously, NIR dyes have been successfully applied for the live animal imaging, due to their great tissue penetrating ability[30, 31] and low background interference caused by animal tissues.[30] Therefore, in this study, we labeled the TAT-Gel and the mAb samples including T84.66-Hep with different NIR dyes, B4 and C5, respectively. The tumor targeting feature of T84.66-Hep/TAT-Gel was demonstrated from the animal images. Localized accumulation of T84.66-Hep-C5 was apparent in the tumor after administration of the T84.66-Hep-C5/TAT-Gel-B4 (Figure 7A), while the images of the control mice (administered with PBS, C5 or IgG-C5) showed no evidence of targeting (Figure 7B). Furthermore, when the T84.66-Hep-C5 and TAT-Gel-B4 were simultaneously imaged in the same mouse after administration of the T84.66-Hep-C5/TAT-Gel-B4, both the components of the DDS were found co-localized in the tumor (Figure 7A and 8C).

Interestingly, higher tumor accumulation of TAT-Gel-B4 was achieved (7-fold increase of AUC) by administration as a complex with IgG-Hep than by injection of TAT-Gel alone (Figure 8A and 8B). This may be explained by extended blood circulation of the TAT-Gel-B4 *via* complex formation (Figure 8B). However, the most dramatic

change in TAT-Gel tumor accumulation was accomplished by the T84.66-Hep-C5/TAT-Gel-B4 administration. Remarkably, 58-fold increased drug exposure (AUC) of TAT-Gel was accomplished by administration of the T84.66-Hep/TAT-Gel, compared with injection of TAT-Gel alone. Overall, the hypothesis that TAT-Gel can be targeted to tumor *via* complex formation with T84.66-Hep was evidenced by the *in vivo* imaging studies.

4.6 Conclusions

In this research, a heparin functionalized mAb, T84.66-Hep, was developed for tumor targeted delivery of a CPP-modified toxin, TAT-Gel. The T84.66-Hep was successfully prepared by chemical conjugation using a heterobifunctional PEG as the cross-linker. Both *in vitro* and *in vivo* assays demonstrated that T84.66-Hep can form a complex with TAT-Gel, and, *via* specific binding to CEA expressed on the tumor cells, T84.66-Hep could provide enhanced delivery of TAT-Gel to the tumor. By administration of TAT-Gel as a complex with T84.66-Hep, significantly enhanced tumor exposure of TAT-Gel (58-fold) was accomplished. Overall, this study demonstrated a convenient but effective strategy to target and deliver highly potent toxins selectively to tumor.

4.7 Tables

Table 4-1. Summary for the ELISA assay results of T84.66 and T84.66-Hep

T84.66 concentration (ng/mL)	10	25	50	75	100
$R_{T84.66}$	91 ± 5	144 ± 9	231 ± 16	258 ± 27	304 ± 14
$R_{T84.66\text{-}Hep}$	66 ± 6**	99 ± 12**	148 ± 25**	177 ± 17*	217 ± 13**
$R_{T84.66\text{-}Hep}/R_{T84.66}$ (%)	73	69	64	69	71

[a]R values are displayed as a.u./min (a.u. is arbitrary unit). Comparison between $R_{T84.66}$ and $R_{T84.66\text{-}Hep}$ was performed using student t-test (unpaired t-test, two tailed) and $*P < 0.05$, $**P < 0.01$. For all experiments, N=3.

4.8 Figures

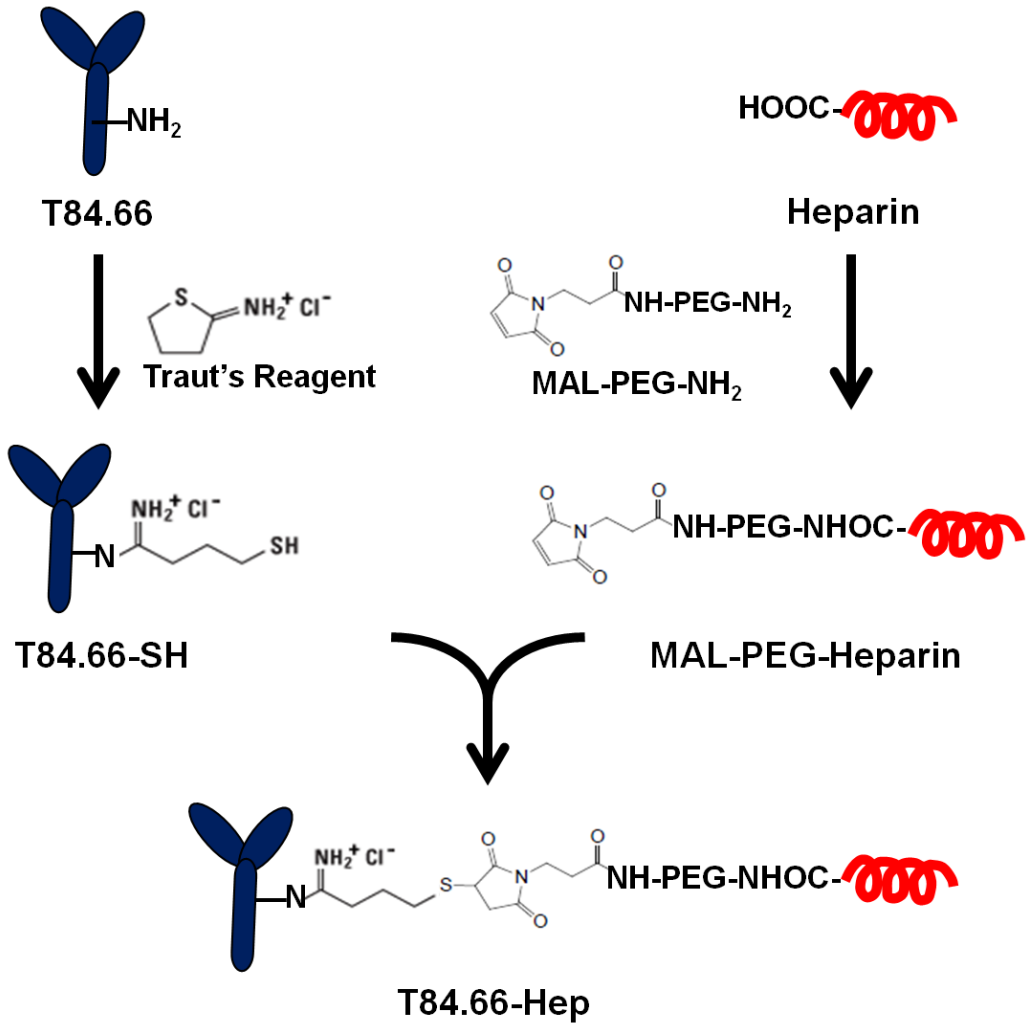

Figure 4-1. Schematic illustration of T84.66-Hep chemical conjugation.

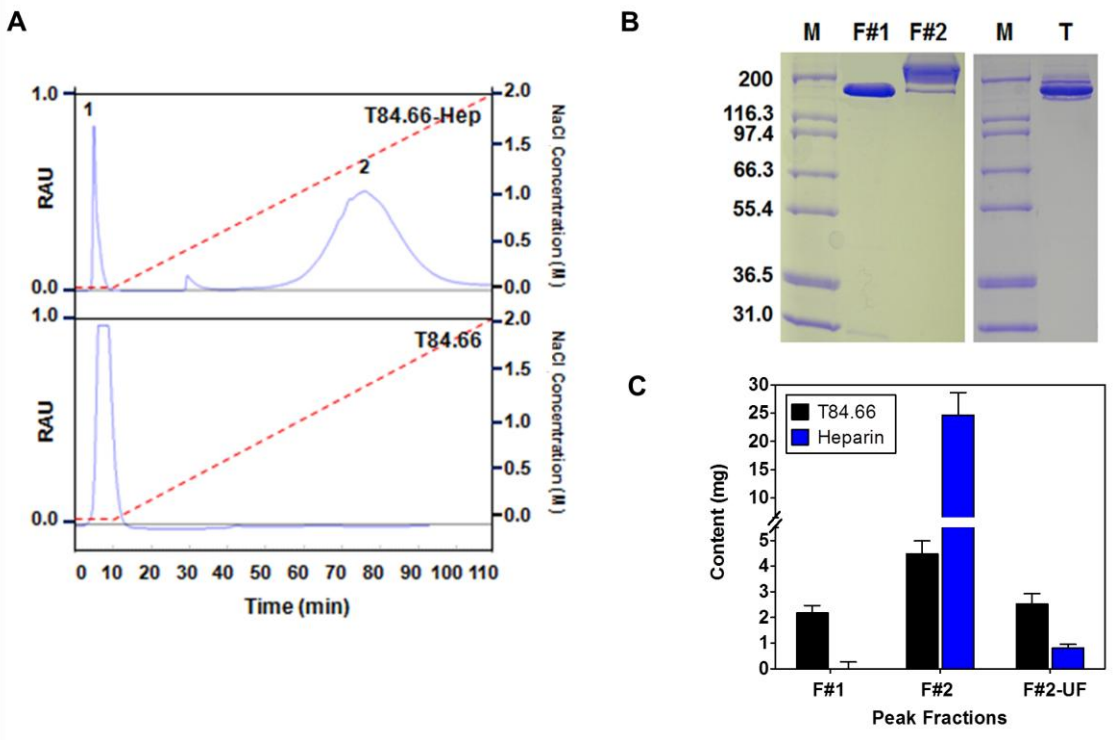

Figure 4-2. Purification of T84.66-Hep.

(A) Chromatograms of T84.66 (upper) and T84.66-Hep (lower) from an anion exchange column. The results are displayed with the RAU (relative absorbance unit) according to the retention time (min). Buffer A: 50 mM phosphate buffer, B: 50 mM PBS (pH 7.4, 2 M NaCl). The NaCl gradient applied for elution of T84.66-Hep is displayed as a red dotted line. T84.66-Hep was eluted at 0.8 - 1.8 M NaCl, while unreacted T84.66 eluted at the beginning without NaCl gradient; (B) SDS-PAGE results of the two separate peak fractions obtained from T84.66-Hep purification by anion exchange column. Lane M: Mark12 protein molecular weight standard (Invitrogen, Carlsbad, CA). Lane 1 and 2: peak fractions 1 and 2 from T84.66-Hep elution. Lane T: T84.66; (C) T84.66 and heparin contents in the peak fractions 1, 2 or 2 after ultrafiltration (molecular weight cut-off: 100 kDa).

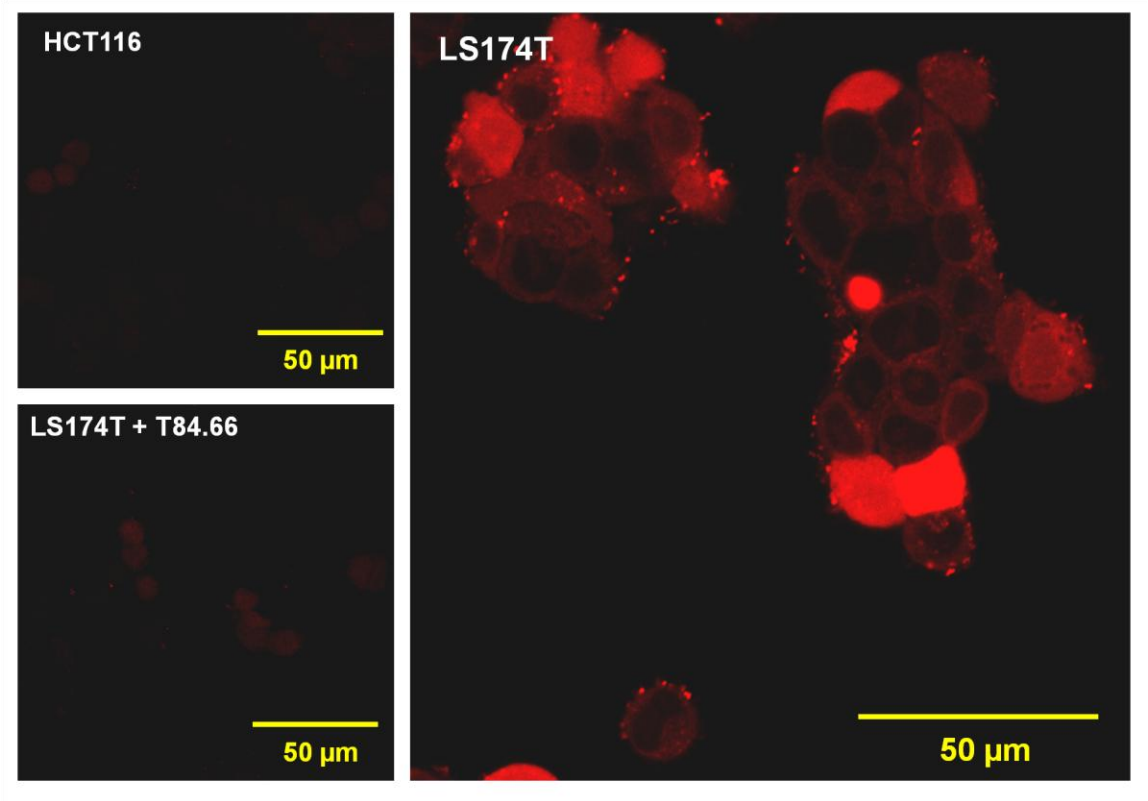

Figure 4-3. Confocal microscopic images of (A) HCT116 and (B) LS174T cells incubated with rhodamine-labeled T84.66-Hep, and (C) LS174T cells incubated with 10-fold molar excess of T84.66 followed by rhodamine-labeled T84.66-Hep.

Cell images were taken by Nikon A1R-A1 confocal laser microscope (Nikon Instruments Inc., Melville, NY).

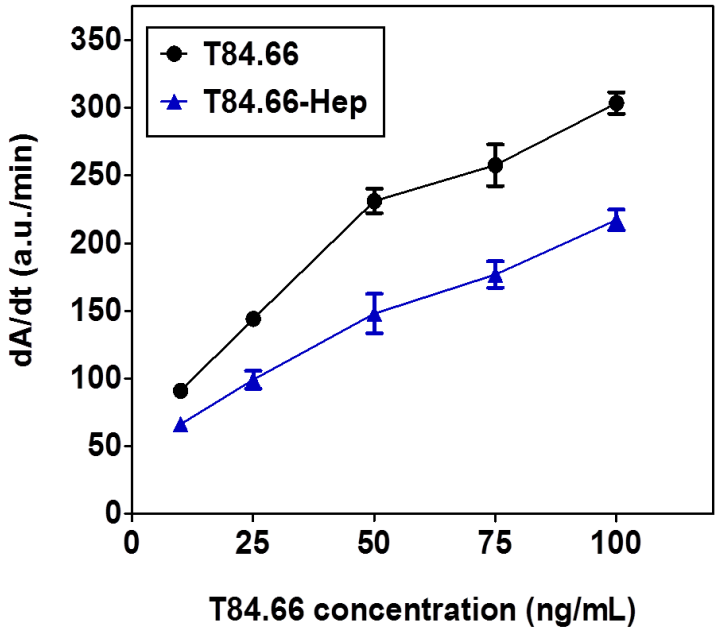

Figure 4-4. ELISA assay results of T84.66 and T84.66-Hep tested against recombinant carcinoembryonic antigen (rCEA, R&D SYSTEMS).

T84.66 and T84.66-Hep of different concentrations (0, 10, 25, 50, 75 or 100 ng/mL) were separately incubated with rCEA (400 ng/mL, 250 µL/well) coated on 96-well plates for 2 hours. After wash, the bound T84.66 and T84.66-Hep were further incubated with Fc specific goat anti-mouse IgG-alkaline phosphatase. For detection, 100 µL of p-nitro phenyl phosphate (1-step PNPP, Thermo Scientific) was added to each well and the change in absorbance at 405nm (dA/dt) was monitored by a microplate reader using kinetic mode. (CEA: carcinoembryonic antigen).

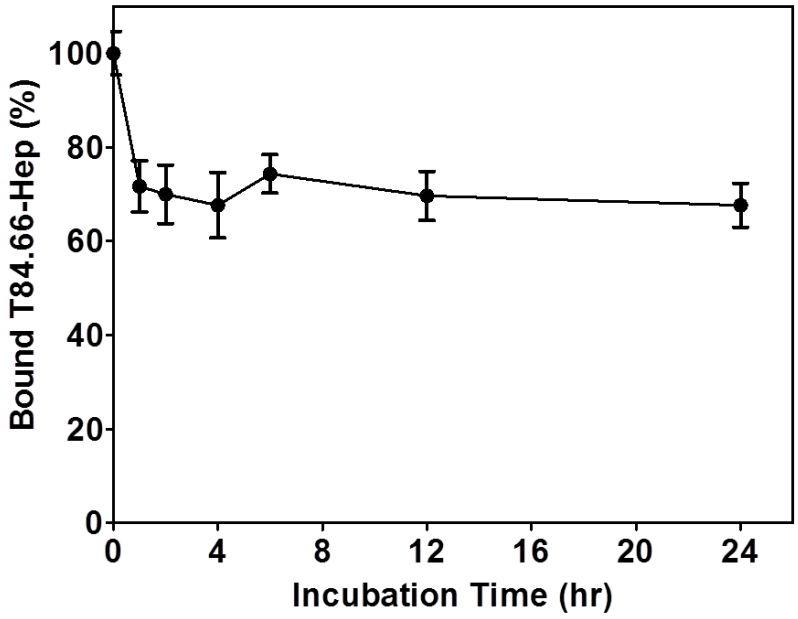

Figure 4-5. *In vitro* plasma stability of T84.66-Hep binding with cationic protamine immobilized beads (Protamine-Agarose, Sigma-Aldrich).

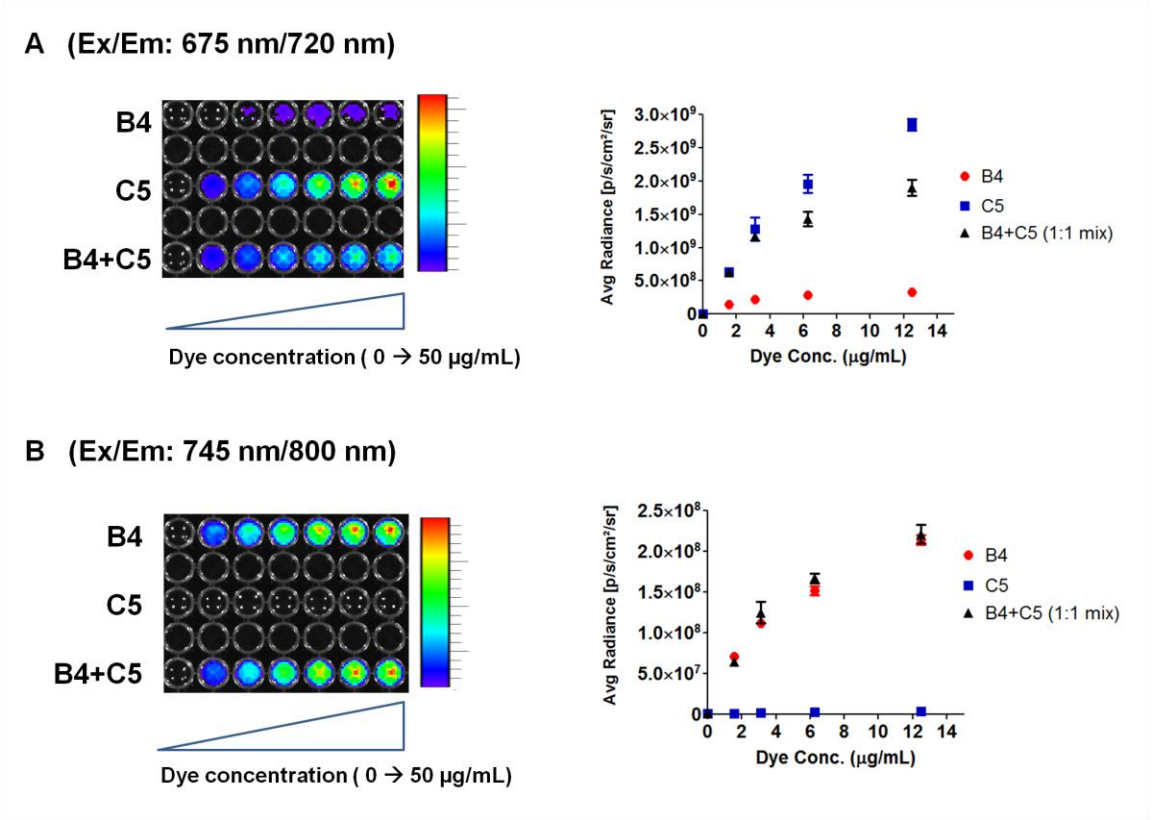

Figure 4-6. Images of C5 and B4 under investigation of interference or quenching.

0 - 50 µg/mL of C5, B4, or mixture of C5 and B4 (1:1) were imaged at Ex/Em wavelength of (A) 675nm/720nm (optimal for detection of C5); and (B) 745nm/800nm (optimal for detection of B4) by IVIS® spectrum imaging system (Xenogen, Alameda, CA). (C5: Dylight 679-C5 dye and B4: Dylight 775-B4 dye)

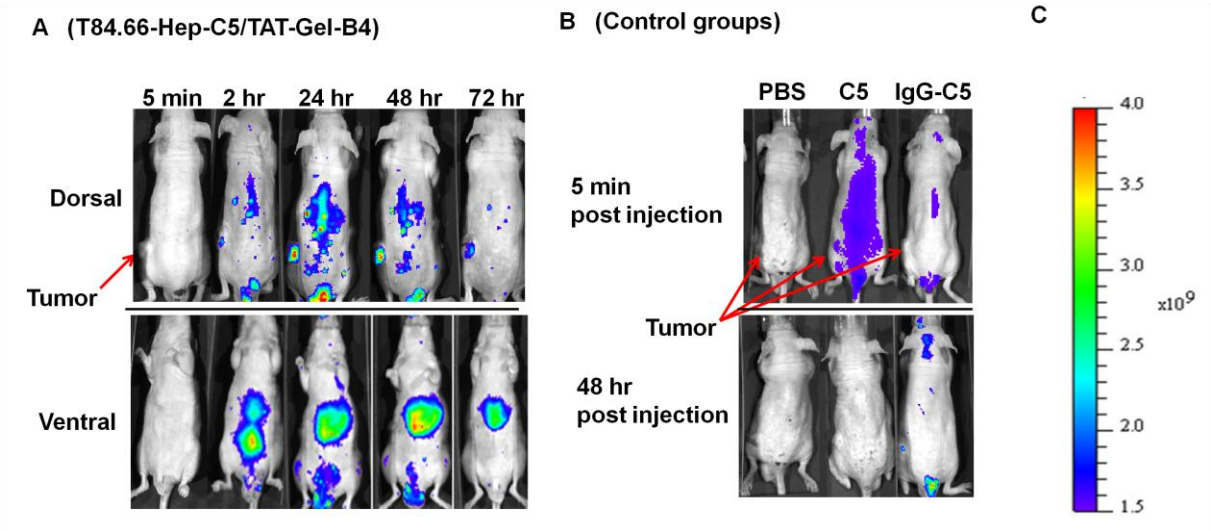

Figure 4-7. Fluorescence images of athymic nude mice bearing LS174T xenograft tumor after *i.v.* injection of (A) T84.66-Hep-C5/TAT-Gel-B4; (B) PBS, C5 or nonspecific murine IgG-C5.

Animal images were taken using Cy5.5 filter at Ex/Em wavelength of 675 nm/720 nm (specific for C5 detection) by IVIS® spectrum imaging system (Xenogen, Alameda, CA). (C5: Dylight 679-C5 dye and B4: Dylight 775-B4 dye)

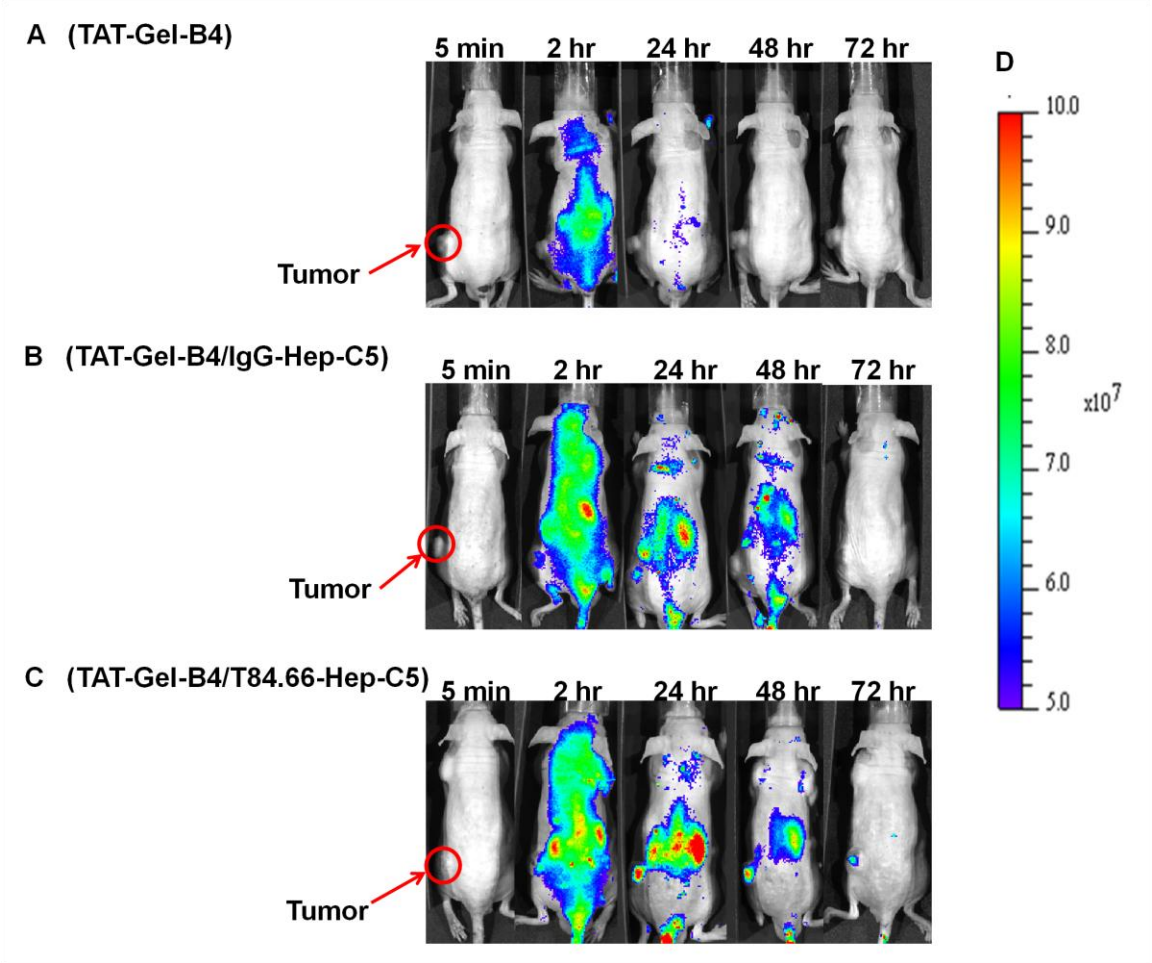

Figure 4-8. Fluorescence images of athymic nude mice bearing LS174T xenograft tumor after *i.v.* injection of (A) TAT-Gel-B4; (B) non-specific IgG-Hep-C5/TAT-Gel-B4; or (C) T84.66-Hep-C5/TAT-Gel-B4.

Animal images were taken using ICG filter with Ex/Em wavelength of 745 nm/800 nm (specific for B4 detection) by the IVIS® spectrum imaging system (Xenogen, Alameda, CA); (D) Scale bar for the relative fluorescence intensity. (C5: Dylight 679-C5 dye and B4: Dylight 775-B4 dye)

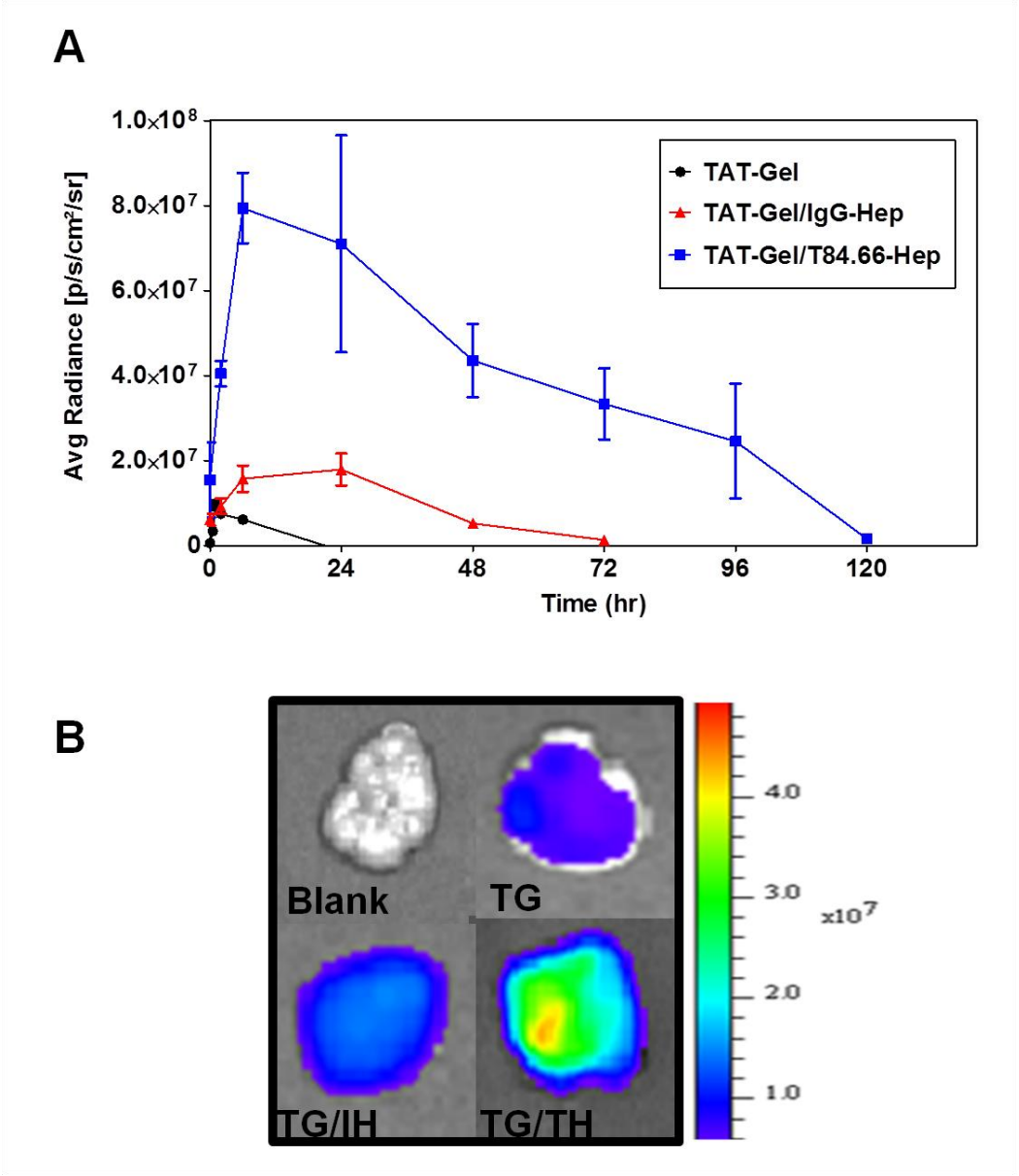

Figure 4-9. Intra-tumor accumulation of TAT-Gel-B4.

(A) Mean fluorescence intensity of TAT-Gel-B4 in tumors after administration of TAT-Gel-B4, IgG-Hep-C5/TAT-Gel-B4, or T84.66-Hep-C5/TAT-Gel-B4. The tumor from each animal image taken by IVIS® spectrum imaging system (Xenogen, Alameda, CA) was designated as the region of interest (ROI) and the fluorescence intensity of each ROI was acquired by subtracting the mean fluorescence intensity of the corresponding ROI on the control blank mice. The images were analyzed using Living Image 2.5 software (Xenogen, Alameda, CA) and the results are displayed with the average radiance (p/s/cm²/sr) according to time (hr); (B) Fluorescence images of the tumors dissected from mice 6hrs after no treatment (blank), or administration of TAT-Gel-B4, IgG-Hep-C5/TAT-Gel-B4, or T84.66-Hep-C5/TAT-Gel-B4.

4.9 References

1. Wu AM, Senter PD. Arming antibodies: prospects and challenges for immunoconjugates. Nat Biotechnol 2005;23:1137-46.
2. Adams GP, Weiner LM. Monoclonal antibody therapy of cancer. Nat Biotechnol 2005;23:1147-57.
3. Gold P, Freedman SO. Specific carcinoembryonic antigens of the human digestive system. J Exp Med 1965;122:467-81.
4. Hammarstrom S. The carcinoembryonic antigen (CEA) family: structures, suggested functions and expression in normal and malignant tissues. Semin Cancer Biol 1999;9:67-81.
5. Meyer T, Gaya AM, Dancey G, Stratford MR, Othman S, Sharma SK, Wellsted D, Taylor NJ, Stirling JJ, Poupard L, Folkes LK, Chan PS, Pedley RB, Chester KA, Owen K, Violet JA, Malaroda A, Green AJ, Buscombe J, Padhani AR, Rustin GJ, Begent RH. A phase I trial of radioimmunotherapy with 131I-A5B7 anti-CEA antibody in combination with combretastatin-A4-phosphate in advanced gastrointestinal carcinomas. Clin Cancer Res 2009;15:4484-92.
6. Shibata S, Raubitschek A, Leong L, Koczywas M, Williams L, Zhan J, Wong JY. A phase I study of a combination of yttrium-90-labeled anti-carcinoembryonic antigen (CEA) antibody and gemcitabine in patients with CEA-producing advanced malignancies. Clin Cancer Res 2009;15:2935-41.
7. Sharkey RM, Hajjar G, Yeldell D, Brenner A, Burton J, Rubin A, Goldenberg DM. A phase I trial combining high-dose 90Y-labeled humanized anti-CEA monoclonal antibody with doxorubicin and peripheral blood stem cell rescue in advanced medullary thyroid cancer. J Nucl Med 2005;46:620-33.
8. Avila AD, Mateo de Acosta C, Lage A. A carcinoembryonic antigen-directed immunotoxin built by linking a monoclonal antibody to a hemolytic toxin. Int J Cancer 1989;43:926-9.
9. Neumaier M, Shively L, Chen FS, Gaida FJ, Ilgen C, Paxton RJ, Shively JE, Riggs AD. Cloning of the genes for T84.66, an antibody that has a high specificity and affinity for carcinoembryonic antigen, and expression of chimeric human/mouse T84.66 genes in myeloma and Chinese hamster ovary cells. Cancer Res 1990;50:2128-34.
10. Urva SR, Balthasar JP. Target mediated disposition of T84.66, a monoclonal anti-CEA antibody: application in the detection of colorectal cancer xenografts. MAbs 2010;2:67-72.
11. Keppler-Hafkemeyer A, Kreitman RJ, Pastan I. Apoptosis induced by immunotoxins used in the treatment of hematologic malignancies. Int J Cancer 2000;87:86-94.
12. Hertler AA, Frankel AE. Immunotoxins: a clinical review of their use in the treatment of malignancies. J Clin Oncol 1989;7:1932-42.
13. Ellman GL. Tissue sulfhydryl groups. Arch Biochem Biophys 1959;82:70-7.

14. Jaques LB, Wollin A. A modified method for the colorimetric determination of heparin. Can J Physiol Pharmacol 1967;45:787-94.
15. Cole AJ, David AE, Wang J, Galban CJ, Hill HL, Yang VC. Polyethylene glycol modified, cross-linked starch-coated iron oxide nanoparticles for enhanced magnetic tumor targeting. Biomaterials 2011;32:2183-93.
16. Urva SR, Yang VC, Balthasar JP. An ELISA for quantification of T84.66, a monoclonal anti-CEA antibody, in mouse plasma. J Immunoassay Immunochem 2010;31:1-9.
17. Troy T, Jekic-McMullen D, Sambucetti L, Rice B. Quantitative comparison of the sensitivity of detection of fluorescent and bioluminescent reporters in animal models. Mol Imaging 2004;3:9-23.
18. Billinton N, Knight AW. Seeing the wood through the trees: a review of techniques for distinguishing green fluorescent protein from endogenous autofluorescence. Anal Biochem 2001;291:175-97.
19. Agnelli G, Piovella F, Buoncristiani P, Severi P, Pini M, D'Angelo A, Beltrametti C, Damiani M, Andrioli GC, Pugliese R, Iorio A, Brambilla G. Enoxaparin plus compression stockings compared with compression stockings alone in the prevention of venous thromboembolism after elective neurosurgery. N Engl J Med 1998;339:80-5.
20. Sun IC, Eun DK, Na JH, Lee S, Kim IJ, Youn IC, Ko CY, Kim HS, Lim D, Choi K, Messersmith PB, Park TG, Kim SY, Kwon IC, Kim K, Ahn CH. Heparin-coated gold nanoparticles for liver-specific CT imaging. Chemistry 2009;15:13341-7.
21. Absar S, Choi S, Yang VC, Kwon YM. Heparin-triggered release of camouflaged tissue plasminogen activator for targeted thrombolysis. J Control Release 2012;157:46-54.
22. Kwon YM, Li YT, Liang JF, Park YJ, Chang LC, Yang VC. PTD-modified ATTEMPTS system for enhanced asparaginase therapy: a proof-of-concept investigation. J Control Release 2008;130:252-8.
23. Nagarajan M, Rao VS. Conformational studies of proteoglycans: theoretical studies on the conformation of heparin. Biopolymers 1979;18:1407-20.
24. Chertok B, David AE, Yang VC. Magnetically-enabled and MR-monitored selective brain tumor protein delivery in rats via magnetic nanocarriers. Biomaterials 2011;32:6245-53.
25. Liang JF, Park YJ, Song H, Li YT, Yang VC. ATTEMPTS: a heparin/protamine-based prodrug approach for delivery of thrombolytic drugs. J Control Release 2001;72:145-56.
26. Shively JE, Conrad HE. Formation of anhydrosugars in the chemical depolymerization of heparin. Biochemistry 1976;15:3932-42.
27. Wang XH, Li DP, Wang WJ, Feng QL, Cui FZ, Xu YX, Song XH. Covalent immobilization of chitosan and heparin on PLGA surface. Int J Biol Macromol 2003;33:95-100.
28. Magzoub M, Graslund A. Cell-penetrating peptides: [corrected] from inception to application. Q Rev Biophys 2004;37:147-95.
29. Park YJ, Chang LC, Liang JF, Moon C, Chung CP, Yang VC. Nontoxic membrane translocation peptide from protamine, low molecular weight

protamine (LMWP), for enhanced intracellular protein delivery: in vitro and in vivo study. FASEB J 2005;19:1555-7.
30. Frangioni JV. In vivo near-infrared fluorescence imaging. Curr Opin Chem Biol 2003;7:626-34.
31. Zou P, Xu S, Povoski SP, Wang A, Johnson MA, Martin EW, Jr., Subramaniam V, Xu R, Sun D. Near-infrared fluorescence labeled anti-TAG-72 monoclonal antibodies for tumor imaging in colorectal cancer xenograft mice. Mol Pharm 2009;6:428-40.

Chapter 5

Application of CPP-modified ATTEMPTS for Enhanced Toxin-Based Colorectal Cancer Therapy: Proof-of-Concept Investigation

5.1 Abstract

In the previous chapters, the two components of the CPP-modified ATTEMPTS, recombinant TAT-gelonin chimera (TAT-Gel) and T84.66 and heparin chemical conjugate (T84.66-Hep), were successfully produced and characterized for their potencies. On this basis, the aim for this chapter was to combine the two components into a DDS and evaluate the feasibility of applying CPP-modified ATTEMPTS for toxin-based colorectal cancer therapy.

Cytotoxicity studies revealed that T84.66-Hep can effectively block the TAT-Gel cell internalization, as T84.66-Hep/TAT-Gel complex yielded markedly reduced cell death, compared with incubation of the cells with TAT-Gel alone. However, when protamine was added to the cells pre-treated with the T84.66-Hep/TAT-Gel complex, significantly higher level of cytotoxicity was observed, indicating successful reversal of the heparin-mediated block of TAT. The PK and biodistribution studies further showed that TAT-Gel could tightly bind with T84.66-Hep in the blood circulation and be

delivered to tumor. By administered as a complex with T84.66-Hep, the PK profiles of TAT-Gel were markedly changed (17-fold increase of the plasma half-life) and, obvious through biodistribution studies, significantly enhanced tumor exposure to TAT-Gel (58-fold) was accomplished, in comparison with injection of TAT-Gel alone.

Based on the above encouraging results, the *in vivo* toxicity and therapeutic efficacy of TAT-Gel in conjunction with the CPP-modified ATTEMPTS was evaluated in an s.c. LS174T xenograft tumor mouse model. Compared with TAT-Gel, the T84.66-Hep/TAT-Gel complex displayed significantly reduced toxicity. Furthermore, by T84.66-Hep/TAT-Gel complex treatment followed with protamine injection (T84.66-Hep/TAT-Gel+Pro) after 24 hrs, the most significant therapeutic effects (70% inhibition of tumor growth) were accomplished, while no therapeutic effects were observed by administration of TAT-Gel alone even at close to its maximum tolerable dose (MTD). Overall, this study demonstrated the feasibility of CPP-modified ATTEMPTS application for enhanced toxin-based cancer therapies.

5.2 Introduction

The previous chapters provided data for production and characterization of TAT-Gel and T84.66-Hep, the two components of the CPP-modified ATTEMPTS. TAT-Gel was proven for its great tumoricidal activity, which was further found controllable by heparin/protamine-mediated regulation (Chapter 3). Moreover, it was realized that T84.66-Hep can deliver TAT-Gel selectively to tumor by forming a tight complex (see Chapter 4). Based on the previous findings, in this chapter, the functionality of CPP-modified ATTEMPTS is investigated *in vitro* and *in vivo*.

The DDS is first evaluated *in vitro* by cytotoxicity studies on LS174T human adenocarcinoma cell line, using similar protocols described in Chapter 3. Cytotoxicity levels are assessed for the T84.66-Hep/TAT-Gels after preparation with various T84.66-Hep-to-TAT-Gel molar ratios. The effect of protamine addition to the T84.66-Hep/TAT-Gel cytotoxcity is also investigated, using different protamine-to-T84.66-Hep molar ratios and addition time points.

After the *in vitro* characterizations, the *in vivo* stability, tumor targeting and acute toxicity of the T84.66-Hep/TAT-Gel is further investigated by PK, biodistribution and MTD determination studies. Based on the T84.66-Hep/TAT-Gel behavior profiles in the body and the severity of toxicity, the dosing regimen and the protamine administration time are determined. Finally, the therapeutic efficacy of TAT-Gel with the CPP-modified ATTEMPTS is evaluated using a LS174T xenograft tumor bearing nude mice. Eventually, the feasibility to apply this DDS for toxin-based cancer therapy is explored.

5.3 Materials and Methods

5.3.1 Cell Culture

LS174T human adenocarcinoma cells were purchased from American Type Culture Collection (ATCC) (Manassas, VA). The cells were cultured in a 75 cm^2 flask and maintained in a humidified incubator at 37°C (5% CO_2). The cells were cultured in DMEM with 2 mM L-glutamine, high glucose, 1% (v/v) penicillin-streptomycin, and 10% FBS. Culture media in the flasks was replaced by fresh media every two days, and

the cells were sub-cultured when it was confluent, by detaching with 0.25% trypsin-EDTA.

5.3.2 *In Vitro* Evaluation of CPP-Modified ATTEMPTS

The T84.66-Hep block of TAT-Gel cell internalization and protamine-induced reversal of the heparin-mediated block was evaluated *via* cytotoxicity study using XTT assay. LS174T cells were dispensed into 96-well plates at a density of 5×10^3 cells per well. When the cells were attached on the bottom of the plates, TAT-Gel and T84.66-Hep/TAT-Gel were separately added to the wells (TAT-Gel concentration: 10^{-10} - 10^{-5} M, N=3). T84.66-Hep/TAT-Gel was prepared by mixing the TAT-Gel with T84.66-Hep (Hep:TAT = 3:1, 1:1, 1:3, 1:5 or 1:10) and incubation for 30 min at 4°C. To evaluate the protamine-induced reversal of the T84.66-Hep block, different amount of protamine sulfate (Hep:Pro molar ratio = 1:2, 1:1, 1:0.3 or 1:0.2) was immediately added to the cells pre-incubated with T84.66-Hep/TAT-Gel (Hep:TAT = 1:3). Additionally, to evaluate the effect of protamine addition time to the reversal of the T84.66-Hep inhibition, cells were first incubated with T84.66-Hep/TAT-Gel (Hep:TAT = 1:3, 1 μM TAT-Gel conc.) and, at different time points (2 hr-, 6 hr-, 24 hr-, 48 hr-post-incubation with T84.66-Hep/TAT-Gel), washed with PBS and then treated with protamine (Hep:Pro = 1:10). Cells were incubated at 37 °C for total 72 hrs after treatment of TAT-Gel or T84.66-Hep/TAT-Gel and the relative cell proliferation was measured by XTT assay.

5.3.3 Animal Studies

All animal experiments were conducted according to protocols approved by the University of Michigan Committee on Use and Care of Animals (UCUCA).

NIR Dye Labeling

The T84.66 and T84.66-Hep were labeled with Dylight 679-C5 (C5) and the rGel and TAT-Gel were labeled with Dylight 775-B4 (B4), following the vendor's protocol (Thermo Scientific, Rockford, IL). Briefly, the protein samples (10 mg/mL in 20 mM sodium bicarbonate buffer; pH 9.3) were incubated with 5-fold molar excess of the NIR dyes (10 mg/mL in DMF) for 2 hrs at room temperature, and the labeled proteins were purified using dye removal resins (Thermo Scientific, Rockford, IL).

Plasma Pharmacokinetics (PK) Analyses of T84.66, T84.66-Hep, rGel, TAT-Gel and T84.66-Hep/TAT-Gel

PK studies for T84.66, T84.66-Hep, rGel, TAT-Gel and T84.66-Hep/TAT-Gel were performed with C57BL/6 mice (body weight: 25 ~ 28 g, Charles Rivers Laboratories, Raleigh, NC). Three days after arrival, the mice were randomly divided into 5 groups and administered with: 1) 11 mg/kg of T84.66-C5, 2) 11 mg/kg of T84.66-Hep-C5, 3) 5 mg/kg of rGel-B4, 4) 5 mg/kg of TAT-Gel-B4 or 5) T84.66-Hep/TAT-Gel (11 mg/kg of T84.66-Hep and 5 mg/kg of TAT-Gel) *via* tail vein injection. At intended time points, blood was collected and the plasma samples were obtained by centrifugation at 3000 rpm for 5 min. To determine the PK profiles of T84.66, blood was withdrawn at 0 hr, 1hr, 2 hr, 6 hr, 24 hr, 48 hr, 72 hr, 96 hr, 168 hr, 240 hr, 288 hr and 504 hr post-injection (total 12 time points), and for the T84.66-Hep, blood was collected at 0 hr, 0.5 hr, 1 hr, 2 hr, 4 hr, 6 hr, 12 hr, 24 hr and 48 hr post-injection (total 9 time points). To obtain the PK profiles of rGel and TAT-Gel, blood was taken at 0 min, 2 min, 5 min, 10 min and 30 min post-injection (total 5 time points), and for the T84.66-Hep/TAT-Gel,

blood was collected at 0 min, 5 min, 15 min, 30 min, 1 hr, 2 hr, 3 hr, 4 hr, 6 hr, 12 hr and 24 hr post-injection (total 11 time points).

The plasma samples were dispensed in a black 96 well plate and the fluorescence intensity of each well was measured *via* the IVIS® spectrum imaging system (Xenogen, Alameda, CA). The Ex/Em wavelength of 675 nm/720 nm was used for measurement of the T84.66-C5 and the T84.66-Hep-C5 and the Ex/Em wavelength of 745 nm/800 nm was utilized for assessment of both the rGel-B4 and TAT-Gel-B4. Exposure time (2 s), binning (8), *f/*stop (4 for C5 labeled-T84.66 and T84.66-Hep, 1 for B4 labeled-rGel and TAT-Gel) and fields of view (25 cm x 25 cm) were used identically for imaging the samples. Each well of the images was designated as region of interest (ROI) and the fluorescence intensity was analyzed using Living Image 2.5 software (Xenogen, Alameda, CA). The fluorescence intensity of each ROI was determined by subtracting the mean fluorescence intensity of blank wells. The plasma concentration of T84.66, T84.66-Hep, rGel and TAT-Gel was calculated using standard curves prepared with the NIR dye labeled standard solutions, and their PK profiles were analyzed by Phoenix WinNonlin 6.3 (Pharsight, Sunnyvale, CA).

LS174T S.C. Xenograft Tumor Mice Model

Male athymic nude mice (body weight: 23 ~ 27 g, 6 weeks old) were purchased from Charles Rivers Laboratories (Raleigh, NC). Mice were housed in sterile animal facilities and fed by standard chow diet. At day 0 (three days after arrival), LS174T cells (5×10^6 cells/mice) were implanted (s.c.) in the left flank region of the mice. For the biodistribution studies, after tumor implantation, the mice were fed by special alfalfa-free diet (AIN-76A rodent diet, gamma-irradiated, Research Diets, Inc, New Brunswick, NJ)

to reduce the autofluorescence during the tissue imaging.[1] The tumor growth and the body weight were monitored daily. The tumor size was measured using a vernier caliper and the volume was calculated by the formula of V (mm^3) = (w^2 x l) / 2. In the equation, w is the width and l is the length of the tumor. The biodistribution and the efficacy studies were performed when the average tumor size reached 500 mm^3 (at day 25) and 30 mm^3 (at day 3), respectively.

Biodistribution of TAT-Gel and T84.66-Hep/TAT-Gel

The tissue distribution of TAT-Gel and T84.66-Hep/TAT-Gel was determined in LS174T xenograft tumor bearing mice. When the average tumor size reached about 500 mm^3, the mice were administered with either 5 mg/kg of TAT-Gel-B4 or 2) T84.66-Hep-C5/TAT-Gel-B4 (11 mg/kg of T84.66-Hep-C5 and 5 mg/kg of TAT-Gel-B4) *via* tail vein injection. The mice injected with TAT-Gel were euthanized at 15 min, 1 hr, 5 hr and 24 hr post-injection, and the T84.66-Hep/TAT-Gel injected mice were euthanized at 2 hr, 24 hr, 48 hr and 72 hr post-injection, and the major organs including tumor, heart, liver, spleen, lung, kidney and intestine were harvested. The fluorescence intensity of each tissue was measured immediately by IVIS® spectrum imaging system (Xenogen, Alameda, CA) and analyzed using Living Image 2.5 software (Xenogen, Alameda, CA). The relative fluorescence intensity of each tissue sample was calculated by subtracting the mean fluorescence intensity of corresponding tissue from the blank mouse.

Determination of Maximum Tolerable Dose (MTD)

The MTD of TAT-Gel and T84.66-Hep/TAT-Gel was tested in C57BL/6 mice (body weight: 26 - 29 g, 6 weeks old, Charles Rivers Laboratories). The MTD was defined as the maximum drug dose administered once bolus to non-tumor bearing mice

without mortality. The mice were administered with either TAT-Gel (dose: 9 mg/kg, 18 mg/kg, 36 mg/kg and 72 mg/kg) or T84.66-Hep/TAT-Gel (dose: T84.66-Hep 20 mg/kg with TAT-Gel 9 mg/kg, T84.66-Hep 40 mg/kg with TAT-Gel 18 mg/kg and T84.66-Hep 80 mg/kg with TAT-Gel 36 mg/kg) *via* tail vein injection (N=3). The T84.66-Hep/TAT-Gel was prepared by mixing the T84.66-Hep with the TAT-Gel and incubating for 30 min at room temperature. The mortality of the mice was monitored for 24 hr post-injection.

In Vivo Efficacy Studies

Three days after tumor implantation (at day 3) when average tumor size reached 30 mm^3, LS174T xenograft tumor mice were randomly divided into 5 groups and received: 1) PBS, 2) TAT-Gel (7 mg/kg), 3) T84.66-Hep/TAT-Gel (21 mg/kg T84.66-Hep and 7 mg/kg TAT-Gel), 4) T84.66-Hep/TAT-Gel+Pro (21 mg/kg T84.66-Hep, 7 mg/kg TAT-Gel and 10 mg/kg protamine) or 5) protamine (10 mg/kg) treatment. Each mouse was treated three times with the above recipe at day 3, 6 and 9 *via* tail vein injection. For each treatment, the T84.66-Hep/TAT-Gel was freshly prepared by mixing T84.66-Hep with TAT-Gel and incubating for 30 min at 4ºC. For the T84.66-Hep/TAT-Gel+Pro treatment, the T84.66-Hep/TAT-Gel was prepared and administered as above, and protamine was injected *via* tail vein 24 hr post-injection of the complex. The tumor size and body weight of the mice was measured daily.

5.3.4 Statistical Analysis

All measurements are presented as mean ± standard deviation. Statistically significant differences among groups were determined using the one-way ANOVA and Tukey's multiple comparison test as post-hoc test (Prism version 5.0, GraphPad, San

Diego, CA). Results that yielded p-values less than 0.05 were considered to be statistically significant.

5.4 Results

5.4.1 *In Vitro* Evaluation of CPP-Modified ATTEMPTS

The heparin inhibition of TAT-Gel cell internalization and protamine-induced reversal of the heparin block was evaluated by cytotoxicity studies on LS174T cells. The results are shown in Figure 1 and the IC_{50} values are summarized in Table 1. Treatment of cells with T84.66-Hep/TAT-Gel showed no cell death (at concentration up to 5 μM of TAT-Gel) with above 1:3 molar ratio (heparin:TAT), while high level of cytotoxicity (IC_{50}: 15.7 ± 12.2 nM) was observed by treatment with TAT-Gel alone (see Figure 1A and Table 1). In comparison, when protamine was added to the cells pre-incubated with the T84.66-Hep/TAT-Gel, significantly enhanced cytotoxicity was observed. Notably, T84.66-Hep/TAT-Gel+Pro treatment (with heparin-to-protamine molar ratios of 1:2 to 1:0.2) yielded IC_{50} values close to that of TAT-Gel (Figure 1B and Table 1). Moreover, this protamine-induced reversal of the heparin block was available even after 48 hrs post-treatment of the T84.66-Hep/TAT-Gel (Figure 1C).

5.4.2 PK Profiles

The PK profiles of T84.66, T84.66-Hep, rGel, TAT-Gel and T84.66-Hep/TAT-Gel were determined using C57BL/6 mice. The plasma concentration *vs.* time profile for each sample is shown in Figure 2 and the various PK parameters (e.g., plasma half-live ($t_{1/2}$), clearance (CL), area under the curve (AUC) and volume of distribution at steady-state (Vss)) calculated by multi-compartment model analyses are summarized in Table 2

and 3. The plasma concentration profile of T84.66 fit a 2-compartment model and the plasma half-life of T84.66 was 2.5 days (Figure 2A and Table 2). In comparison, the T84.66-Hep profile fit better a 1-compartment model and showed a relatively shorter plasma half-life (2.76 ± 0.80 hr). The conjugation with heparin might have affected the FcRn receptor binding of the T84.66, thereby, impeding the recycling of the antibody in the blood circulation. This possibility was supported by severely hampered T84.66-Hep binding to protein G resins (data not shown). When the T84.66-Hep was administered as a complex with TAT-Gel, the kinetics fit a 2-compartment model and T84.66-Hep had even shorter plasma half-life (2.22 ± 0.54 hr) (Figure 2A and Table 2).

The rGel and TAT-Gel both showed a similar monophasic plasma concentration profile and were rapidly cleared from the blood circulation ($t_{1/2}$ of rGel: 3.7 min (± 0.6) and $t_{1/2}$ of TAT-Gel: 4.7 min (± 0.5)) (Figure 2B and Table 3). As a comparison, TAT-Gel as a complex with T84.66-Hep yielded significantly prolonged plasma half-life (68 ± 24 min) and the plasma profile fit better a 2-compartment model (Figure 2B and Table 3).

Comparison of the PK parameters of the TAT-Gel indicated that, *via* complex formation with the T84.66-Hep, the CL of TAT-Gel was reduced by 3-fold (15.56 ± 3.07 $mL \cdot hr^{-1}$ → 5.00 ± 0.56 $mL \cdot hr^{-1}$) leading to significantly increased AUC (8.94 ± 1.75 $mg \cdot hr \cdot L^{-1}$ → 27.27 ± 3.09 $mg \cdot hr \cdot L^{-1}$). The Vss of TAT-Gel was also increased by 3-fold (1.72 ± 0.31 mL → 4.94 ± 1.99 mL), suggesting more extensive distribution of TAT-Gel outside the blood circulation (Table 3).

5.4.3 Biodistribution Profiles of TAT-Gel and T84.66-Hep/TAT-Gel

Tissue distribution of TAT-Gel and T84.66-Hep/TAT-Gel was evaluated in LS174T xenograft bearing nude mice. Figure 3A shows the images of dissected tissues

harvested from the mice administered with TAT-Gel-B4, at 15 min, 1 hr, 5 hr or 24 hr post-injection. The relative fluorescence intensity of each tissue is shown in Figure 3B. Figure 4A and 4B show the tissue distribution profiles of T84.66-Hep-C5 and TAT-Gel-B4 in the tissues collected from the mice administered with T84.66-Hep-C5/TAT-Gel-B4, at 2 hr, 24 hr, 48 hr or 72 hr post-injection. The relative fluorescence intensity of each tissue is also shown in Figure 4A and 4B.

Certain background autofluorescence was detected only from the intestine when imaged at Ex/Em wavelength of 675nm/720 nm, but not at 745nm/800 nm (Figure 3A, 4A and 4B). The TAT-Gel-B4 was mainly distributed in kidney and liver, but only weak fluorescence signal was detected in the tumor (Figure 3A and 3B). In comparison, after administration of T84.66-Hep-C5/TAT-Gel-B4, T84.66-Hep-C5 was observed largely in the liver and tumor (Figure 4A), and TAT-Gel-B4 was found mainly in the kidney, tumor and liver (Figure 4B). Based on the tissue images, it was clearly realized that enhanced tumor accumulation of TAT-Gel-B4 was accomplished by administered as a complex with T84.66-Hep-C5 (Figure 3 and 4B).

The fluorescence intensities of both the T84.66-Hep-C5 and TAT-Gel-B4 peaked in the tumor 24 hr after administration of the T84.66-Hep-C5/TAT-Gel-B4 (Figure 4A and 4B). Furthermore, both the tumor-to-kidney and the tumor-to-liver distribution ratios of the TAT-Gel-B4 reached their maximum levels at 24 hr post-injection of the T84.66-Hep-C5/TAT-Gel-B4 (Figure 4B). Therefore, 24 hr-post injection of the T84.66-Hep/TAT-Gel was considered optimal for protamine administration.

5.4.4 Maximum Tolerable Dose (MTD) Assay

The MTD of TAT-Gel and T84.66-Hep/TAT-Gel was determined using non-tumor bearing C57BL/6 mice. Injection of more than 18 mg/kg TAT-Gel caused death of all the mice in the group (N = 3) within 24 hr post-injection, but no mice died at lower than 9 mg/kg dose. Therefore, the MTD of the TAT-Gel was determined as 9 mg/kg. In case of the T84.66-Hep/TAT-Gel, no mouse was dead even by administration of 80 mg/kg T84.66-Hep and 36 mg/kg TAT-Gel complex. As the above complex dose was considered high, no studies were further performed for determining the MTD of the T84.66-Hep/TAT-Gel.

5.4.5 *In Vivo* Efficacy Studies

The efficacy of TAT-Gel to treat colorectal cancer in conjunction of CPP-modified ATTEMPTS was evaluated in LS174T xenograft tumor mice model. The results are shown in Figure 5A and 5B. The tumor volumes of the mice treated with PBS, TAT-Gel or protamine continued exponential growth and, at day 40, reached average size of 1935.6 ± 429.6 mm^3, 1981.9 ± 312.9 mm^3 and 2182.3 ± 417.2 mm^3, respectively. Notably, no therapeutic effect was observed with TAT-Gel treatment even at dose (7 mg/kg) close to its MTD (9 mg/kg). In comparison, remarkably, T84.66-Hep/TAT-Gel+Pro treatment yielded a 70% inhibition of the tumor growth (583.1 ± 202.2 mm^3 at day 40, $p < 0.001$***). The mice treated with T84.66-Hep/TAT-Gel without protamine also yielded a 31% inhibition of tumor growth (1331.1 ± 365.5 mm^3 at day 40, $p < 0.05$*).

During the efficacy studies, whereas the body weight of mice treated with PBS or protamine continuously increased, the mice received TAT-Gel (15% weight loss by day 10), T84.66-Hep/TAT-Gel (1% weight loss by day 10) or T84.66-Hep/TAT-Gel+Pro

(8.5% weight loss by day 10) treatment experienced temporary loss of weight specifically during the sample treatment (Figure 5C). However, no other apparent symptoms of toxicity were observed and, since the last treatment at day 9, the body weight of the mice received TAT-Gel, T84.66-Hep/TAT-Gel or T84.66-Hep/TAT-Gel+Pro treatment gradually increased and eventually caught up that of the control mice (Figure 5C).

5.5 Discussion

While great anti-cancer activity of TAT-Gel was reported, its utilization for cancer therapy remains a challenge, due to potential toxicity issues induced by nonspecific internalization[2]. In this research, we explored *in vitro* and *in vivo* the feasibility to apply the CPP-modified ATTEMPTS for toxin-based colorectal cancer therapy.

The T84.66 mAb was chosen as the targeting moiety of the DD. Besides its excellent targeting ability against CEA over-expressed tumors (e.g., colorectal cancer)[3], additionally, the non-internalizing property of the T84.66 was also a crucial factor.[4] To utilize the great translocation ability of the CPP, ideally, the targeted mAb-Hep/CPP-drug should stably remain on the surface of the tumor cells until the CPP-drug is triggered release by protamine.

Once the TAT-Gel and T84.66-Hep were both synthesized, the ‘prodrug’ feature of the DDS was determined in cytotoxicity studies. Dose dependent inhibition of TAT-Gel cell internalization was observed by T84.66-Hep. Especially, with molar ratios of above 1:3 (Hep:TAT), the T84.66-Hep/TAT-Gel yielded no cytotoxicity (up to 5 μM of TAT-Gel) (Figure 1A), suggesting that TAT-Gel cell internalization is completely

blocked by the T84.66-Hep. As a comparison, addition of protamine to the cells pre-treated with the T84.66-Hep/TAT-Gel significantly enhanced the cytotoxic effect which was close to that observed from the cells treated with TAT-Gel alone (Figure 1B).

The 'targeting' feature of the DDS was realized by biodistribution studies. Compared with the tumor images harvested from the TAT-Gel administered mice (Figure 3), significantly higher accumulation of TAT-Gel was observed in the tumors dissected from the mice administered with the T84.66-Hep-TAT-Gel (Figure 4B). This result was in good accordance with the previous findings (Chapter 4). Remarkably, 58-fold enhanced tumor exposure of TAT-Gel was accomplished by the complex formation with the T84.66-Hep.

The *in vivo* complex stability of the T84.66-Hep/TAT-Gel was evidenced by the PK and biodistribution profiles (Figure 2 and 4). Similar to the rGel, the TAT-Gel was rapidly eliminated ($t_{1/2}$: 4.7 ± 0.5 min) by renal excretion (supported by high disposition of TAT-Gel in the kidney (Figure 3)), following a monophasic plasma profile. However, by complex formation with T84.66-Hep, the plasma concentration profile of TAT-Gel better fit a 2-compartment model, and the clearance rate was markedly reduced by 3-fold, resulting in significant increase of plasma half-life (17-fold, 68 ± 24 min) (Figure 2B). Meanwhile, the plasma concentration profiles of the T84.66-Hep as a complex with the TAT-Gel also fit a 2-compartment model, and the plasma half-life was significantly reduced (Figure 2A). This plasma stability of the T84.66-Hep/TAT-Gel was further confirmed from the tissue distribution profiles. Both the T84.66-Hep and TAT-Gel displayed similar accumulation profiles in the tumor along the time (Figure 4A and 4B).

The tissue distribution profiles, however, also raised certain issues. T84.66-Hep showed high disposition in the liver but low in the kidney, while highest disposition of TAT-Gel was observed in the kidney (Figure 4A and 4B). A possible explanation for this is the presence of unbound or weakly bound TAT-Gel in the sample as we applied no purification step after the complex formation. In regard to this problem, optimizations of the mixing ratio of T84.66-Hep and TAT-Gel, or applications of more stringent binding condition (e.g., higher salt concentration) and purification steps appears to be necessary for solving the problem of TAT-Gel loss.

Encouraged by the promising outcome from the feature characterization, the *in vivo* efficacy was evaluated using the nude mice with LS174T xenograft bearing mice. The results are shown in Figure 5. TAT-Gel yielded no therapeutic effect even with dose close to the MTD (9 mg/kg). This result was somewhat expected because TAT-Gel displayed a short plasma half-life (4.7 ± 0.5 min) (see Figure 2 and Table 3) and very low tumor accumulation (see Figure 3). In comparison, when the mice were treated with T84.66-Hep/TAT-Gel, delayed tumor growth (31% inhibition of tumor growth, $p < 0.05$*) was observed (Figure 5A and 5B). Possibly, certain portion of the TAT-Gel might have been released from the T84.66-Hep after delivered to the tumor. However, the most crucial finding of this study was observed from the treatment group. Remarkably, administration T84.66-Hep/TAT-Gel followed by injection of protamine (24 hr post-injection of complex) yielded the highest therapeutic effect (70% inhibition of tumor growth) (Figure 5A and 5B). This result substantiates the hypothesis that protamine can reverse the inhibition of T84.66-Hep block *in vivo* and enable the release of TAT-Gel.

The *in vivo* toxicity of TAT-Gel was assessed through MTD assays. The TAT-Gel caused severe acute toxicity with above 18 mg/kg dose, which caused death of all the tested mice within 24 hrs. This toxicity level of TAT-Gel was greater than that reported for gelonin (LD_{50} ~ 75 mg/kg)[5] presumably due to enhanced nonspecific cellular uptake in various organs. However, when TAT-Gel was administered as a complex with T84.66-Hep, significantly reduced level of toxicity (no death of mice even with 36 mg/kg dose) was observed. This reduced toxicity by complex formation with T84.66-Hep was further evidenced by the body weight profile during the efficacy studies (Figure 5C). The average body weight of the T84.66-Hep/TAT-Gel treated mice was similar to that of the control mice (PBS treatment) along the time, while the treatment with TAT-Gel and T84.66-Hep/TAT-Gel+Pro induced significant body weight loss during the treatment. A possible explanation for the body weight loss of the treatment group could be due to toxicity caused by the TAT-Gel released from T84.66-Hep by protamine. However, importantly, the body weight of the mice was regained gradually since the last treatment (at day 9) and no other symptoms were observed.

5.6 Conclusions

Overall, the feasibility to apply CPP-modified ATTEMPTS for toxin-based colorectal cancer therapy was explored in this research. Through *in vitro* and *in vivo* studies, appropriate functioning of both the 'targeting' and 'prodrug' features of the DDS was confirmed. Targeted delivery of TAT-Gel to tumor *via* complex formation with the T84.66-Hep was evidenced by PK and biodistribution studies. Also, through *in vitro* cytotoxicity assays and *in vivo* efficacy studies, the protamine induced reversal of

T84.66-Hep block was realized. Although further optimization is in need in preparation and purification of T84.66-Hep/TAT-Gel, this study clearly demonstrated that the DDS can provide enhanced therapeutic efficacy as well as reduced toxicity.

5.7 Tables

Table 5-1. Summary for the cytotoxicity study results (IC_{50}) after TAT-Gel, T84.66-Hep/TAT-Gel or T84.66-Hep/TAT-Gel+Pro treatment

TAT-Gel	T84.66-Hep/TAT-Gel		T84.66-Hep/TAT-Gel+Pro	
IC_{50}	Hep:TAT	IC_{50}	Hep:Pro	IC_{50}
15.7 ± 12.2	1:0.3	> 5000	1:2	9.7 ± 1.5
	1:1	> 5000	1:1	6.2 ± 2.2
	1:3	> 5000	1:0.3	19.2 ± 9.1
	1:5	> 5000	1:0.2	6.8 ± 3.6
	1:10	2100 ± 520		

IC_{50} values are displayed as nM. For all experiments, N=3.

Table 5-2. Summary for PK profiles of T84.66, T84.66-Hep and T84.66-Hep as a complex with TAT-Gel

Samples	$t_{1/2}$ (β) (hr)	CL ($mL \cdot hr^{-1}$)	AUC ($mg \cdot hr \cdot L^{-1}$)	Vss (mL)
T84.66	> 2.5 days	n.a.	n.a.	n.a.
T84.66-Hep	2.8 ± 0.8	0.3 ± 0.1	1400 ± 330	1.1 ± 0.1
T84.66-Hep/TAT-Gel	2.2 ± 0.5	$0.9 \pm 0.2^{***}$	$460 \pm 110^{***}$	$2.3 \pm 0.3^{****}$

n.a.: not applicable. ***$P < 0.001$, ****$P < 0.0001$ by student t-test (unpaired t-test, two tailed). For all experiments, N=5. ($t_{1/2\ (\beta)}$: plasma half-life calculated by slope of terminal phase, CL: clearance rate from plasma, AUC: area under the concentration/time curve, Vss: volume of distribution at steady-state)

Table 5-3. Summary for PK profiles of rGel, TAT-Gel and TAT-Gel as complex with T84.66-Hep

Samples	$T_{1/2}$ (β) (min)	CL ($mL \cdot hr^{-1}$)	AUC ($mg \cdot hr \cdot L^{-1}$)	Vss (mL)
rGel	3.7 ± 0.6	22.1 ± 5.3	6.5 ± 1.4	1.9 ± 0.5
TAT-Gel	4.7 ± 0.5	16.3 ± 3.1	8.9 ± 1.8	1.7 ± 0.3
TAT-Gel/T84.66-Hep	68 ± 24***	5.0 ± 0.6**	27.1 ± 3.1***	4.9 ± 2.2**

** $P < 0.001$, *** $P < 0.0001$. For all experiments, N=5. ($t_{1/2\ (\beta)}$: plasma half-life calculated by slope of terminal phase, CL: clearance rate from plasma, AUC: area under the concentration/time curve, Vss: volume of distribution at steady-state)

5.8 Figures

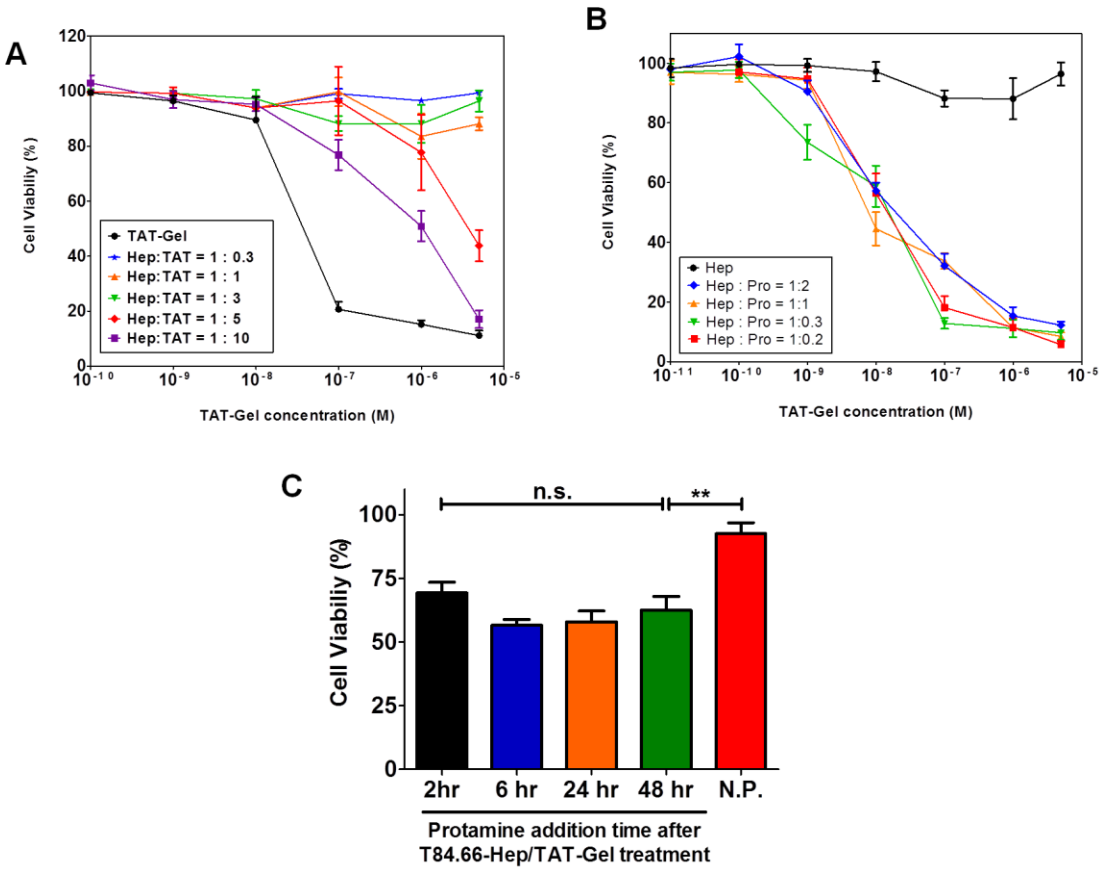

Figure 5-1. *In vitro* evaluation of CPP-modified ATTEMPTS on LS174T cells by XTT assay.

(A) T84.66-Hep-mediated inhibition of TAT-Gel cell internalization; Reversal of T84.66-Hep block by protamine with different concentration (B) or addition time (C) ((N=3). n.s.: not significant, ** $P < 0.001$. (N.P.: no protamine)

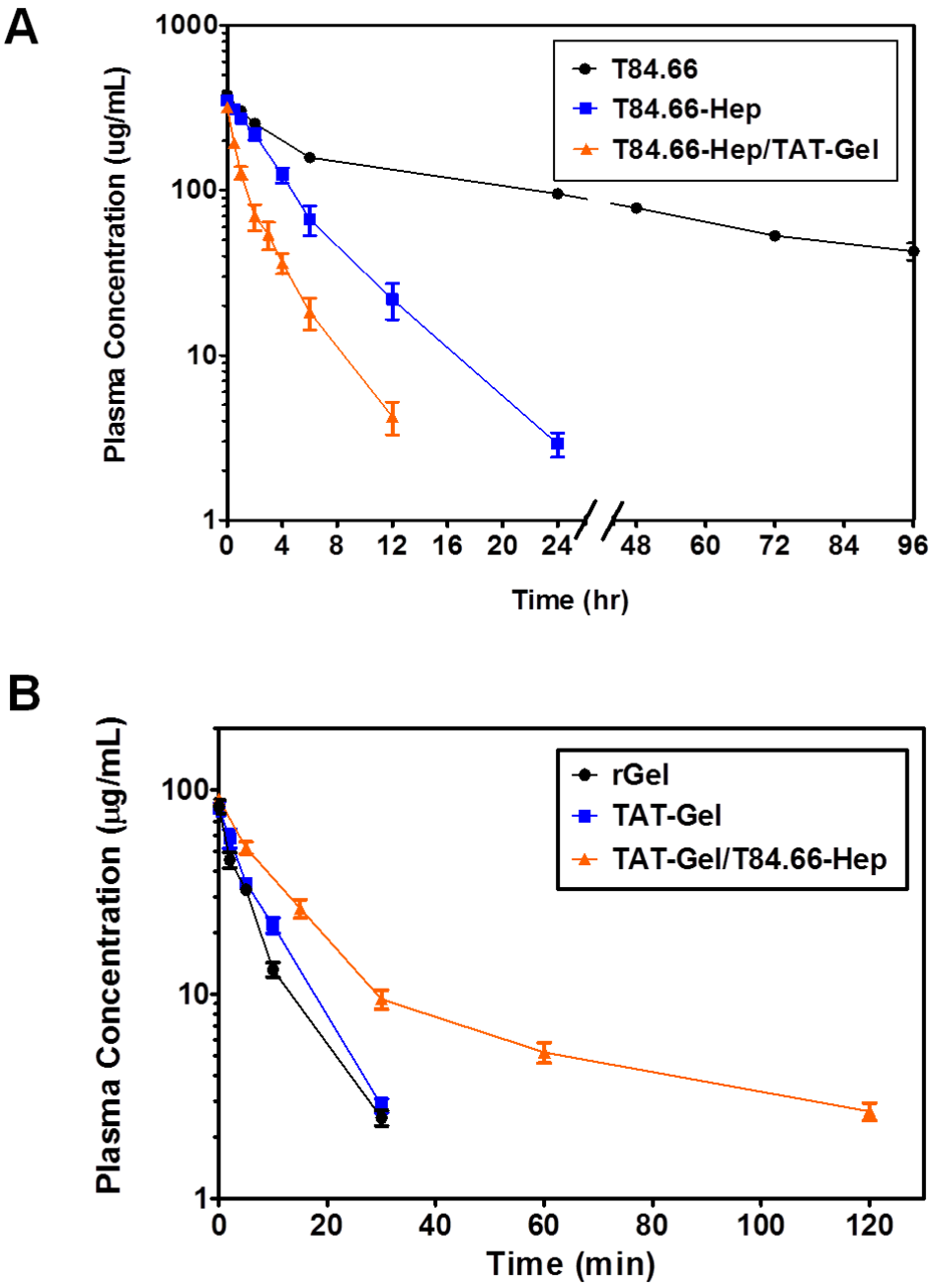

Figure 5-2. Plasma clearance of T84.66, T84.66-Hep, rGel, TAT-Gel and T84.66-Hep/TAT-Gel in mice.

(A) PK of T84.66, T84.66-Hep and T84.66-Hep as a complex with TAT-Gel; (B) PK of rGel, TAT-Gel and TAT-Gel as a complex with T84.66-Hep. Each symbol represents the mean concentration, and error bars indicate the standard deviation (N = 5).

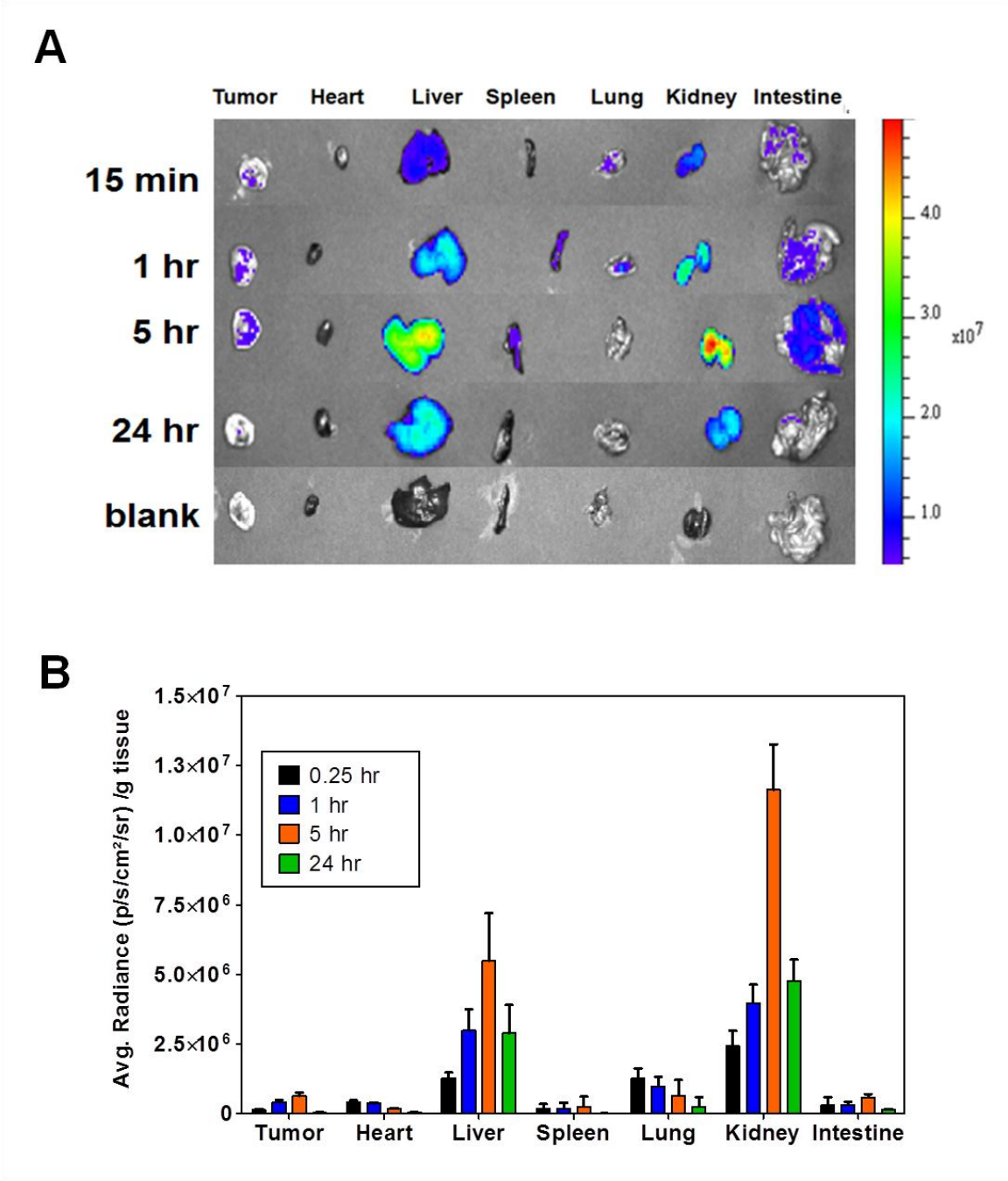

Figure 5-3. Tissue distribution of TAT-Gel in athymic nude mice bearing LS174T xenograft tumor.

(A) Representative images of the dissected mice organs sacrificed at 15 min, 1 hr, 5 hr or 24 h post-administration of TAT-Gel-B4. (B) Relative fluorescence intensity of each organ normalized by the tissue weight (displayed as average radiance per gram tissue).

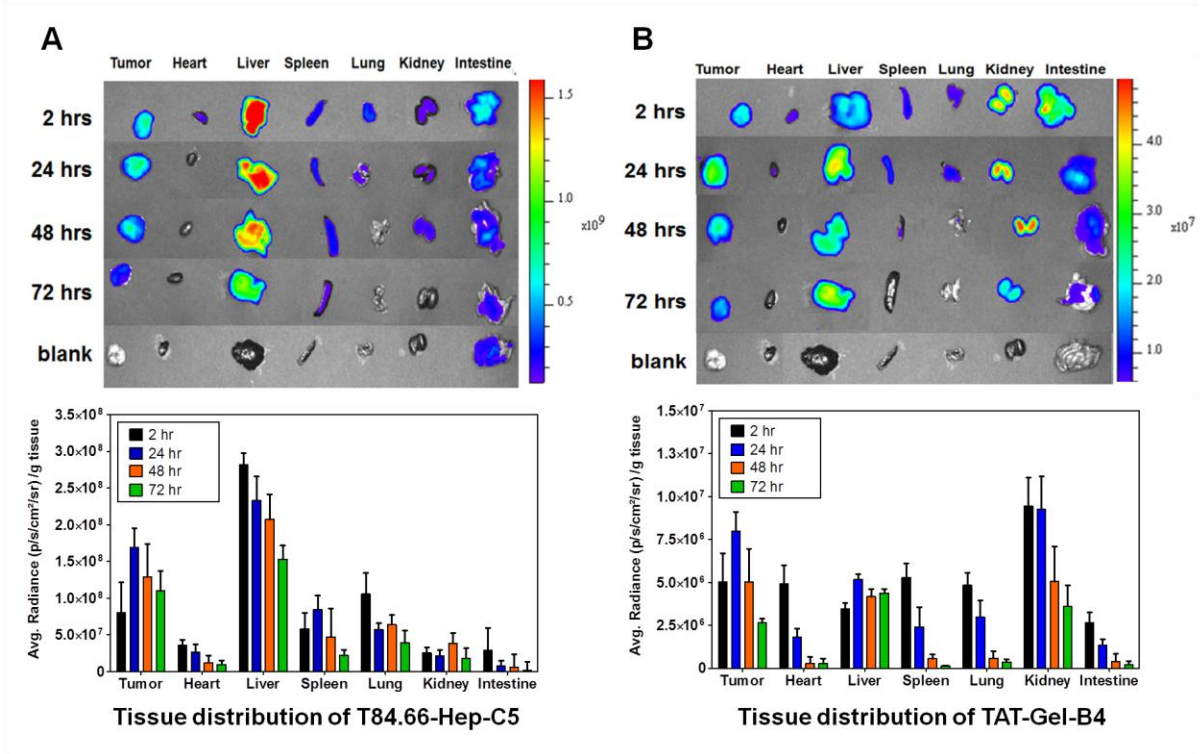

Figure 5-4. Tissue distribution of T84.66-Hep (A) and TAT-Gel (B) in athymic nude mice bearing LS174T xenograft tumor after administration of T84.66-Hep-C5/TAT-Gel-B4.

At 2 hr, 24 hr, 48 hr or 72 hr post-administration of T84.66-Hep-C5/TAT-Gel-B4, mice were sacrificed and dissected organs were imaged. Relative fluorescence intensity of each organ was calculated by subtracting the mean fluorescence intensity of corresponding organ from the blank mouse. The relative fluorescence intensity was further normalized by the tissue weight and displayed as average radiance per gram tissue.

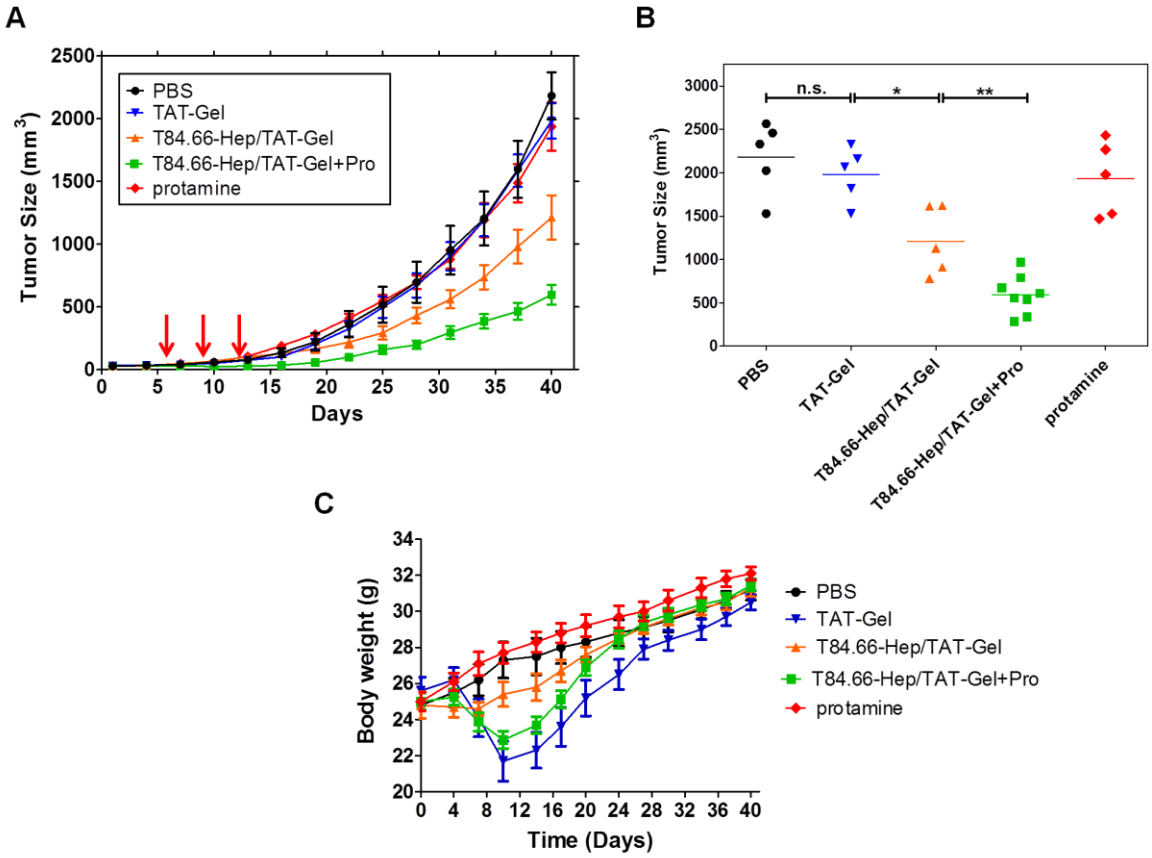

Figure 5-5. *In vivo* efficacy study results in an LS174T s.c. xenograft tumor mice model.

(A) Tumor volume profiles as a function of time (days). When the tumor size reached ~ 30 mm^3 (at day 3), mice were divided into 5 groups (N=5) and received PBS (circle), TAT-Gel (triangle), T84.66-Hep/TAT-Gel (reversed triangle), T84.66-Hep/TAT-Gel+Pro (square) or protamine (diamond) treatment. The treatment was given by tail vein injection at day 3, 6 and 9. For T84.66-Hep/TAT-Gel+Pro treatment, the T84.66-Hep/TAT-Gel was administered at day 3, 6 and 9 and protamine was given 24 hrs after each treatment of the T84.66-Hep/TAT-Gel. Tumor size was measured daily using a vernier caliper after tumor inoculation (day 0) and the volume (mm^3) was calculated by the following equation, $V = (a^2 \times b) / 2$. In this equation, *a* represents the width and *b* represents the length of the tumor. (B) Average tumor size of each group at day 40 when the tumor size of the PBS treated group reached 2000 mm^3. Data represent mean ± SD. *** $P < 0.0001$. (C) Body weight change of each group during treatment.

5.9 References

1. Billinton N, Knight AW. Seeing the wood through the trees: a review of techniques for distinguishing green fluorescent protein from endogenous autofluorescence. Anal Biochem 2001;291:175-97.
2. Schwarze SR, Ho A, Vocero-Akbani A, Dowdy SF. In vivo protein transduction: delivery of a biologically active protein into the mouse. Science 1999;285:1569-72.
3. Urva SR, Balthasar JP. Target mediated disposition of T84.66, a monoclonal anti-CEA antibody: application in the detection of colorectal cancer xenografts. MAbs 2010;2:67-72.
4. Bryan JN, Lewis MR, Henry CJ, Owen NK, Zhang J, Mohsin H, Jia F, Sivaguru G, Anderson CJ. Development of a two-antibody model for the evaluation of copper-64 radioimmunotherapy. Vet Comp Oncol 2004;2:82-90.
5. Woodhams J, Lou PJ, Selbo PK, Mosse A, Oukrif D, MacRobert A, Novelli M, Peng Q, Berg K, Bown SG. Intracellular re-localisation by photochemical internalisation enhances the cytotoxic effect of gelonin--quantitative studies in normal rat liver. J Control Release 2010;142:347-53.

Chapter 6

Conclusions

6.1 Summary

In this research, CPP-modification was employed to facilitate the intracellular delivery of gelonin. Two model CPPs, TAT and LMWP, were successfully linked to gelonin *via* chemical conjugation and genetic recombination method. The prepared CPP-modified gelonins (cG-L, rG-L and TAT-Gel) possessed equivalent N-glycosidase activity to that of unmodified rGel. Moreover, the CPP-modified gelonins displayed a markedly improved cell uptake and significantly enhanced tumoricidal activities, compared with the rGel.

Although CPP-modification successfully enhanced the anti-cancer activity of gelonin, it also aggravated the potential toxicity concerns due to nonspecific fashion of the CPP-mediated cell uptake. To overcome this non-selective cell penetration of the CPP-modified gelonins, a modified ATTMEPTS was investigated for the applicability. Preliminary *in vitro* and *in vivo* studies demonstrated that the cell internalization of TAT-Gel could be effectively regulated by masking the positive charge of TAT with heparin, and reversing this block by protamine.

In order to provide specific tumor targeting properties for TAT-Gel, a heparin functionalized mAb, T84.66-Hep, was developed by chemical conjugation. The prepared

T84.66-Hep possessed specific CEA binding ability and was able to bind tightly to cationic protamine. Through live animal imaging, it was proven that T84.66-Hep can selectively deliver TAT-Gel to tumor *via* complex formation.

Once the two components of the DDS, the TAT-Gel and the T84.66-Hep, were prepared and characterized, the functionality of the CPP-modified ATTEMPTS was evaluated *in vitro* and *in vivo*. Through PK, biodistribution, toxicity and efficacy studies, appropriate functioning of the key features, 'mAb mediated active tumor targeting' and 'prodrug' were demonstrated.

Overall, this dissertation research provides the evidence that CPPs may serve as tools to enhance the anti-cancer activity of potent but cell-impermeable macromolecules, such as protein toxins. Also, this research demonstrates that CPP-modified ATTEMPTS can provide an effective way to selectively and safely deliver the CPP-modified macromolecules to the tumor site.

6.2 Future Studies

Based on the promising results of the proof-of-concept *in vivo* results, further optimizations for preparation of the CPP-modified ATTEMPTS system are currently proceeding in our laboratory. To reduce the unbound fraction of the TAT-Gel in the sample, application of a purification step or optimization of the incubation condition is considered. Also, to improve the binding strength between the TAT-Gel and T84.66-Hep, different approaches (e.g., insertion of a tandem peptide sequence in between TAT and gelonin, addition of more cationic residues in adjacent to the TAT peptide) are currently underway. Furthermore, expanded PK and biodistribution studies will be performed for

PBPK (physiologically based PK) modeling, and thereby, protamine administration time will be optimized.